

Shibuya

ISSN 0385-2520

**Rock Magnetism
and
Paleogeophysics**

volume 8

1981

Published by the

ROCK MAGNETISM AND PALEOGEOPHYSICS RESEARCH GROUP IN JAPAN

PREFACE

This volume is an annual progress report of the Rock Magnetism and Pleogeophysics Research Group in Japan for the year 1981. As the previous volumes were so, this volume is a collection of summaries or extended abstracts of various research works carried out in our group. Many of the reports contain materials which may be revised or updated as the research activity continues. In this respect, this volume contains many tentative results.

Except for the ones written as pure progress reports, most of the papers in this volume will eventually be published elsewhere in full detail and length. When the names of the journals in which a paper is to be published is available, they are indicated at the end of individual papers. This volume may be referenced, but if a paper appears in an academic journal, the readers are requested to quote the paper from such a journal.

We hope that this volume is a useful source of advance information for recent works on rock magnetism and paleogeophysics in Japan. We thank Dr. T. Nakajima for the kind arrangement in printing this volume.

December 1981

Masaru KONO

Editor

CONTENTS

Preface	i
Contents	ii
Rock Magnetism and Paleogeophysics Symposium 13	iv
PALEOMAGNETISM: CENOZOIC	
M. Koyama Paleomagnetism of the Cezoic Deposits in the North- Eastern Part of the Izu Peninsula, Central Japan	1
L. Chun, K. Maenaka, S. Sasajima Preliminary Study of Paleomagnetism of Some Late Cezoic Basalt Group in Datong Province, North China	9
K. Heki, H. Tsunakawa Paleomagnetism of the Shimokura Dike Swarm, Nrotheset Japan-An Estimation of the Activity Duration of a Dike Swarm-	17
T. Nakajima, Y. Morimoto Paleomagnetism and Fission Track Age of the Miocene Volcanic Rocks from Okutango Peninsula, Japan	22
T. Tosha, H. Tsunakawa. Paleomagnetism of the Shidara Dike Swarm, Central Japan - An Estimation of Paleo- intensity in Miocene -	28
M. Torii, T. Matsuda, S. Ishida, Natural Remanent Magnetization of the Miocene Phonolite from Northern Kenya	34
PALEOMAGNETISM: CRETACEOUS AND EARLIER	
H. Domen, H. Muneoka, A Progress Report on Paleomagnetic Study on Cretaceous Rocks	38
H. Ito, K. Tokieda, Y. Notsu Paleomagnetic Results of Cretaceous Granitic Rocks in Eastern Chugoku, Southwest Japan	40
Y. Otofujii, J. Y. Oh, T. Hirajima, K. D. Min, S. Sasajima Paleomagnetism and K-Ar Age of Cretaceous Rocks from Korean Peninsula...Gyeongsang Supergroup in South Korea....	46
H. Shibuya, S. Sasajima, A Paleomagnetic Study on Silurian- Devonian System in Kurosegawa Tectonic Zone, Southwest Japan	53
ROCK MAGNETIC PROPERTIES	
H. Domen, Preliminary Report on Thermomagnetic Analysis of Volcanic Ash Erupted from Mount St. Helens, U.S.A., 1980	57

H. Domen	On Thermomagnetic Property of An Icelandic Matsuyama Reversed Rock	59
Y. Otofujii, I. Katsura, and S. Sasajima	Origin of Decay of A Past-Depositional Remanent Magnetization in Wet Sediments During Desiccation	61
I. Katsura, and S. Sasajima	Note on the Experimental Acquisition of Remanence in Sediment During a Field Reversal	67
Y. Hamano, K. Yomogida	Magnetic Susceptibility Anisotropy of Chondritic Meteorites	75
GEOCHEMISTRY, DATING, AND MAGNETIC METHODS		
H. Tanaka,	Magnetic Surveying of Archeological Sites	81
T. Sato	Electron Spin Resonance Dating of Calcareous Microfossils in Deep-Sea Sediment	85
M. Kono	Magnetic Field in a Circular Symmetric coil	89
I. Kaneoka	Noble Gas Constraints on the Layered Structure of the Mantle	94
J. Matsuda, K. Notsu, T. Kikukawa and K. Yaskawa	Sr Isotopes in Volcanic Rocks from the South Pacific Ocean: Samoa, Rarotonga, Rurutu, and Marquesas	100
M. Yoshida, Y. Fujiwara, M. Homma, Y. Igarashi and T. Tonosaki	Magnetostratigraphy and Chronology of the Late Neogene to Quaternary Deposits in the Tokachi District, Hokkaido, Japan	106
Author Index		110

ROCK MAGNETISM AND PALEOGEOPHYSICS SYMPOSIUM 13

The thirteenth Rock Magnetism and Paleogeophysics Symposium was held on 27th and 28th July, 1981 at Ohtaki Seminar House, Hokkaido. The following papers were presented.

27th July Morning

1. S.Okada, T.Uno and S.Nakamura (Tottori Univ.) Strati-
graphy and paleomagnetism of Ohginosan volcano, in Tottori and Hyogo
Prefecture.
2. M.Koyama and N.Niitsuma (Shizuoka Univ.) Rock Magnetic
investigation of the Kotai Formation,
Makinohara, Shizuoka Prefecture.
3. M.Koyama (Shizuoka Univ.) Late Cenozoic paleomagnetic
stratigraphy in northeastern Izu
Peninsula.
4. K.Hirooka, N.Tsuda (Toyama Univ.), S.Nishimura, S.Sasajima
(Kyoto Univ.), K.H.Thio and F.Hehwwatt (Geol.Surv. of
Indonesia) Paleomagnetic stratigraphy of
Kharasanbung, Jawa, Indonesia.
5. K.Momose (Shinshu Univ.), H.Nagai and M.Funaki (National
Inst. Polar Res.) Magnetic properties of Fe-Ni Alloy.

27th July Afternoon

6. K.Kodama (Tokyo Univ.) Paleomagnetism of the Ogasawara
Islands.
7. K.Kodama (Tokyo Univ.), K.Shimamura, T.Taira and M.Okamura
(Kouchi Univ.) Paleomagnetism of the Shimanto Belt,
Shikoku.
8. M.Yoshida (Hokkaido Univ.) Paleomagnetic investigation
of Pliocene pumice flow deposits
distributed in the Tokachi plain,
eastern Hokkaido.
9. K.Manabe (Fukushima Univ.) Magnetic properties of the
swamp deposits.
10. Liu Chun (Geol.Inst.Academia Sinica), S.Sasajima (Kyoto
Univ.) and K.Maenaka (Hanazono Univ.) Paleomagnetism
of Late Cenozoic basalts, Tatung,
China.

27th July Evening

11. T.Tosha (Tokyo Univ.) Application of the Ring Core type
Flux gate magnetometer.
12. H.Ito (Shimane Univ.) Paleomagnetic properties of
granites.
13. M.Homma (Girls' Senior Highschool attached to Tokyo College
of Home Economy) Magnetic properties of Joso Clay.
14. H.Sakai and K.Hirooka (Toyama Univ.) Magnetic aniso-
tropy of the igneous rocks.

PALEOMAGNETISM OF THE CENOZOIC DEPOSITS IN THE NORTH-EASTERN PART OF THE IZU PENINSULA, CENTRAL JAPAN

Masato KOYAMA

Institute of Geosciences, Shizuoka University, Shizuoka, 422, JAPAN

1. Introduction

The Izu Peninsula is located on the boundary between the Eurasia plate and the Philippine Sea plate, and is thought to be the block colliding with the Honshu arc. The Peninsula is characterized by intense volcanic activities and crustal movements since Miocene. There are many active faults such as Tanna fault and Irozaki fault, which are related with the 1930 North Izu earthquake and the 1974 Izu Hanto Oki earthquake, respectively, and there are many other active crustal movements such as the abnormal upheaval since 1975 near the Hiekawa pass in the north-eastern part of the Peninsula, the 1978 Izu-Oshima Kinkai earthquake, and the swarm earthquakes off Kawana near Ito city since 1978.

The author has studied the geology and paleomagnetism in the north-eastern part of the Izu Peninsula to quantify the crustal deformation since 1 m.y.B.P. (Fig.1). The tectonic movements in this area and some problems for discussing tectonics using paleomagnetic data have been revealed and are reported here.

2. Geology

The formations distributed in this area consist mainly of volcanics and are divided into four groups which have unconformable relationships with each other: the Yugashima Group, Hiekawa Group, Jo Group, and Atami Group, in ascending order (Fig. 2,3).

The Yugashima Group consists of pumice tuff in the lower part (Kadono Formation), and pumice tuff, calcareous sandstone, tuffaceous sandstone, and basaltic lavas in the upper part (Shimoshiraiwa Formation). This Group is distributed in the north-western part of this area. The age of this Group is middle to late Miocene.

The Hiekawa Group consists of pumice tuff, tuffaceous siltstone, dacitic and basaltic lavas and their pyroclastics in the lower part (Mukai Tuff) and basaltic lavas and their pyroclastics in the upper part (Umegi Formation). This Group is distributed widely along the Oomi and Hie rivers. The age of this Group is Pliocene.

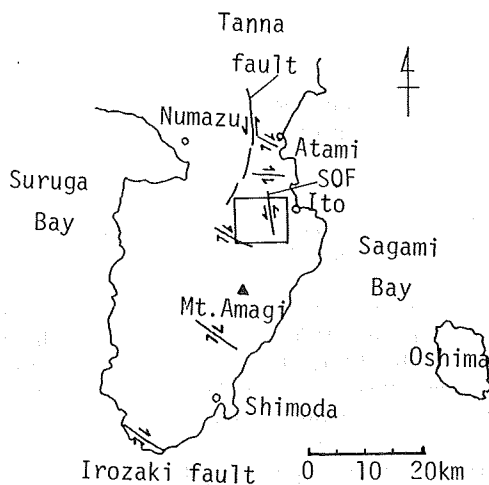


Fig.1. Index map showing the studied area (rectangle). Note the Tanna fault and the Sukumoyama-Okuno fault.

SOF: Sukumoyama-Okuno fault

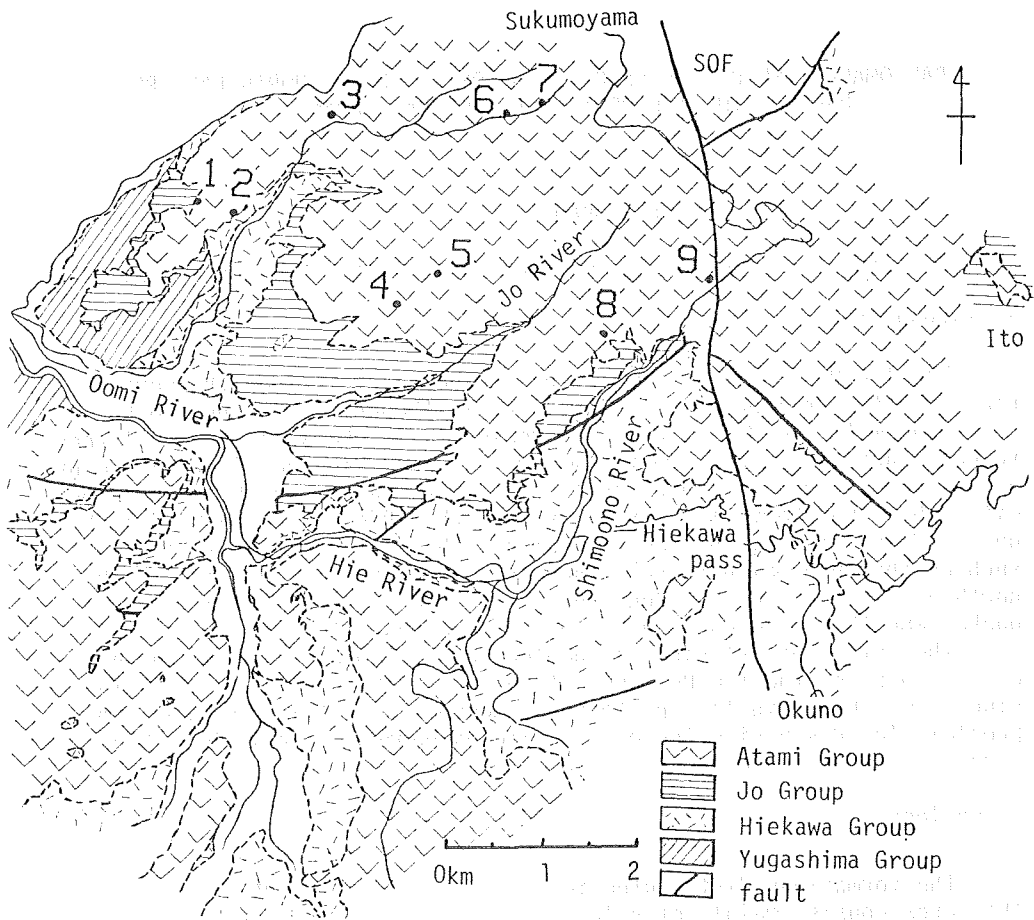


Fig.2. Geologic map showing the sampling sites. The numbers indicate site numbers.

The Jo Group consists of siltstone and sandstone in the lower part (Yokoyama Siltstone), and andesitic lavas and their pyroclastics (Shimo-onogawa Andesite) and tuffaceous conglomerate (Oono Conglomerate) in the upper part. This Group is distributed along the Jo and Shimoono rivers in the central part of this area. The age of this Group is early Pleistocene (from the Olduvai Event to the Jaramillo Event).

The Atami Group consists of andesitic lavas and their pyroclastics (Usami Volcanic-products, Tenshi Volcanic-products, Amagi-main-body Volcanic-products and Hiekawatoge Andesite) in the lower and middle parts, and dacitic and basaltic lavas and their pyroclastics (Oomuroyama Volcanics) in the upper part. This Group consists of terrestrial volcanic-products and is distributed widely in this area. Two units of lava flows named US-2 and US-4 in the lower part of the Usami Volcanic-products are traced over about 5 km from east to west. The age of this Group is early Pleistocene to Holocene (from the Jaramillo Event to the Brunhes Normal Epoch).

The geologic structure in this area is generally simple. Strata are almost horizontal except in the north-western part of this area where strata show a monoclinial structure with eastward to southeastward dip of

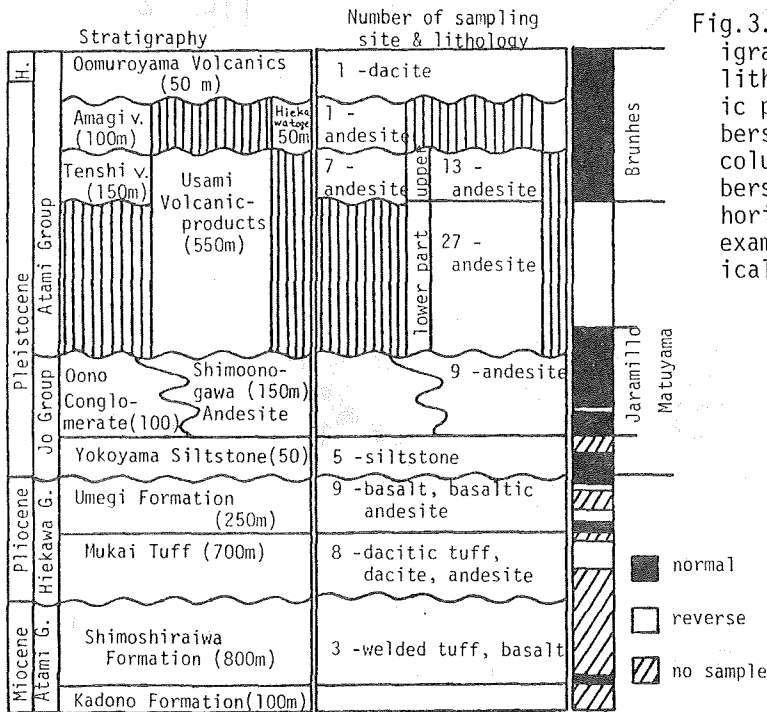


Fig.3. Schematic stratigraphic succession, lithology and magnetic polarity. The numbers in the middle column indicate numbers of the sampling horizons which were examined paleomagnetically.

20° to 70°. There is a fault named the Sukumoyama-Okuno fault near the Hiekawa pass in the eastern part of this area. The fault has the strike of nearly N-S with a vertical downward displacement of 100 to 200 m in the eastern block. This displacement is indicated by the level change of the base of the Usami Volcanic-products. The facies of the Usami Volcanic-products in the western block is different from that in the eastern block. Well-traced lava flows in the western block, for example US-2 and 4 cannot be traced into the eastern block. This fact suggests that the Sukumoyama-Okuno fault has a nature of strike-slip faults. The age of the formation of the fault should be younger than that of the uppermost of the Usami Volcanic-products, which corresponds to the early Brunhes Normal Epoch.

The Sukumoyama-Okuno fault is thought to be a southward extension of the Tanna fault as regards the position and the age.

3. Samples and Measurements

The samples for paleomagnetic measurements are collected at nine sites from two sets of lavas (US-2 and US-4) in the lower part of the Usami Volcanic-products (Fig.2). The US-2 is the andesitic lava of 5-50 m thick. The US-4 consists of four andesitic lavas of 3-10 m thick, which successively lie upon one another and have similar lithology. All the four lavas of the US-4 crop out near the site 9, and in the other sites one lava flow crops out which is correlated with one of the four lavas.

The bottom surfaces of the US-2 and 4 lava flows dip 20° northeastward at the site 9, and dip less than 10° at the other sites. These dips are thought to be initial ones, because the present structure of the Usami Volcanic-products is almost horizontal. Therefore, the bedding correction has not been introduced for the analysis.

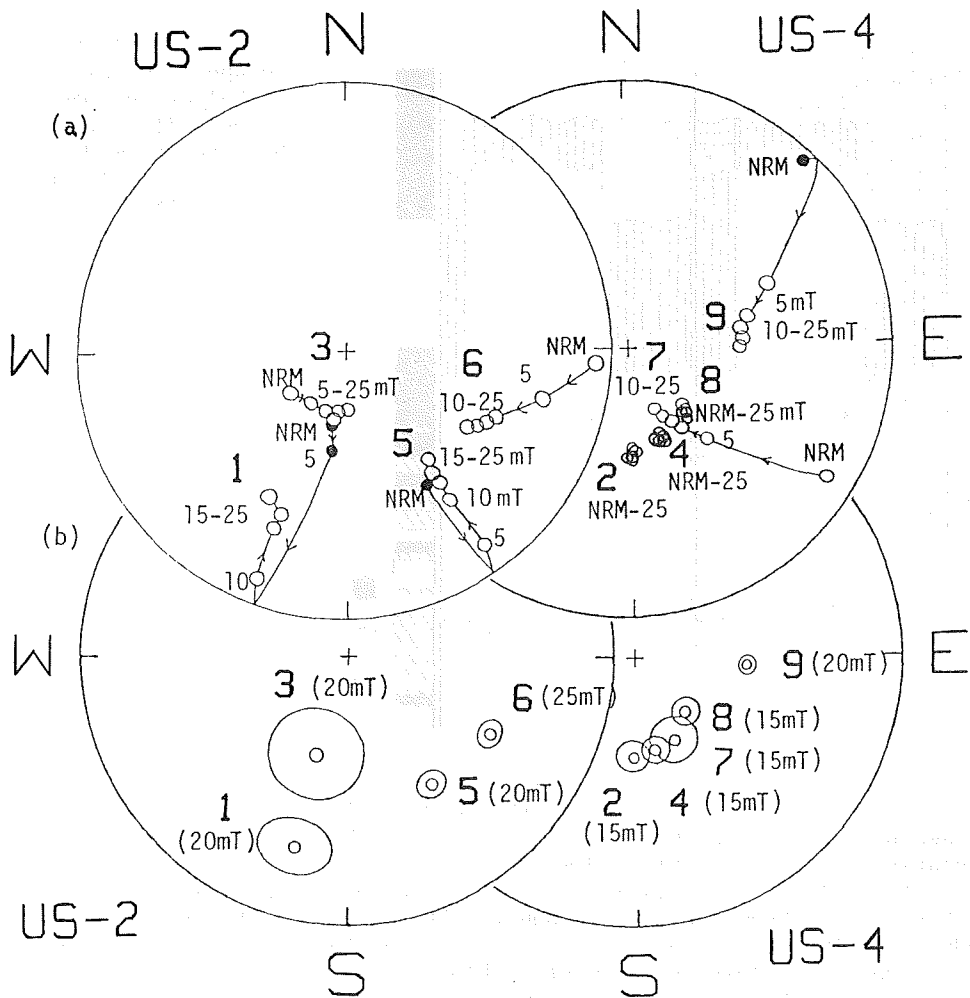


Fig.4. (a) Changes in the remanent magnetization of the lava flows US-2 (left circle) and US-4 (right circle) during stepwise AF-demagnetizations. The numbers in this figure indicate the site number and AF-demagnetization field in mT.

(b) Changes in directions of remanent magnetization of the lava flows US-2 (left circle) and US-4 (right circle) at each site after the 15-25 mT AF-demagnetizations. Size of outer circle at each point shows α_{95} confidence limit. The numbers indicate the site number and AF-demagnetization field in mT.

The four lavas of the US-4 near the site 9 were already sampled and measured paleomagnetically by Kono (1968) (sample number: UV06-09). According to his data the dispersion of the remanent magnetizations of these samples after 12 mT AF-demagnetization is small ($\alpha_{95} = 5.2^\circ$). This fact suggests that the direction of the geomagnetic field was in coincidence with about 5° error while these four lavas erupted, and therefore, within this angle the four lavas can be treated as one set.

Three cored samples with 35 mm diameter were collected from one site using an engine drill, and cut into 32 mm-long pieces. 3 to 6 samples were measured at each site with a high sensitive automatic astatic magnetometer (Niitsuma and Koyama, 1981) and a ring-core type flux-gate spinner magnetometer (Niitsuma and Koyama, 1982). AF-demagnetizations were carried out with a three axial alternating field demagnetizer (Niitsuma and Koyama, 1981, 1982).

4. Results

Changes in remanent magnetization during AF-demagnetization and the directions of remanent magnetization after AF-demagnetization of the US-2 and 4 samples are shown in Fig.4. The changes in directions of remanent magnetization of the US-4 samples during AF-demagnetization are smaller than those of the US-2 samples. Intensities of NRM range from 2.5×10^{-1} to 2.4×10^0 A/m. The ratio between the intensity of NRM and after 15 mT AF-demagnetization of the US-4 samples (1.1 to 2.8) are smaller than that of the US-2 samples (1.6 to 3.6). The dispersion of the remanent magnetizations after AF-demagnetization of the US-4 samples ($\alpha_{95} = 2.8^\circ - 7.0^\circ$) is smaller than that of the US-2 samples ($4.0^\circ - 14.1^\circ$).

Directions of the remanent magnetization of the US-4 samples from one site significantly differ from the other, and the counter-clockwise rotation of declination tends to get larger from western sites to eastern ones (Fig.5), but inclinations do not change significantly (Fig.6). Similar changes in remanent magnetization are detected also in the US-2 samples. These facts suggest that the rotation took place in this area after the eruption of the US-2 and 4 lavas, and the amount of rotation tended to get larger eastward.

5. Discussions and Conclusions

(1) There is an interesting relationship between the counter-clockwise rotation of the remanent magnetization and the distance between sampling sites and the Sukumoyama-Okuno fault (Fig.5). In Fig.5, the counter-clockwise rotation tends to get larger toward the origin of the horizontal axis, which indicates the position of the Sukumoyama-Okuno fault. These horizontal counter-clockwise rotations should be related with the drag rotation along the left-lateral strike-slip fault as shown in Fig.7.

(2) In order to determine the age of the initial phase of the rotation along the fault, the paleomagnetic directions of underlying formations were examined. Most of the samples were collected as hand specimens, except several sites where samples were collected using an engine drill. The hand-sampled blocks were cut into rectangular prism with a base 25×25 mm and a height of 32 mm. The paleomagnetic measurements were made on 1 to 3 specimens for one site, after 15-19 mT AF-demagnetization.

The remanent magnetizations of the formations underlying the Usami Volcanic-products after bedding correction are plotted in Figs.5 and 6. Fig.5 shows that the counter-clockwise rotations of declinations of remanent magnetization also exist in the underlying formations. There is no difference in the amount of rotations between the Usami Volcanic-products and the underlying formations. This fact means that the displacement along the Sukumoyama-Okuno fault started after the eruption of the Usami Volcanic-products. This estimation agrees with other available geologic data.

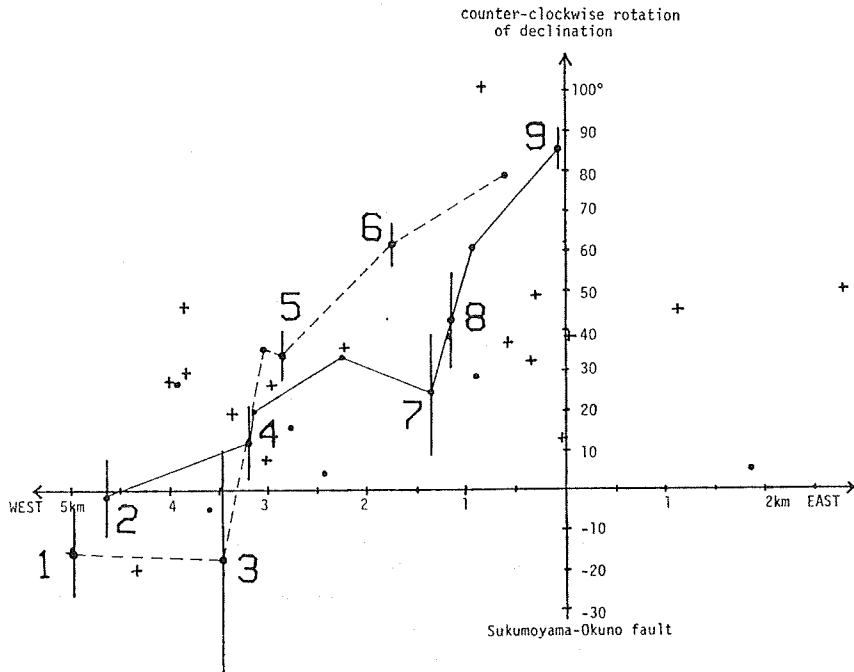


Fig.5. Relationship between counter-clockwise rotations of declinations of remanent magnetization and distances from the Sukumoyama-Okuno fault. Declinations of the US-4 and US-2 lava flows are shown by points connected with solid line and dotted line, respectively.
 ●: declination of remanent magnetization of sample from the Usami Volcanic-products, +: declination of remanent magnetization of sample from the formations underlying the Usami Volcanic-products.

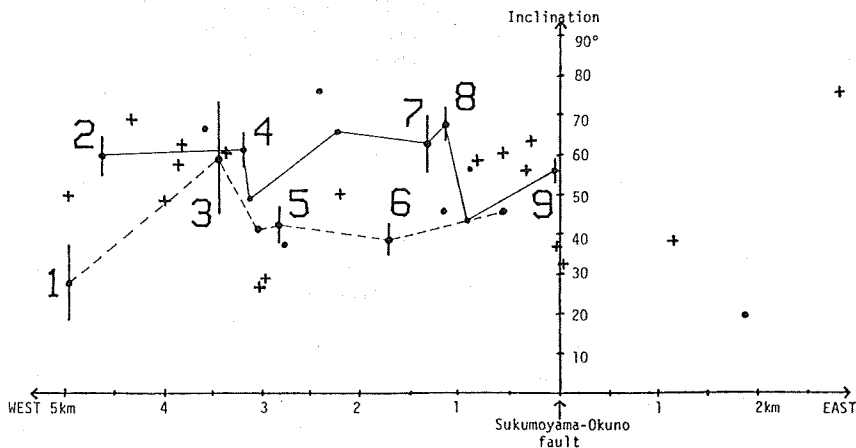


Fig.6. Relationship between absolute inclination of remanent magnetization and distances from the Sukumoyama-Okuno fault. The symbols are the same as in Fig.5.

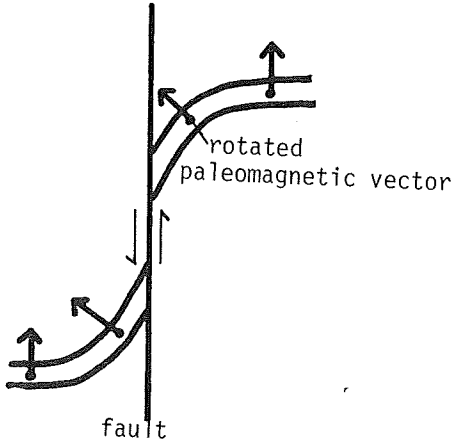


Fig.7. Schematic diagram showing the rotation of paleomagnetic vectors caused by the drag along the left-lateral strike-slip fault.

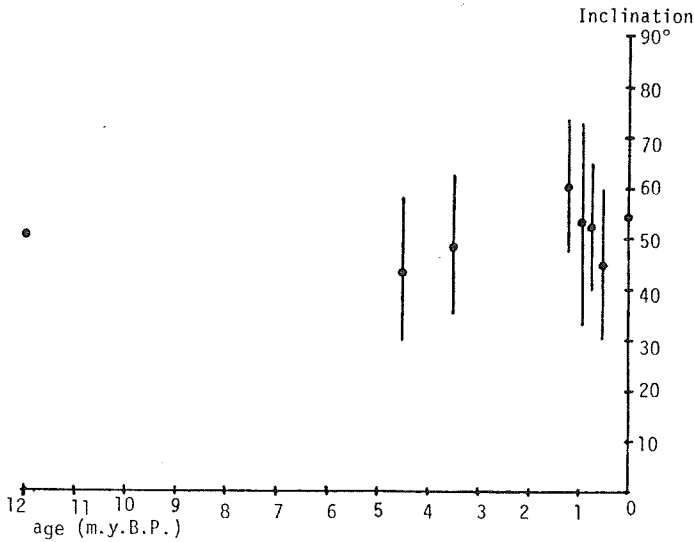


Fig.8. Relationship between the mean of absolute inclinations of remanent magnetization of each formation and its geologic age.

(3) There is no difference between the inclinations of remanent magnetization of each formation and of the present geomagnetic field in this area (Fig.8). This fact suggests that there was no large variation in latitudes, which can be detected as the change of inclination of remanent magnetization since late Miocene time.

Many studies about tectonic rotations and tectonic movements using paleomagnetic data have been reported so far. In this study it is revealed that in such a relatively small area, several tens degree difference in the declination of paleomagnetic vectors was found and the formations were deformed by the movement of a fault. In order to discuss tectonic movements, it is necessary to take into account the possibility of the deformation on a 2 to 3 km scale as in this area, and to use samples collected from several different positions in a same horizon, based on detailed geologic study.

References

Kono, M. (1968) J. Geomag. Geoelectr., 20, 353.
Koyama, M. (1982) (to be published in Geosci. Rep. Shizuoka Univ., 7.)
Niitsuma, N. and Koyama, M. (1981) Geosci. Rep. Shizuoka Univ., 6, 35.
Niitsuma, N. and Koyama, M. (1982) (to be published in Geosci. Rep. Shizuoka Univ., 7.)

(to be published in J. Geomag. Geoelectr.)

PRELIMINARY STUDY OF PALEOMAGNETISM OF SOME LATE CENOZOIC
BASALT GROUPS IN DATONG PROVINCE, NORTH CHINA

Liu CHUN*, Kazuaki MAENAKA** and Sadao SASAJIMA***

* Institute of Geology, Academia Sinica, Beijing, China

** Hanazono College, Kyoto 616, Japan

*** Department of Geology & Mineralogy, Faculty of Science,
Kyoto University, Kyoto 606, Japan

Introduction

In Shanxi-Datong Province of Northern part of China, lying 200 km westward from Beijing City, late Cenozoic volcanic groups are widely distributed. In China, the distributions of Plio-Pleistocene volcanic rocks are concentrated in North-east County and Datong Province described in this paper, so the Datong basalt groups have attracted the attention of geologist in China. Since Teilhard de Chardin & Yang (1931) firstly surveyed the ruins of Quaternary volcano in this region, continuing studies of this subjects have been carried out by many researchers (Barbour & Pien 1930, Yin 1932, Lebedenskii 1958, Wang & Ou 1958, Cao 1959, and Yang 1961). Yin (1932) classified Datong volcanoes into some types basing on their forms, and reported that their activity had initiated at Early Pleistocene and continued until the Age of deposition of loess. Lebedenskii (1958) discussed the type of activity of 12 volcanoes in Datong area and the age of volcanic activity. He concluded that the latest eruption of Datong volcanoes was in historical age, and consequently that the Datong volcanoes were not extinct but dormant volcano. Yin (1976) resurveyed the Datong volcanic area. He separated the Datong volcanic area into two parts; east and west. He insisted that the volcanic activity of the eastern part had begun at middle to late of Middle Pleistocene and finished at early of Late Pleistocene, while that of the western part had started at early of Late Pleistocene and ended at 60 or 70 thousand years ago. He thought that the eruption of Datong volcanoes was an instantaneous episode in geological past and they became inactive volcanoes which had already stopped their volcanic activity in spite of young volcano. Jia et al. (1976) examined such a divergence of opinion on Datong volcanoes from view point of archaeology. They estimated the age of the volcanic activity of Datong volcanoes to be 100 thousands years ago and supported the aspect of Datong inactive volcanoes proposed by Yin (1976).

April of 1981, one of writers (Liu Chun) with his collaborators surveyed in some fields of Datong volcanic area. We clarified that these basalt groups were Pleistocene eruptive products and the stratigraphical sequence of these basalt groups could be determined as illustrated in Fig. 1 (presented by Zhou et al. 1982) from the relation with loess deposits and "Nihowan bed", representative Quaternary sediments in China, with which Datong basalt groups contacted. Loess deposits with a great thickness and a complete sequence are widely distributed in north-western part of China. The study of loess has long been stressed in China. To determine absolute ages of loess has an important significance to the development of not only geology but also archaeology, anthropology and so on.

Liu Chun collected some basalt rocks, loess samples baked by the flowing of basalt, and loess samples from some localities in Datong area, and measured the paleomagnetic direction in cooperation with the researchers in Japan. In this paper, the preliminary result is described.

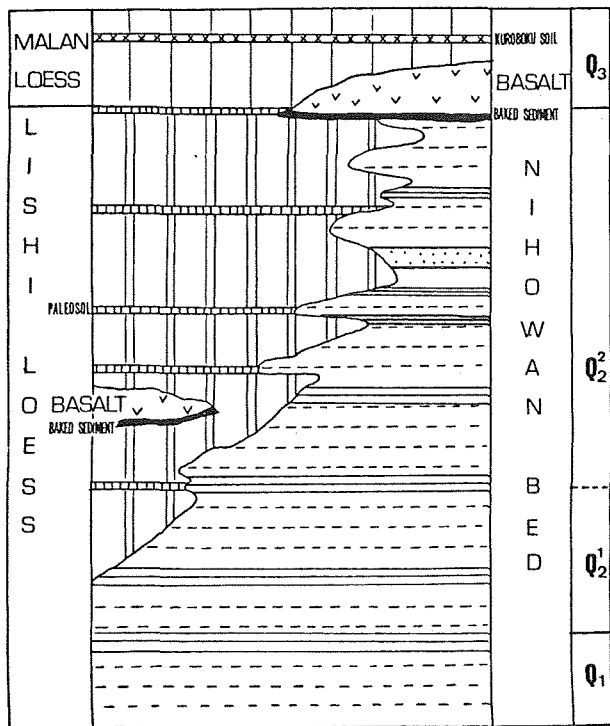


Fig. 1, The general stratigraphical sequence of Datong basalt groups.

Geological outline and samples

Zhou et al. (1982), summarizing the present results of field syuvey and forerunner's results, concluded that the Datong volcanic area was no doubt separated into two areas; eastern and western parts. Their geological ages are Pleistocene, and the age of the western part is generally younger than that of the eastern part. The oriented samples for paleomagnetic purpose from three sites as shown in Fig. 2 are collected by handy core-drilling machine. Geological outline of sampling sites are as follows.

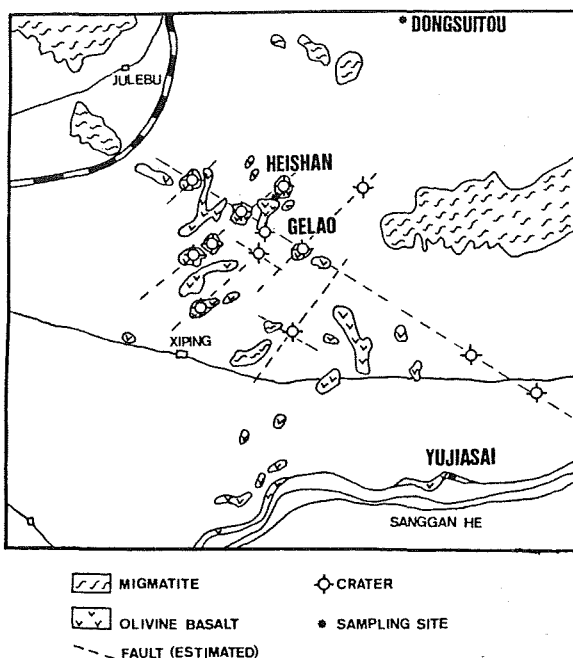


Fig. 2, Distribution map of Datong basalt and sampling sites.

1. Heishan section (site B)

This site locates at the valley of westward from Gelao village (113.5°E, 40.1°N). Fig. 3 shows the stratigraphic succession of this site. The total thickness of the upper basalt, basaltic scoria and the lower basalt is about 5 m. These basaltic layers overly Lishi loess and are overlain by Malan loess. The baked loess layer with the thickness of 50 cm lies directly under the lower basalt layer. Li et al. (1981) obtained the geological age of 0.16 MY by the method of thermoluminescence (TL) using quartz grains (grain sizes range in 2.5-8.2 μm) extracted from this baked loess layer. From this site, total 20 orientated samples of basalt, basaltic scoria, baked loess and unbaked loess are collected.

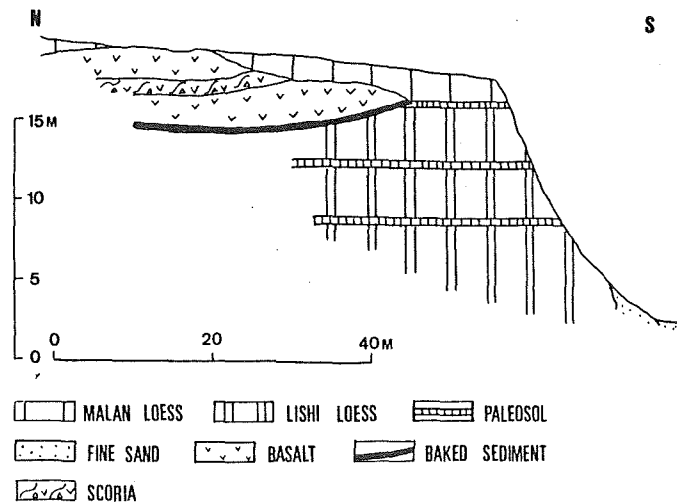


Fig. 3, Cross section of Datong basalt at Heishan site (site B).

2. Dongsuitou section (site T)

This site situates nearby Dongsuitou dam, Dongsuitou village (113.6°E, 40.1°N). This is the place where the loess of middle Pleistocene is well developed. The basalt layer in this section is eruptive product in the time of the fifth paleosol in Lishi loess as illustrated in Fig. 4. Among Lishi and Malan loess, 13 layers of buried paleosols can be found. The paleoclimatic significance of the fifth layer paleosol in the Lishi loess is discussed by An & Wei (1980). Li et al. (1981) obtained 0.21 MY TL age using quartz grains extracted from baked loess layer contacted directly under the basaltic layer. From this site, total 14 samples are taken.

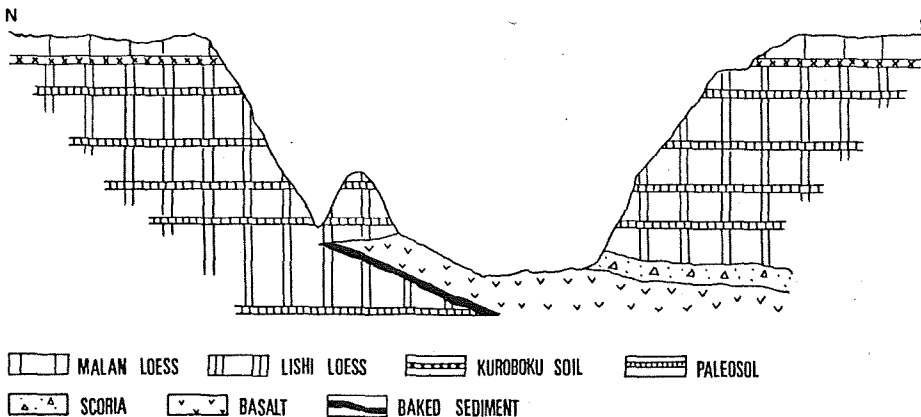


Fig. 4, Cross section of Datong basalt at Dongsuitou section (site T).

3. Yujiasai section (site Y)

This site situates eastward from Yujiasai village (113.9°E, 40°N). Basalt layer in this site overlies clay bed as shown in Fig. 5. The baked sediment layer with 40 cm thick lies directly under the basalt layer. From this site, 4 basalt samples and 14 baked sediment samples are taken.

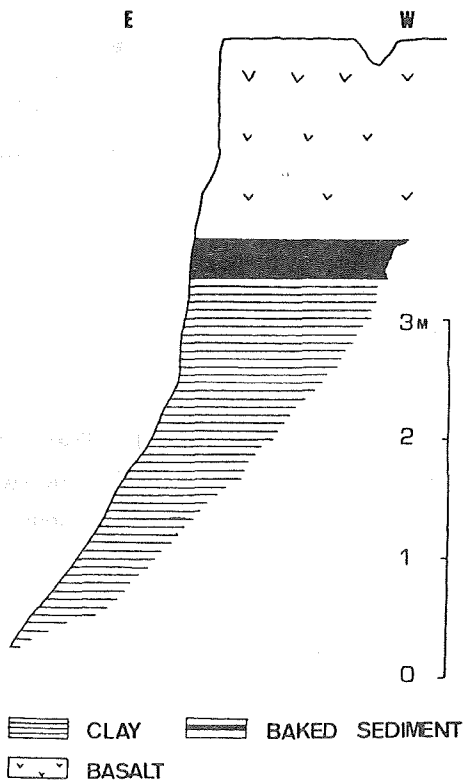


Fig. 5, Cross section of Datong basalt at Yujiasai section (Site Y).

Result of paleomagnetic measurement and discussions

One to three core specimens with one inch are cut from each core samples. The direction and the intensity of the remanent magnetizations of specimens were measured by Schonstedt type spinner magnetometer (SSM-1A) at Kyoto University in Japan. The measured results are described in the following sections.

1. Natural remanent magnetization (NRM)

The intensity of the measured NRM of basalt, baked loess, and loess samples are as follows; basalt $(60-220) \times 10^{-7}$ emu/cc
 baked loess $(0.9-40) \times 10^{-7}$ emu/cc
 loess $(0.3-3) \times 10^{-7}$ emu/cc.

The intensity of remanence, even if the same kinds of rocks, is not steady, but it is generally said that it becomes weaker in order of basalt, baked loess and loess. It is considered that the difference of the mechanism of remanence acquisition between basalt and loess may reflect in the difference of the intensity of their remanence. The one of the most impressive feature is that the intensity of the remanence of the baked loess becomes weaker according to the increased distance from the baked contact with the basalt. It can be imagined that the loess becomes not well baked proportional to the distance from the baked contact.

The directions of measured NRMs are listed in Table 1. The dispersion of the direction, even if in the case of specimens taken from the sample, is rather large, so the magnetic cleaning by the alternating

Table 1 Paleomagnetic results of Datong basalt groups.

Sample Number	Material	N	R	M	After Cleaning		Virtual pole position		
		Declination	Inclination	Declination	Inclination	Latitude	Longitude		
Yujiasai section									
Y-8	basalt	115.2		22.8	76.9	66.0			
Y-7	basalt	357.4		23.0	349.1	45.4			
Y-6-1	basalt	105.1		48.7	336.2	61.1			
Y-6-2	basalt	35.1		71.5	347.4	60.6			
Y-5-1	basalt	120.0		38.4	26.7	67.7			
Y-5-2	basalt	130.0		35.6	31.1	71.0			
Y-4-1	basalt	77.8		50.7	354.6	66.0			
Y-4-2	basalt	104.5		51.3	27.4	68.8			
Y-4-3	basalt	118.5		42.9	36.6	69.9			
Y-3	basalt	305.9		35.4	356.5	58.9			
Y-2	basalt	303.1		31.6	355.6	55.6			
Y-1-1	basalt	328.8		21.0	349.8	51.3			
Y-1-2	basalt	317.9		21.3	342.9	62.0			
				Mean*	358.2	63.0	85.2	309.0	
Y-9	baked clay	334.3		66.7	317.9	53.7			
Y-10	baked clay	46.1		65.2	3.5	63.3			
Y-11	baked clay	9.6		69.7	16.5	54.9			
Y-12	baked clay	7.4		54.9	5.2	53.2			
				Mean	350.7	58.4	82.8	19.7	
Heishan section									
B-1-1	basalt	35.4		39.8	26.9	44.1			
B-1-2	basalt	39.3		38.1	41.5	43.0			
B-2	basalt	40.3		35.2	38.3	39.5			
B-3-1	basalt	41.0		46.7	36.3	46.4			
B-3-2	basalt	33.0		38.0	35.1	43.3			
B-4-1	basalt	28.3		37.7	39.5	37.7			
B-4-2	basalt	26.5		37.6	37.9	38.3			
B-5	basalt	358.1		33.5	354.2	35.0			
B-7	basalt	11.1		28.0	14.6	35.9			
B-8	basalt	43.0		33.2	38.6	40.5			
B-9	basalt	0.1		26.1	315.1	35.2			
				Mean	14.4	42.6	70.5	260.9	
B-10-1	basaltic scoria	184.8		-31.6	212.8	-8.4			
B-10-2	basaltic scoria	61.2		76.1	214.5	-8.4			
				Mean	208.6	-8.4	-45.9	70.3	
B-11	basalt	48.1		6.5	24.0	18.7			
B-12	basalt	73.8		27.9	59.6	43.3			
B-13	basalt	59.0		11.0	47.0	44.2			
				Mean	36.7	36.4	53.2	224.0	
B-15	baked loess	45.0		35.2	13.2	41.2			
B-17	baked loess	32.5		40.3	4.3	26.4			
				Mean	3.3	33.9	68.4	285.0	
B-18	loess	14.9		49.9	59.4	76.2			
B-19	loess	4.7		77.1	9.5	45.0			
B-20	loess	10.3		63.0	355.9	59.1			
				Mean	7.1	61.9	83.8	170.9	
Dongsuitou section									
T-10-1	basalt	12.4		57.3	352.3	55.8			
T-10-2	basalt	4.0		55.5	7.3	58.1			
T-11	basalt	343.3		57.7	341.9	52.8			
				Mean	345.3	55.0	77.5	39.9	
R-2-1	baked loess	342.4		59.8	333.1	42.9			
R-2-2	baked loess	350.7		61.9	347.3	47.5			
R-2-3	baked loess	344.9		58.4	336.2	56.5			
R-2-4	baked loess	349.5		56.2	359.3	56.1			
R-2-5	baked loess	347.2		55.2	348.7	46.4			
R-2-6	baked loess	342.0		60.8	341.1	62.9			
R-2-7	baked loess	346.3		52.4	351.5	49.0			
R-2-8	baked loess	355.2		58.7	354.5	60.2			
R-1-1	baked loess	352.4		66.4	351.7	51.3			
R-1-2	baked loess	344.7		62.9	347.4	63.1			
R-1-3	baked loess	353.7		67.2	6.4	66.3			
R-1-4	baked loess	350.7		69.5	359.2	48.8			
				Mean	350.9	57.6	82.7	11.3	
L-2-1	loess	334.9		54.6	335.3	55.2	66.3	24.3	

current (A.C.) field demagnetization method was tried out to obtain a reliable data.

2. A.C. demagnetization

Pilot specimens were demagnetized progressively in alternating field up to a peak field of 1500 Oe. The examples of A.C. demagnetization on these specimens are shown in Figs. 6 and 7. Fig. 6 shows the result of basalt specimens from site Y. As shown in lower diagram of Fig. 6, demagnetization curve shows a sudden decrease in intensity. The median demagnetization field of basalt specimens from site Y is very low (50 Oe) and the change of the direction is also great, but it seems to stabilize up to 200 Oe. In the case of this specimen, the directional changes with increasing peak field up to 200 Oe give an improvement of the grouping. The median demagnetizing field of baked loess specimens from site T is also low (100 Oe) but the change of the direction is not so great as shown in Fig. 7. Considering from the result of these preliminary test, A.C. demagnetization of all specimens were done in peak field of 200 Oe to isolate stable remanent magnetization from NRM. The data after A.C. cleaning are also listed in Table 1.

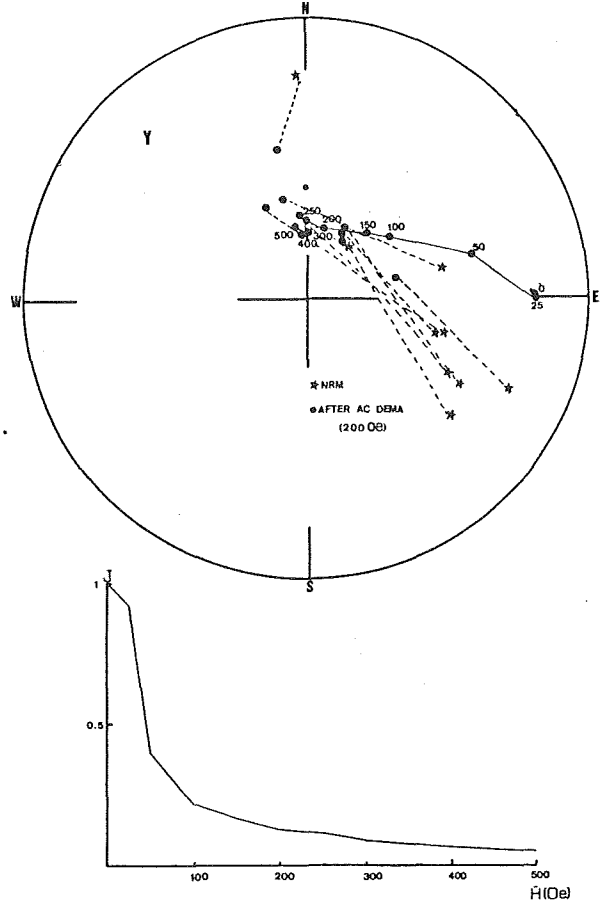


Fig. 6, The A.C. demagnetization of basalt specimens from site Y.

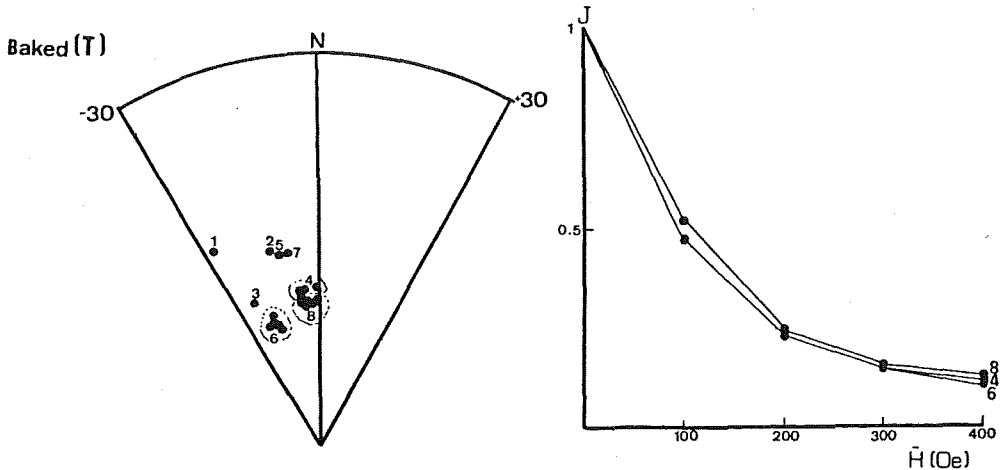
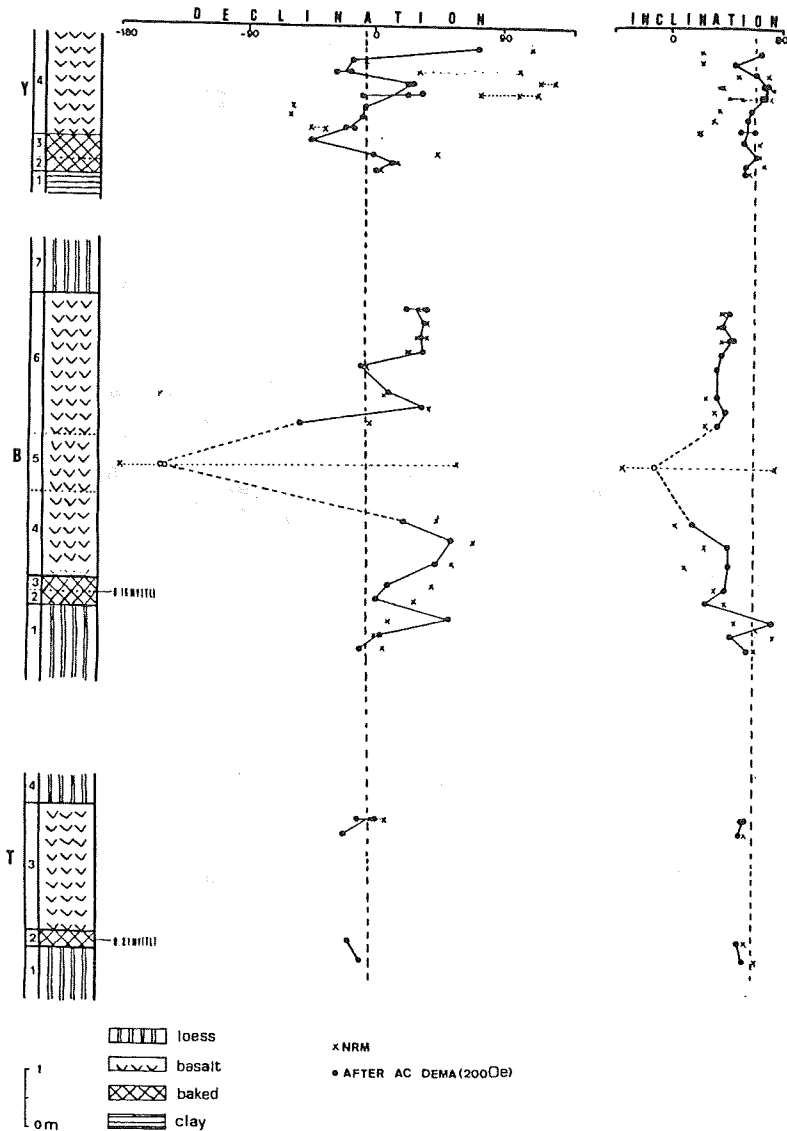


Fig. 7, The A.C. demagnetization of baked loess specimens from site T.

3. Paleo-secular variation

The directions of the remanence after cleaning listed in Table 1 show that the remanence of all specimens have the same direction in spite of the difference of the mechanism of remanence acquisition. The value of the declination and inclination is, roughly speaking, close to the present value at Datong, but in the case of the specimen from site B eastward declination and shallow inclination are prominent. The amplitude of the paleo-secular variation is larger compared to that of archaeo-secular variation.



4. Blake event

Fig. 8 shows a paleomagnetic stratigraphy of

Fig. 8, Paleomagnetic stratigraphy of Datong basalt groups.

Datong basalt groups. As shown in this figure, all Lishi loess and basalt erupted in the age of the deposition of Lishi loess have normal polarity except one layer. The reversed layer having reversed polarity is basaltic scoria layer at site B. The study of mineralogical and petrological composition shows that there are no difference between basaltic scoria, overlying and underlying basalt. So, it is considered that the reversed magnetization of basaltic scoria is due to the reversal of geomagnetic field. Li et al. (1981) obtained 0.16 MY T.L. age on quartz grains extracted from the baked loess at the horizon of 3 m under the scoria layer. The age of the basaltic scoria is estimated to be about 0.10 MY judging from the thickness between the scoria and the baked loess layers. Consequently,

the reversed polarity of the basaltic scoria is considered to be correlated to the Blake event.

5. Virtual geomagnetic pole path

In Table 1, the mean direction of the remanence of the collected specimens from Datong and the position of virtual geomagnetic pole (VGP) are also calculated. Thus obtained VGP cluster around the geographic pole as shown in Fig. 9. A pole path is also given in this figure. A pole path during the geomagnetic field reversal at Blake event seems to travel the low latitude in Pacific Ocean.

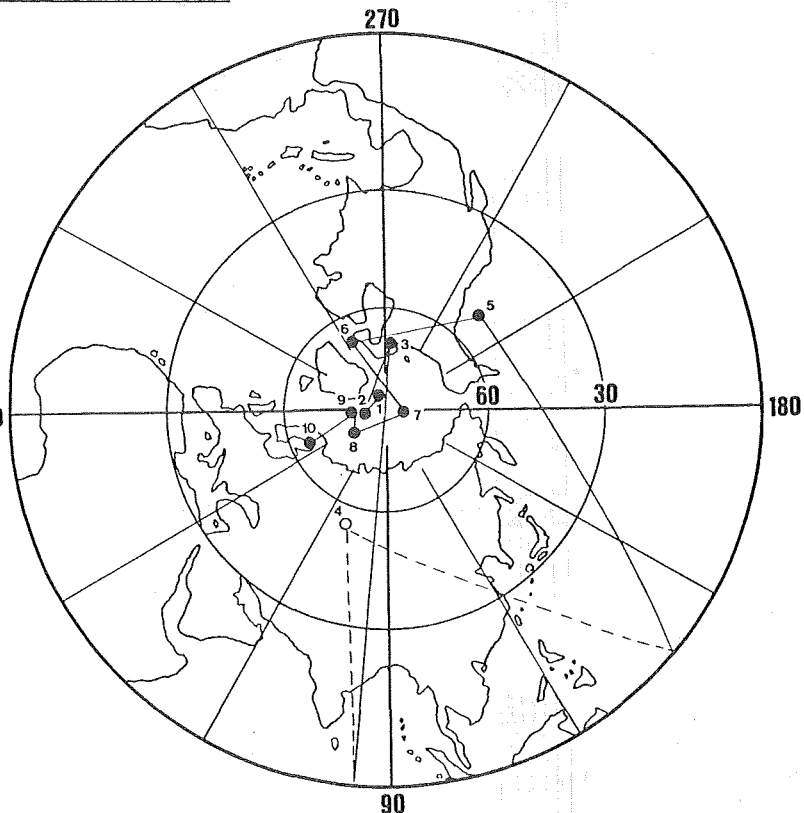


Fig. 9, Pole path during a geomagnetic field reversal at Blake event.

Hirooka (1977) suggested that the VGP during a reversal of geomagnetic field in late Pleistocene have a tendency of grouping in low latitude of Indian Ocean, Europe, and middle to east of Pacific Ocean. This is not contradict to the present data.

References

- An, Z. and L. Wei (1980) *Acta Pedologica Sinica*, 17, 1.
 Barbour, G.B. and M.L. Pien (1930) *Bull. Geol. Soc. China*, 9, 361.
 Cao, J.X. (1959) *Quaternaria Sinica*, 2, 60.
 Hirooka, K. (1977) *Japan Quaternary Res.*, 16, 105.
 Jia, L., C. Zhang and J. Wei (1976) *Acta Geographica*, 1.
 Lebedenskii, B.I. (1958) *Datong Volcanic Group* (Science Publisher, Peking), 80.
 Li, H., Y. Mei, J. Sun and F. Ji (1981) *Seismology and Geology*, 3, 20.
 Teilhard de Chardin P. and Z. Yang (1931) *Acta Geologica*, 8.
 Wang, N. and Y. Ou (1958) *Quaternaria Sinica*, 1, 174.
 Yang, J. (1961) *Science Rep. Peking Univ.*, 7.
 Yin, Z. (1932) *Bull. Geol. Soc. China*, 12, 355.
 Yin, Z. (1976) *Culture*, 2, 51.
 Zhou, K., C. Liu, B. Yuan and J. Sun (1982) in preparation.

PALEOMAGNETISM OF THE SHIMOKURA DIKE SWARM, NORTHEAST JAPAN
- AN ESTIMATION OF THE ACTIVITY DURATION OF A DIKE SWARM -

Kosuke HEKI and Hideo TSUNAKAWA

Geophysical Institute, University of Tokyo, Bunkyo-ku, Tokyo 113.

Introduction

In the last two years, many dikes were sampled by one of the authors with the purpose of reconstructing the ancient stress field in Japan. It is quite important to reveal the duration of the activity of dike swarms in which they reflect the regional stress field. In June 1980, paleomagnetic samples were taken from 19 dikes of the Shimokura dike swarm, Miyagi prefecture, Northeast Japan, in order to get an estimate on the length of the time span covered by this dike swarm. Paleomagnetic records have been suggested to have some potential of giving a crude estimate of the duration of volcanism (e.g., Kono, 1973). For example, if paleomagnetic samples (i.e., spot readings of the ancient geomagnetic field) were from a short time span compared with the periods of the major spectrum of the geomagnetic secular variation, their directions of the remanent magnetization would yield relatively small angular dispersion due to their poor coverage over the periods of the secular variation. Paleomagnetic data whose time span is comparative to the periods of the secular variation would present relatively larger dispersion. If the samples are revealed to be of some mixed polarities, wider temporal coverage would be stringent.

Geological description of the samples and experimental procedures

Samples were taken from 19 basaltic andesite dikes which is a part of a dike swarm located at the mountainous region of Miyagi prefecture. This dike swarm comprises of more than one hundred dikes and is generally referred to as the Shimokura dike swarm. About 50 dike intrusions crop out along the stream-cut valley of the Okura River a little downstream from Okura dam (Fig.1), and paleomagnetic samples were taken from these exposures. Each dike ranges in width from 40cm to 10m and almost perpendicularly cuts the bedding plane of the tuffaceous host rocks. The bedding of the host rock which was dated as 10Ma by the fission track method is almost horizontal, which indicates that no structural corrections are required to the direction of the natural remanent magnetizations (NRM) of these dikes. The K-Ar dating results indicate these dike intrusions might take place about 8Ma ago.

Four independently oriented samples were taken from each dike using gasoline-powered drills and

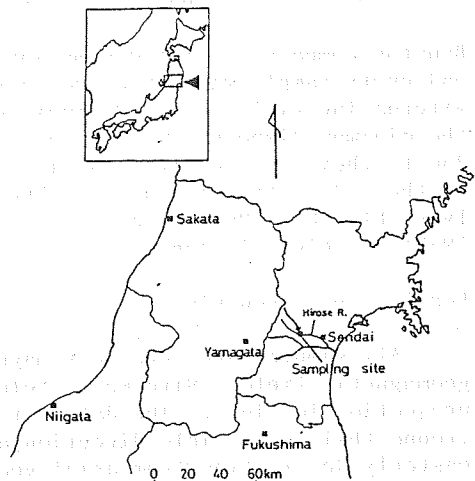


Fig. 1. Sampling site of the Shimokura dike swarm.

Table 1. Paleomagnetic results

Site	N	Incl.	Decl.	k	α_{95}	VGP Lat.	Long.	ODF
OK-1	4	-53.1°	157.9°	625	3.7°	-71.6°	222.9°	5mT
OK-2	4	-62.9	141.0	913	3.0	-60.4	255.1	10
OK-3	4	-66.2	148.6	1205	2.6	-65.2	265.4	5
OK-4	4	-70.8	142.1	333	5.0	-59.6	276.8	10
OK-3&4*	8	-68.5	145.7	356	2.9	-62.6	271.4	-
OK-5	4	-65.5	140.8	269	5.6	-60.2	261.8	15
OK-6	4	-72.2	150.8	399	4.6	-63.1	285.1	10
OK-7	4	-48.2	173.1	271	5.6	-79.3	175.0	5
OK-8	4	-46.7	163.5	38.9	14.9	-72.8	198.6	5
OK-9	4	-60.6	167.9	245	5.9	-80.2	254.0	10
OK-10	4	-64.7	161.4	265	5.7	-74.0	268.0	10
OK-11	4	-61.1	157.7	179	6.9	-72.6	250.6	10
OK-12	4	-75.7	156.0	212	6.3	-61.4	298.0	10
OK-13	4	-57.0	173.1	37.6	15.2	-84.5	225.4	10
OK-15	4	-61.2	177.9	63.0	11.7	-85.7	299.5	15
OK-16	4	-50.8	162.1	98.5	9.3	-73.9	211.2	15
OK-17	4	-73.8	195.5	412	4.5	-66.3	340.2	15

N: number of separately oriented samples, Incl.: inclination of site mean direction, Decl.: declination of site mean direction, k: within-site precision parameter, α_{95} : radius of 95% confidence circle about the mean direction, VGP Lat.: latitude of virtual geomagnetic pole (VGP), Long.: longitude of VGP, ODF: optimum demagnetizing field. *OK-3 and OK-4 are the samples from the same dike.

Brunton compasses. NRM was measured with Schonstedt spinner magnetometer and every sample was subjected to the stepwise demagnetization in alternating field (AF). Optimum demagnetizing steps were determined by the minimum dispersion criterion. Data for five dikes were discarded due to their unstabilities against AF-demagnetization and the largeness of their directional scatter. The other samples proved to have sufficiently stable NRM. Paleomagnetic results and statistical parameters (Fisher, 1953) are given in Table 1.

Results and discussion

All samples are reversely magnetized to the present direction of the geomagnetic field. Site mean field directions are shown on the equal area projection in Fig.2. The data set shows both pretty large dispersion around their mean field direction and slight systematic deviation toward easterly declination from axial geocentric dipole field direction expected in this region. Corresponding virtual geomagnetic poles (VGP) yield an angular standard deviation (ASD) around their mean VGP of $14.1^{\circ} \pm 4.6$ -2.7 .

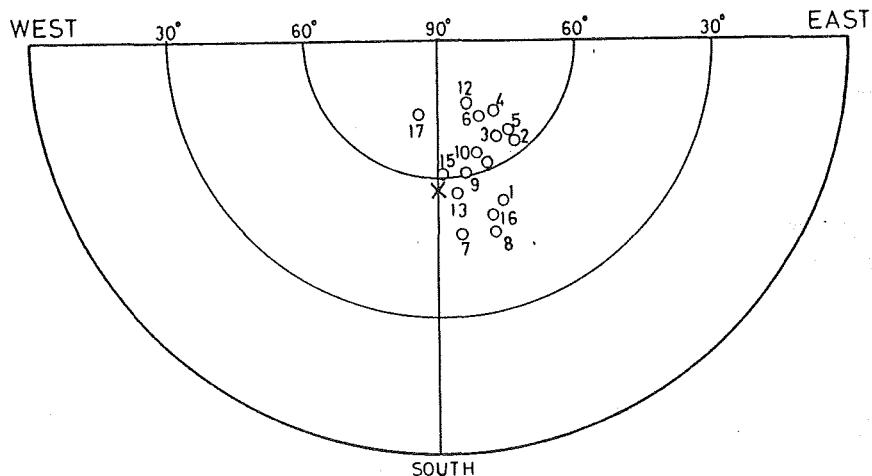


Fig. 2. Mean field direction for each dike. All directions are on the upper hemisphere. Attached numbers indicate the identification numbers of the dikes. × shows the axial geocentric dipole field direction expected in this region.

Its 95% confidence interval was calculated by interpolation from the table presented by Cox (1969).

The magnitude of the paleosecular variation (PSV), or the value of the ASD of VGP's is easily imagined to be in close relationship to the width of a time interval covered by the samples. It would be meaningful to collect the paleomagnetic data sets in Japan and to compare their ASD magnitude among the VGP sets which cover different time spans. The ASD of VGP's are illustrated with their 95% confidence limits as a function of their time spans (Fig. 3). As can be immediately noticed, VGP sets of short time spans (say, less than ten thousand years) such as the archeomagnetic data over the last 2,000 years (Hirooka, 1971), and over the last 10,000 years (Ozima and Aoki, 1972) show relatively small values of ASD. ASD reaches about $14^{\circ}\sim 15^{\circ}$ and keeps nearly constant after the time span comes up to a few tens of thousands of years and marked increase does not appear for longer time spans as far as 10^6 years. It would be reasonable to consider the ASD of Higashi-Izu monogenetic volcano group and Kagoshima pyroclastic flow deposits (Heki, 1980), Hakone Old Somma (Nagata et al., 1963; some unpublished data), Usami volcano (Kono, 1968) and Japanese data compiled over Brunhes epoch (McElhinny and Merrill, 1975) almost equal within their errors. The value of $14^{\circ}\sim 15^{\circ}$ matches very well with the other data in the vicinity of latitude 35° in the worldwide summaries for the Brunhes epoch, presented by McElhinny and Merrill (1975). This suggests that the ASD value of $14^{\circ}\sim 15^{\circ}$ may represent the PSV in Japanese region (Fig. 4).

Ozima and Aoki (1972) suggested the existence of some effects that ASD tends to get large for the data of old ages due to the integrated effects of some inter-site tectonics. However, at least for Japanese data the ASD is almost constant for the time span between 4×10^4 and 10^6 years and the inter-site tectonic movements as the cause of larger ASDs for older data are not needed in interpreting the PSV in this time range, although such effects may certainly exist to some extent.

Between-site ASD of the Shimokura dike swarm is $14.1^{\circ+4.6}_{-2.7}$, which can be included in the group of the VGP sets whose ASDs are thought to have the representative value for Japanese region. Following suggestion is derived accordingly that the time span covered by the Shimokura dike

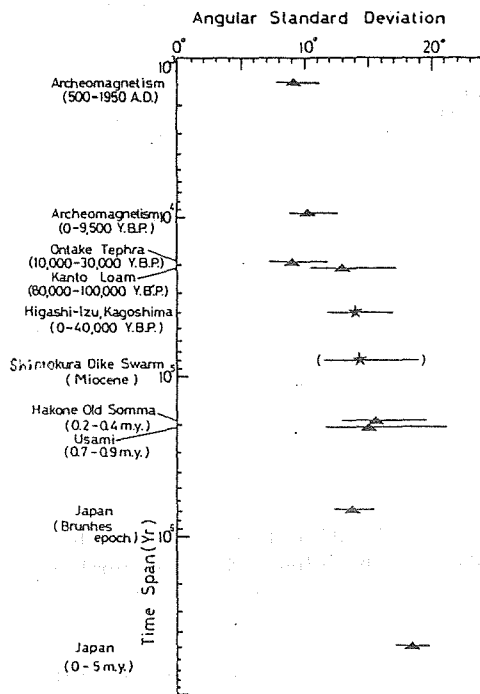


Fig. 3. Variation of ASD of VGP sets with their time spans in Japan. Error bars indicate 95% confidence intervals. The time span of the Shimokura dike swarm has not been accurately determined.

swarm may be at least longer than a few tens of thousands of years. On the other hand, the remanent magnetization of the entire samples taken from the Shimokura dike swarm shows reversed polarity. It is possible that these dikes intruded selectively in the time range when geomagnetic field had reversed polarity although the time span covered both several normal and reversed polarity intervals, but it would be more plausible that these dike intrusions occurred within a single polarity interval. This suggests that the time span would be shorter than the time constant of geomagnetic polarity transitions in the Late Cenozoic, say 10^6 years (e.g., McDougall, 1979).

There remains another problem on the deviation between the mean field direction of the Shimokura dike swarm and the axial geocentric dipole field expected at the sampling locality, that is, the declination of the Shimokura dike swarm show significant easterly shift as if there had occurred slight counterclockwise tectonic rotation about the vertical axis. There are two ways of the interpretation. The first interpretation is to attribute this shift to an actual regional tectonic rotation in a counterclockwise sense, but this should wait for some accumulation of other evidence to be justified. The second interpretation is to consider long-term nondipole field as is not to be averaged out even over the time span longer than a few tens of

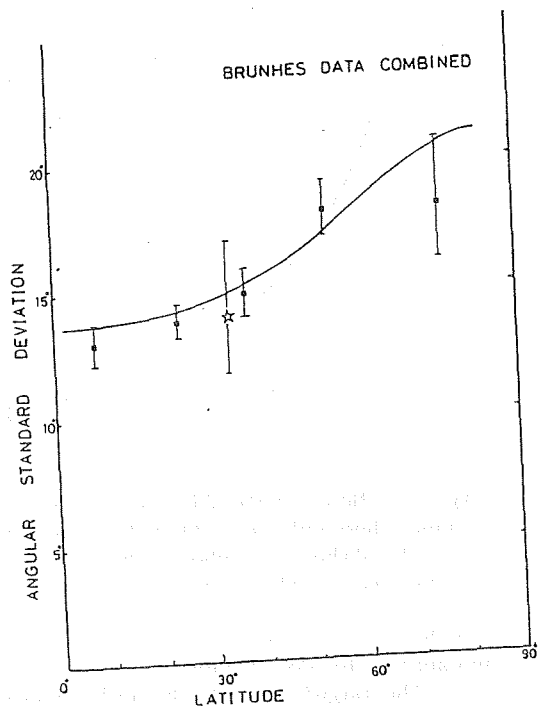


Fig. 4. Worldwide summarized ASDs of VGPs for Brunhes epoch found by averaging over 15° latitude strip by McElhinny and Merrill (1975). The star indicates the ASD of VGPs of Higashi-Izu monogenetic volcano group and Kagoshima pyroclastic flow deposits (Heki, 1980). Curve represents the latitude dependence of ASD expected from 11° of dipole wobble and the latitude variation of the ASD of the present nondipole field.

thousands of years. Such long-term nondipole components have been well investigated in the last decade (Wilson, 1971; Merrill and McElhinny, 1977; and many others). However, it is still difficult to discuss declination anomalies because of the shortness of the resolution of the ordinary paleomagnetic data. It should be noticed that even when such a long-term nondipole anomaly exists (in other words, even when true mean VGP does not coincide with the geographic pole), the ASD of VGPs becomes somewhat larger but never gets smaller, which means that the estimated lower limit of the activity duration of the dike swarm remains still reasonable. Anyway, it is fair to say it is premature to present any crucial interpretations upon this declination shift, but it does not affect the estimation of the activity duration of the Shimokura dike swarm.

References

- Cox, A. (1969) *Geophys. J. R. astr. Soc.*, 18, 545.
Fisher, R. A. (1953) *Proc. Roy. Soc., Ser. A*, 217, 295.
Heki, K. (1980) *Rock Mag. Paleogeophys.*, 7, 72.
Hirooka, K. (1971) *Mem. Fac. Sci. Kyoto Univ., Ser. Geol. Mineral.*, 38, 167.
Hirooka, K., C. Tobita, T. Yokoyama, and S. Nakaya (1977a) *Rock mag. Paleogeophys.*, 4, 81.
Hirooka, K., S. Sakai, and T. Yokoyama (1977b) *Rock mag. Paleogeophys.*, 4, 88.
Kono, M. (1968) *J. Geomag. Geoelectr.*, 20, 353.
Kono, M. (1973) *J. Geophys. Res.*, 78, 5972.
McDougall, I. (1979) *The Earth, Its origin, structure and evolution*, edited by M. W. McElhinny (Academic Press, London) p. 543.
McElhinny, M. W. and R. T. Merrill (1975) *Rev. Geophys. Space Phys.*, 13, 687.
Merrill, R. T. and M. W. McElhinny (1977) *Rev. Geophys. Space Phys.*, 15, 309.
Ozima, M. and Y. Aoki (1972) *J. Geomag. Geoelectr.*, 24, 471.
Wilson, R. L. (1971) *Geophys. J. R. astr. Soc.*, 22, 491.

PALEOMAGNETISM AND FISSION TRACK AGE OF THE MIOCENE VOLCANIC
ROCKS FROM OKUTANGO PENINSULA, JAPAN

Tadashi NAKAJIMA and Yuichiro MORIMOTO*

Geological Laboratory, Faculty of Education, Fukui University,
Bunkyo, Fukui 910, Japan

In order to clarify the stratigraphic correlation of Miocene formations of Hokuriku Sedimentary Basin belonging to the so-called "Green-tuff" region, we continue paleomagnetic investigation and fission track (FT) age determination in the region.

Miocene volcanic rocks related to the "Green-tuff" volcanism are widely distributed in Okutango Peninsula, Kyoto Prefecture. The volcanostratigraphy of this area has been described in detail by Ikebe et al. (1965) and Azuma (1977). In this note will be given the preliminary results of the paleomagnetic measurement and the FT age determination of the Miocene volcanic rocks.

Fission Track Age

The Miocene Hokutan Group in Okutango Peninsula is subdivided

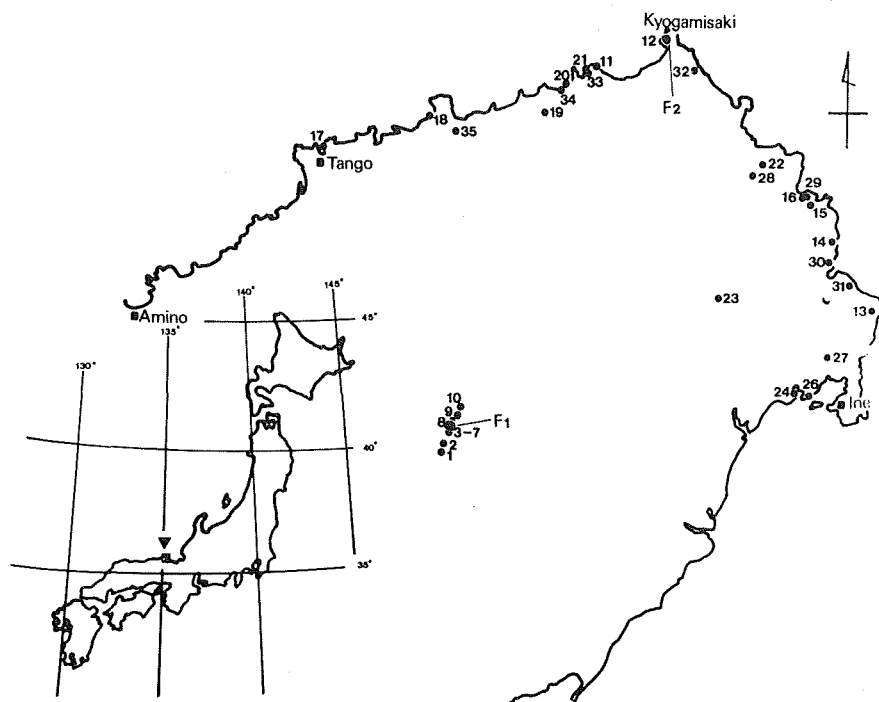


Fig. 1 Sampling locality.
1 - 35; paleomagnetism
F1 and F2; Fission track dating

Table 1 Stratigraphic Sequences of Sampling Site.

HOKUTAN GROUP

(Upper Miocene)

Tango Formation

Kyogamisaki andesites	S12, S32	F2 (10.2 Ma)
Taiza basalts	S17	
Norihara dacites	S18, S35	
Sodeshi dacites	S11	
(Owa andesites	S21, S33	
Nakahama andesites	S20, S34	
Honjyohama andesites	S14, S15, S16, S22 S28, S29	

(Middle Miocene)

Amino Formation

Choen ss. & sh.		
Honzaka rhyolites	S19, S30	

Toyooka Formation

Sugano andesites	S19, S30	
Takine cg./Hide rhyolites	S24, S26	
Oshima ss. & cg.		
Matsuo cg.		

(Lower Miocene)

Seya Formation

Kigo tuffite		F1 (15.8 Ma)
Uchiyama cg.		

Yoka Formation

Horikoshi andesites	S2, S3, S4, S5, S6, S7	
Hata andesites	S1	
Noma andesites	S8, S9, S10	

Takayanagi Formation

Torakuji cg. & SS.

Stratigraphy of the Hokutan group	Paleomagnetic Sampling Site	FT Sampling Site
--------------------------------------	--------------------------------	---------------------

into six formations, namely, the Takayanagi, the Yoka, the Seya, the Toyooka, the Amino and the Tango Formations in ascending order as shown in Table 1 (Ikebe et al., 1965; Azuma, 1977).

Kigo tuffites (F1) in the Seya Formation (lower Miocene) and Kyogamisaki andesites (F2) in the Tango Formation (upper Miocene) were dated 15.8 Ma and 10.2 Ma by the FT method. F1 and F2 in Fig. 1 show the sampling localities, at Yoshizu, Yaei-cho and at Kyogamisaki, Tango-cho, respectively. The FT ages were determined by the grain-by-grain method on zircon crystals separated from the tuffite and the andesite samples. Detailed description of the dating method can be referred to the paper by Yokoyama et al. (1980).

Zircon crystals were separated from the rock samples by the standard method with heavy solution and isodynamic separator. Zircons were etched for 5 hours in a mixture of 52 % HF and 98 % H₂SO₄ in a volume ratio of 1 : 1 at 185 ± 5 °C in a teflon capsule within a screw type stainless container (Nishimura and Yokoyama, 1975). For the reactor run, the zircons were packed in polycarbonate sheet and irradiated in KUR-1 reactor of Kyoto university. Neutron flux was also obtained by the fission track method (Hashimoto et al., 1969).

The results of the FT dating are listed in Table 2. We used $7.03 \times 10^{-7} \text{ y}^{-1}$ for the decay constant of the spontaneous fission of ²³⁸U (Fleischer et al., 1975).

Table 2 Results of Fission Track Age Determination.

F1	Yoshizu	1.08×10^6	4.28×10^6	1.05 (± 3.5 %)	15.8 ± 4.1
F2	Kyogamisaki	1.02×10^5	6.27×10^5	"	10.2 ± 1.2

Site	Spontaneous FT Density (cm ⁻²)	Induced FT Density (cm ⁻²)	Neutron Dose ($\times 10^{15}$ cm ⁻²)	Age (Ma)
------	--	--	--	------------

The obtained ages are consistent with the stratigraphic relation of the Hokutan Group.

Miura (1979) correlated the Yoka and the Seya Formations with the lower Miocene Ito-o Formation of Niu Mountainland in Fukui Prefecture. The Nunogataki and the Sasagawa volcanic members of the Ito-o Formation had been dated 16 Ma and 18.6 Ma, respectively, by the FT method (Hirooka et al., 1972). The Nunogataki member is correlated to the Seya Formation of the Hokutan Group, and the FT ages of both formations agree with each other. The Sasagawa member which is correlated to the Yoka Formation is the lowest member of the Ito-o Formation.

The period of volcanic activity in the Hokutan Group is considered to be within the time between 10 Ma to 19 Ma by comparing the FT ages with the stratigraphic correlation between the Hokutan Group and the Ito-o Formation.

Paleomagnetism

About 350 oriented samples were collected from 35 sites as shown in Fig. 1. Stratigraphic relations of sampling sites are shown in Table 1. The NRM direction of the samples was measured by means of an astatic magnetometer. After the measurement of NRM, each sample was demagnetized in alternating field (AF) in steps with peak field values of 50, 100, 200, 300, and 400 Oe. Stable component direction of the NRM was determined as the mean direction of magnetization at the AF demagnetization stage where the angular dispersion (α_{95}) was the smallest. If the α_{95} was larger than 20° at the best convergence, the unit was classified as unstable and paleomagnetic results were not considered. The stable directions to the AF demagnetization are obtained from only 14 sites in Okutango Peninsula. The data of the stable direction are listed in table 3.

The stable direction of NRM of each volcanic member and the mean direction of them are plotted in Fig. 2. The two intermediate directions of Noma andesites were excluded from the calculation of the mean direction. The mean direction ($D=10.7^\circ W, I=50.7^\circ$) lies nearly close to the direction of the geocentric axial dipole field ($D=0^\circ, I=55.1^\circ$) within the limit of the error angle ($\alpha_{95}=19.8^\circ$).

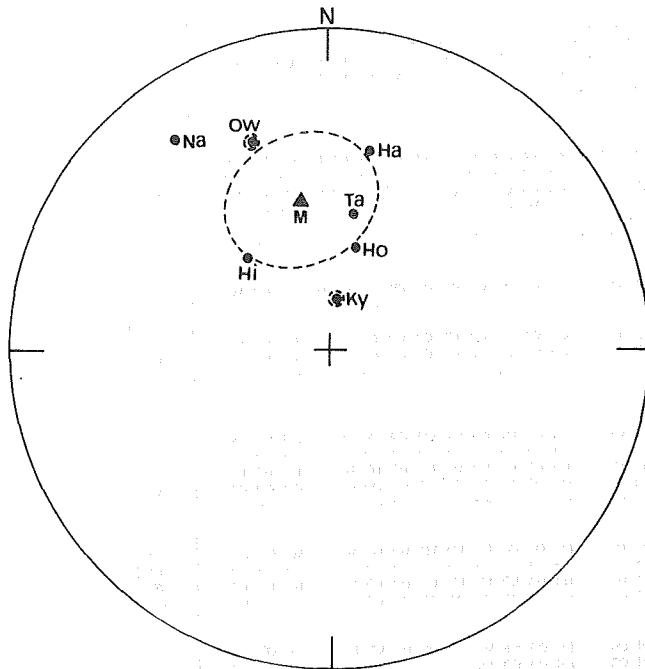


Fig. 2 The direction of NRM plotted on Schmidt equal area projection.
Ky; Kyogamisaki (south seeking pole)
Ta; Taiza Ow; Owa (South seeking pole)
Na; Nakahama Hi; Hide Ho; Horikoshi
Ha; Hata M; Mean

Table 3 Results of Paleomagnetic Measurement.

Kyogamisaki	S12	35.8	135.2	100	8	159.2	-74.9	6.0	85.4	400	-60.9	294.9
	S32	35.8	135.2	100	9	-141.1	-75.7	6.4	65.9	400	-53.9	344.1
	(Mean)				2	-171.8	-77.1	32.2	62.2			
Taiza	S17	35.7	135.1	100	6	10.4	54.1	2.2	959.3	>400	81.4	229.2
Owa	S33	35.8	135.2	200	6	160.4	-30.7	4.9	186.7	200	64.0	182.4
Nakahama	S34	35.8	135.2	200	8	-36.1	19.8	3.9	207.9	150	48.5	16.2
Hide	S26	35.7	135.3	100	6	-41.3	58.1	14.4	22.6	250	57.3	63.3
Horikoshi	S 3	35.6	135.2	200	8	33.8	42.7	19.3	9.2	100	59.0	236.3
	S 4	35.6	135.2	100	8	28.4	69.5	4.1	185.2	150	63.4	174.7
	S 5	35.6	135.2	200	9	3.4	69.1	3.7	193.6	300	72.8	142.4
	S 6	35.6	135.2	100	10	0.1	62.4	6.6	55.1	150	81.9	135.8
	S 7	35.6	135.2	100	8	2.6	65.2	4.7	141.1	200	78.2	144.0
	(Mean)				5	15.9	62.7	13.0	35.8			
Hata	S 1	35.6	135.1	100	7	12.0	36.4	7.1	74.1	350	71.3	277.5
Noma	S 8	35.7	135.2	100	5	-129.6	55.9	11.7	43.5	250	-4.3	96.6
	S10	35.7	135.2	50	6	6.2	-10.2	7.7	76.9	100	48.8	305.8

Site	Lat. (°N)	Lon. (°E)	AF (Oe)	N	D (°E)	I (°)	α_{95} (°)	k	MDF (Oe)	VGP	
										Lat. (°N)	Lon. (°E)

However, this mean direction is significantly different from those of the Cretaceous ($D=56.9^{\circ}E$, $I=61.6^{\circ}$) and the Paleogene ($D=41.3^{\circ}E$, $I=51.1^{\circ}$) of Southwest Japan compiled by Sasajima (1980). The northeasterly declinations which are characteristic of the paleomagnetic directions from Southwest Japan may suggest the clockwise rotation of Southwest Japan as proposed by Sasajima (1980). By comparing the paleomagnetic data from Southwest Japan with that from Korea, Otofujii and Matsuda (1981) concluded that the clockwise rotation of Southwest Japan began in a younger period than 33 Ma - 27 Ma. Although the amount of data is poor, the present results seem to suggest that the clockwise rotation had ended in a period of volcanic activity in the Hokutan Group (19 Ma - 10 Ma).

References

- Azuma, Y. (1977) *Kyoto Chigaku*, No. 6, 1 (in Japanese).
Fleischer, R.L. and R.M.Walker (1975) *Neuclear tracks in solid*, Calf. Univ. Press.
Hashimoto, T., S.Iwata, S.Nishimura, T.Nakanishi and M.Sakanoue (1969) Paper 9 th. Japan Con. Radioisotopes, 231 (in Japanese).
Hirooka, K., T.Okude and S.Nishimura (1972) *Mem. Fac. Educ. Fukui Univ.*, 22(II), 1 (in Japanese).
Ikebe, N., K.Wadatsumi and T.Matsumoto (1965) *Field Guide Book, Tajima-Tango*, 72 th. Conf. Geol. Soc. Japan (in Japanese).
Miura, S. (1979) *Mem. Geol. Soc. Japan*, No. 16, 149 (in Japanese).
Nishimura, S. and T.Yokoyama (1975) *Paleolimnol. Lake Biwa Japanese Pleistocene*, 3, 138.
Otofujii, Y. and T.Matsuda (1981) Paper 70 th. Conf. Soc. Terrestrial Mag. Electr. Japan, 175 (in Japanese).
Sasajima, S. (1980) *Paleoreconstruction of the continents geodynamics series*, 2, 115.
Yokoyama, T., T.Matsuda and K.Takemura (1980) *Quaternary Res.*, 19, 301 (in Japanese).

*Present address; Takefu-Daisan Junior High School, Murakuni, Takefu, Fukui 915, Japan.

PALEOMAGNETISM OF THE SHIDARA DIKE SWARM, CENTRAL JAPAN
- AN ESTIMATION OF PALEOINTENSITY IN MIOCENE -

Toshiyuki TOSHA and Hideo TSUNAKAWA

Geophysical Institute, Faculty of Science, University of Tokyo
Bunkyo-ku, Tokyo 113

Introduction

Igneous rocks have stable remanence and acquired the magnetic moment in proportion to the geomagnetic field during their cooling. Since these remanences are usually intensive and undisturbable by some later tectonic processes, it is relatively easy for us to measure them in order to study the geomagnetic behaviour in the ancient age.

Dikes occur as a sheet of igneous rocks and may be intruded in the relatively short period. We can possibly obtain a lot of samples in the narrow region that are sufficient to average out the secular variation.

There are abundant studies which have provided the evidence of generally small intensity during the polarity change of geomagnetic field. (e.g. Hillhouse and Cox, 1976). They showed that a substantial decrease, perhaps to about 10% of the initial field intensity, took place. However, for the most part these conclusions were derived from the magnetization change of the sedimentary rocks. In contrast to the studies which reported the small field intensity during the transition time, another determination have attracted the attention that the strong field have been recorded by lava flows. (e.g. Shaw, 1977). The anomalously strong field have been also reported using baked clay of prehistoric aboriginal fireplace. (Barbetti and McElhinny, 1976). Fuller et al. (1979) suggested that although high intensities of geomagnetic field might be a common, they only exist for the short period within the transition stage.

This paper is a preliminary report of paleomagnetism and paleointensity estimate using the dike swarm.

Geological setting

The Shidara Basin is located in the central Japan. (Fig.1). There are more than 400 dikes which are separated into two major dike swarms. One of the dikes swarm is located in the western part of the Shidara Basin and the other in the eastern. We have carried out the paleomagnetism of the eastern dike swarm.

These dikes dip almost vertically with a strike from N-S to NE-SW. Their strikes are dominated by the N 20°E-trend. Dikes are mostly composed of the alkaline basalts, which have followed the pyroclastic effusion. Corn sheet are found in this region. It might be originated from the same magma source as that of the dike intrusion.

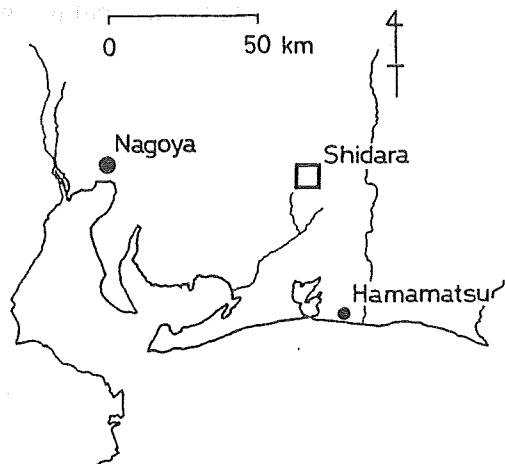


Fig.1. Sampling site of the Shidara dike swarm

Sampling and K-Ar dating

Samples were collected in March 1981 for paleomagnetic study and K-Ar dating. We collected more than four specimens from each of fifteen independent dikes by hand sampling or using a portable gasoline-powered drill. As there is no significant azimuthal error caused by a magnetized dike body, orientation was performed with magnetic compass. Overall orientation errors are estimated to be within 3° for the cores and within 10° for the hand samples. The declination of the present geomagnetic field is $N 6^\circ 10' W$. All the azimuthal angles of the paleomagnetic results have been corrected with this value.

K-Ar dating analysis in the whole rock sample of SDA 09 yielded the age of 15.1 ± 0.5 Ma. Fission track age obtained for the pyroclastic rocks has been reported as that of 16 Ma. (from the data compiled by Kaneoka and Ozima, 1970).

Thermomagnetic analysis

We examined thermomagnetic behavior of magnetic minerals in some specimens. Strong-field magnetization (J_s) versus temperature (T) was measured in a vacuum of about 5×10^{-3} Pa with an automatic recording balance in a field of 3.69×10^5 A/m. Fig. 2 shows an example of the J_s - T curve for the specimen of SDA 09-11. In Fig. 2, we can recognize a slight irreversible change due to heating. The Curie temperature of this specimen can be considered to that of magnetite during heating process, while it decreased during cooling. This difference may be explained by the reduction of slightly oxidized titanomagnetite.

From the thermomagnetic analysis, magnetic minerals of this dike is suggested to have been exposed initially to the high-temperature oxidization and to show no negative feature for the paleointensity measurement. (e.g. Smith, 1967).

Paleomagnetic measurement

The remanence and the anisotropy of susceptibility were measured by a Schonstedt Spinner magnetometer with six-spin. Measurements of low field susceptibility were carried out a Bison susceptibility bridge.

Each specimen was subjected to alternating field demagnetization up to, usually, 50 mT in a step of 5 mT. A typical example of demagnetization curve is given in Fig. 3. (Zijderveld, 1967). We calculated the precision parameter of Fisher's statistics (k) for four specimens at each AF step. The mean direction of each site was determined from the maximum value of k . The specimens whose value of k was smaller than 30 were rejected as inconsistency among one site. Six out of fifteen results were rejected in this reason.

Murthy et al. (1980) reported dual magnetic behaviour in intrusive rocks. The specimens by which the reliable results were obtained, however,

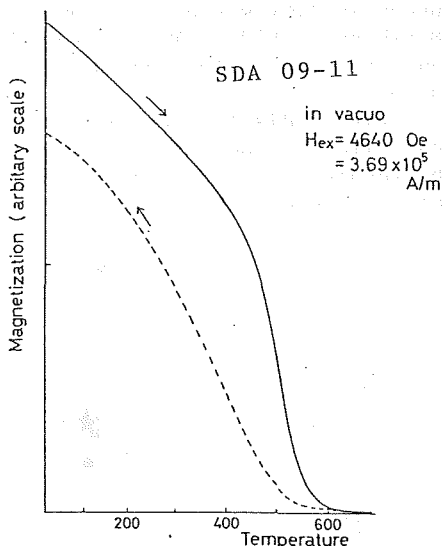


Fig. 2. A typical example of J_s - T curve from the site SDA 09

did not show such a behaviour.

Direction of NRM

The direction of the axis of maximum susceptibility lies down the line from N-S to NE-SW. This direction is said to be caused by the elongation of major magnetic grains, so this trend may explained by the reflection of magma flow. (e.g. Thorning and Abrahamsen, 1980). However more data are needed to conclude the relationship between magma flow and the direction of the axis of maximum susceptibility in the Shidara dike swarm.

As the degree of anisotropy (k_{max}/k_{min}) was less than 1.23, the direction error caused by the anisotropy of susceptibility was no more than 6.3° . (McElhinny, 1973). It is no significant error for paleomagnetic investigation.

Fig. 4 displays the AF-cleaned mean direction and Table 1 summarizes the results of paleomagnetic measurements for each dike.

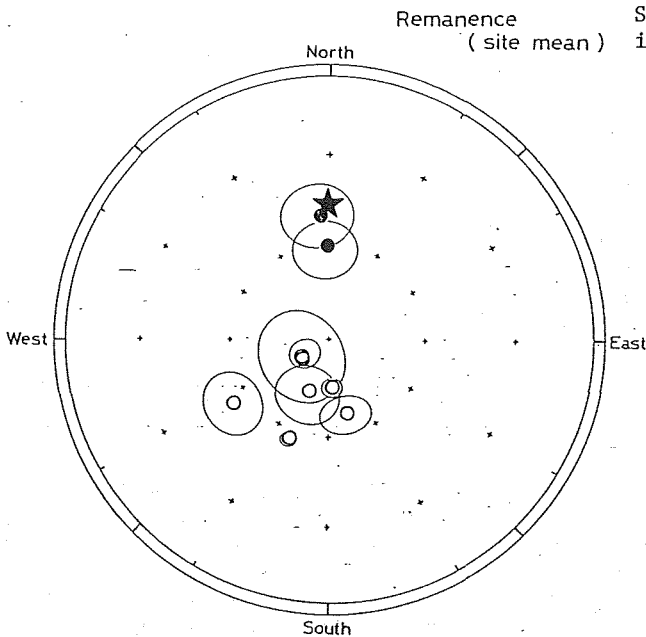


Fig. 4. Site mean direction of AF-cleaned NRM. 95% confidence ovals for individual mean directions are shown as solid lines. Open (solid) symbols indicate negative (positive) inclinations. The star symbol indicates the axial dipole field direction (0° , 49.2°) at the location

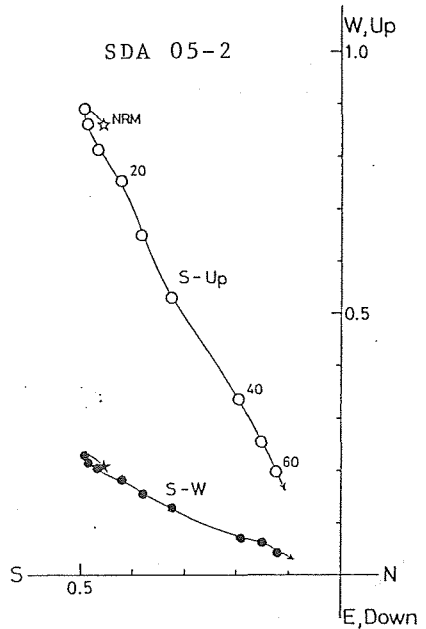


Fig. 3. Variation of direction for the specimens SDA 05-2 during demagnetization. Unit; mT

Dike No.	Inc(°)	Dec(°)	k	α_{95}	ODF(mT)
SDA 01	51.0	354.3	75	10.7	5
SDA 02	-74.9	177.3	719	3.5	50
SDA 03	-71.5	201.2	79	10.4	35
SDA 04	-54.1	234.3	90	9.8	15
SDA 05	-56.7	201.8	1515	2.4	15
SDA 06	61.6	257.4	92	10.0	15
SDA 07	-66.2	167.9	154	7.4	5
SDA 08	-80.8	233.3	40	14.7	10
SDA 09	-80.0	233.8	511	5.5	17.5
present	48.1	353.9			

Table 1. Summary of the paleomagnetic data. Inc,Dec; site mean inclination and declination k, α_{95} ; precision parameter and semiaxis of the 95 % cone of confidence ODF; optimum demagnetization field The direction of present geomagnetic field is also shown in the last line.

The observed directions can be divided into two groups. One group has the normal polarity and the other reversed one. The mean field direction with normal polarity were close to that of Geocentric Axial dipole expected in this region. Some of the dikes with reversed magnetization showed the relatively steep inclination and the westward declination. Considering that dike system might be intruded within relatively short interval, the remanences of these dikes might reflect the transition or excursion of the geomagnetic field.

The rocks which showed normal polarity are porphyritic basalts while the others are aphyric ones. Therefore it is possible to consider that magnetic polarity change occurred at the slightly different stages of the volcanism.

It is worth while examining the paleointensity in the intermediate interval using the Shidara dike swarm.

Paleointensity measurement

Five specimens selected from two sites have been performed. Two of the five specimens are normally magnetized and the other three have recorded in the intermediate geomagnetic field. Paleointensity measurement was carried out by the Thelliers' method of double heating. The results are shown in the form of Arai diagram in Fig. 5. (Nagata et al., 1963). The criteria used on this study in drawing a straight line were similar to those used by Kono (1974).

We obtained no reliable paleointensity estimates from normally magnetized specimens. There are a few adopted points in succeeded specimens. It is one of the reason because they have very sharp magnetic blocking temperature spectra, so it is difficult to control the step-wise temperature. The intensity of NRM component suddenly decrease at the temperature up to 330°C, while it is difficult to predict such sudden reduction. The directions of NRM component, however, did not move so much when experiments going on.

The convex shape at the low temperature is the effect of removing the

VRM component, as is common to the reversally magnetized specimens. (Coe, 1967). Carrying out the reversed magnetized specimens, one may use some technique to cancel out this superposed VRM which masks the properties of low temperature component. One possibility is the AFD. However, until now there is a negative result that AFD destroys the primary information specimens originally has. (Levi, 1975).

Calculated magnetic field intensity and vertical dipole moment are shown in Table 2, where the geomagnetic moment was deduced to about one-third compared to the present one.

The intensity in Miocene transition field recorded in a sequence of the basaltic lavas in southeastern Oregon (15.1±0.3 Ma) was investigated by Goldstein et al. (1969). They showed that polarity change of geomagnetic field occurred in this age and the intensity in the normal field was as large as that of present, while it decreased in the transition stage. Their data are, to some degree, compatible with ours. It is suggested that there were no metastable stage proposed by Fuller et al. (1979) when the intensity of magnetic dipole became larger in Miocene transition stage. However they performed the estimation using the van-Zijl method modified by themselves. The age of K-Ar dating becomes older because of the change of the time-decay constant of K. The field transition which they observed might be the different one which we did.

More specimens are available for us, so much more experiments are needed to obtain the behaviour of geomagnetic moment in the transition interval in Miocene.

Specimen No.	N	T ₁	T ₂	-r	F (×10 ⁻⁴ T)	VDM(×10 ²² Am ²)
SDA 09-5	5	330	460	0.98	0.25 ± 0.03	
SDA 09-6	5	330	460	0.99	0.24 ± 0.02	
SDA 09-7	5	330	460	0.99	0.26 ± 0.02	
mean		(Inclination= -80.0)			0.25 ± 0.04	3.4 ± 0.4
present		(Inclination= 48.1)			0.46	8.0

Table 2. Successful results of paleointensity experiments T₁, T₂; temperature interval (°C) in which linear relation is obtained in NRM-TRM diagram N; number of points in this interval r; correlation coefficient of the regression line F; paleointensity and its standard error VDM; virtual dipole moment calculated from the formula $VDM = \frac{1}{2} Fa^3(1+\cos^2 I)^{1/2}$ where a is the Earth's radius, I the inclination of the site

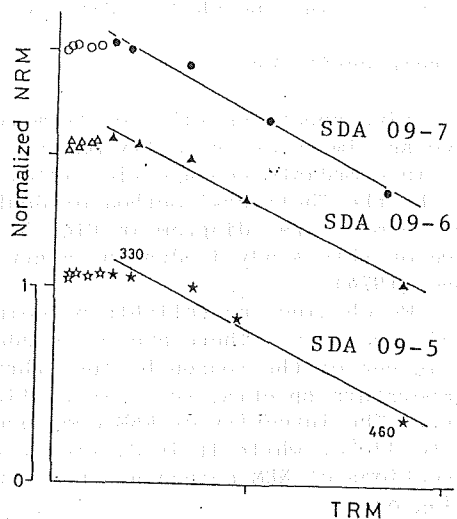


Fig. 5. Successful results of paleointensity experiments shown in Arai diagram. Regression lines were determined from the solid symbols in the temperature interval (°C) indicated by the small numerals.

References

- Barbetti, M.F. and M.W. McElhinny (1976) *Phil.Trans. R. Soc. Lond.*, A281, 515.
- Coe, R.S. (1967) *J.Geomag.Geolectr.*, 19, 157.
- Fuller, M., I. Williams, and K.A. Hoffman (1979) *Rev.Geophys.Space Phys.*, 17, 179.
- Goldstein, M.A., D.W. Strangway, and E.E. Larson (1969) *Earth Planet.Sci.Lett.*, 7, 231.
- Hillhouse, J. and A. Cox (1976) *Earth Planet.Sci.Lett.*, 29, 51.
- Kaneoka, I. and M. Ozima (1970) *Kazan*, 15, 10.
- Kono, M. (1974) *J.Geophys.Res.*, 79, 1135.
- Levi, S. (1975) *J.Geomag.Geolectr.*, 27, 245.
- McElhinny, M.W. (1973) *Paleomagnetism and plate tectonics*, (Cambridge University press, Cambridge), p.357.
- Murthy, G.S., R. Patzold, and C. Brown (1981) *Phys.Earth Planet.Inter.*, 26, 72.
- Nagata, T., Y. Arai, and K. Momose (1963) *J.Geophys Res.*, 68, 5277.
- Shaw, J. (1977) *Geophys.J.R.astr.Soc.*, 48, 263.
- Smith, P.J. (1967) *Geophys.J.R.astr.Soc.*, 12, 239.
- Theilner, E. and O. Theilner (1959) *Ann.Geophys.*, 15, 285.
- Thorning, L. and N. Abrahamsen (1980) *Geophys.J.R.astr.Soc.*, 60, 163.
- Zijderveld, J.D.A. (1967) *IN Method of paleomagnetism*, (Elsevier Publishing Co., Amsterdam), p.254.

Masayuki TORII*, Takaaki MATSUDA** and Shiro ISHIDA*

* Department of Geology and Mineralogy, Kyoto University, Kyoto 606

** Department of Geology, Himeji Institute of Technology, Himeji 671-22

Paleomagnetic study on samples from Miocene succession has been carried out in order to settle a magnetostratigraphy for the vertebrate fossil sites in the Kiriun area, on the northeastern flank of the Kenya Rift Valley (Fig. 1). The geology of this area has been studied by Shackleton (1946) and Ishida et al. (1981). The geologic succession of the Kiriun area is briefly outlined in ascending order as follows:

- (1) Sub-volcanic sediments (lacustrine and fluvial deposit) with intercalated fossil beds unconformably overlies the Precambrian gneiss.
- (2) An aphyric phonolite lava (a-p-l) is discovered to be cropping out only along the narrow gorge at the northeastern part of the Kiriun area. A whole rock K-Ar age of the lava was determined to be 11.4 ± 0.4 Ma (Ishida et al., 1981).
- (3) An aphyric phonolite lava (a-p-u) rests on the other strata which is correlative with the Shackleton's lower Rumuluti Phonolite. A K-Ar age of this rock was reported to be 12.3 ± 0.6 Ma[†] (Baker et al., 1971).
- (4) Uppermost porphyritic phonolite lava (p-p) which is characterized by prominent phenocrysts of anorthoclase and nepheline covers extensive area of this country. This is also correlative to the Shackleton's upper Rumuluti Phonolite, and a K-Ar age is 11.3 ± 0.6 Ma[†] (Baker et al., 1971).

† The ages cited in the text are recalculated by adopting the newly established decay constant and isotope abundance (Steiger and Jäger, 1977).

Volcanism of these plateau phonolites is thought to be a fissure eruption type at the early stage of the rift system (Baker et al., 1971).

Six to ten oriented hand samples were collected at each site; 25 sites from the phonolite lavas, 4 sites from the sediments, and 4 sites from the miscellaneous rock units. A few specimens from each site were firstly subjected to the progressive alternating field demagnetization (AFD) and/or the progressive thermal demagnetization (ThD). Experimental results of typical sites are illustrated in Fig. 2 and 3, including the results of progressive demagnetizations of pilot specimens, NRM directions of before and after partial AFD of the site, and thermomagnetic curves.

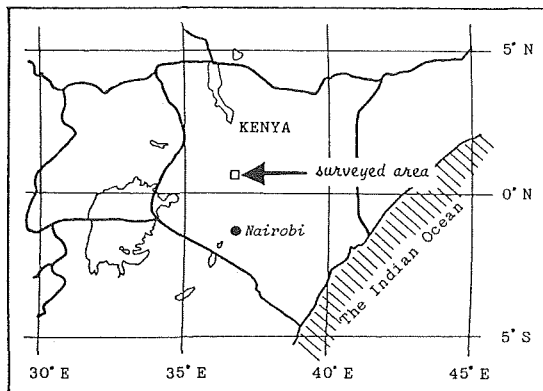


Fig. 1 Location of surveyed area.

Fig. 2 is the case of the successful measurements. A magnetic property of this type is found only in three sites among the total 33 sites. Such sites were situated on the upper surface of the lava plateau of p-p phonolite. As shown in Fig. 2 (a,b), the directions of the NRM show a tight cluster before and after AFD. Median destructive field (MDF) value is about 200 Oe in peak field. It is difficult

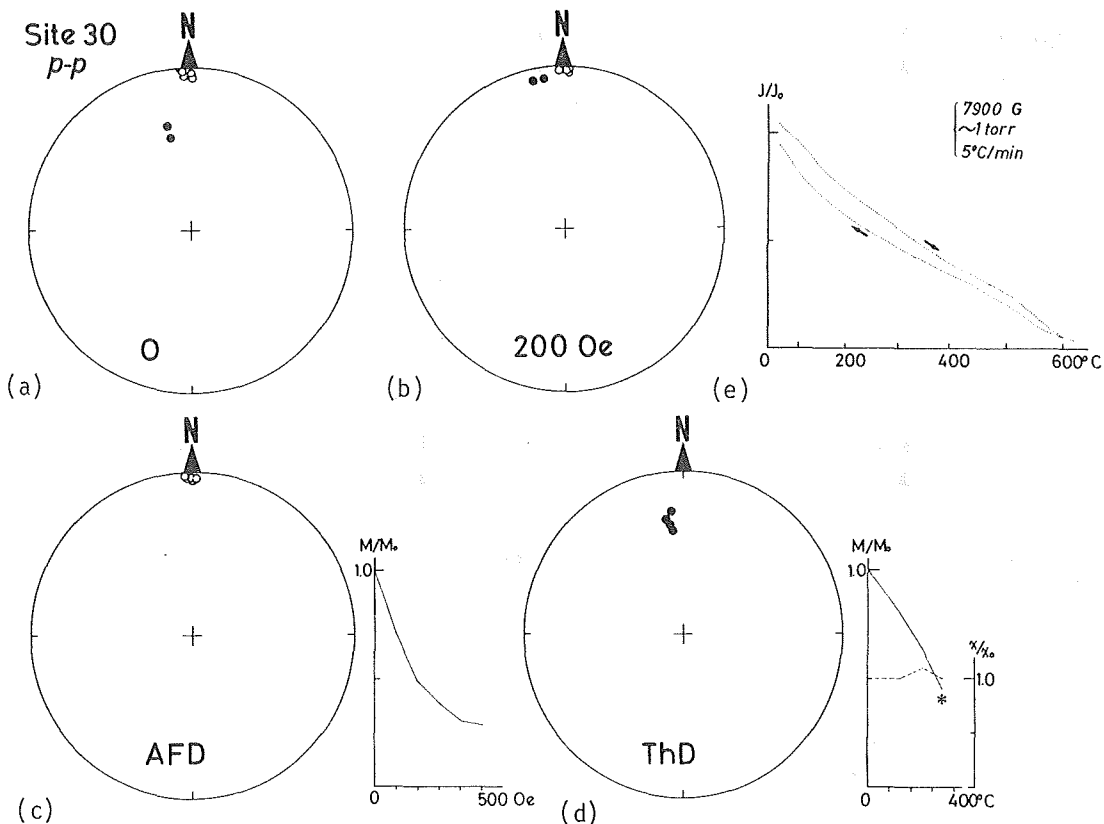


Fig. 2. Typical results of successful site. (a), NRM directions before demagnetization. (b), NRM directions after partial AFD of 200 Oe. (c), Change of direction and intensity of NRM by progressive AFD up to 500 Oe. (d), Change of direction, intensity (solid line), and initial susceptibility by progressive ThD up to 350°C. Asterisk on the curve of intensity indicates an explosion of specimen at 350°C. (e), Thermomagnetic curve of heating and cooling processes by an automatic recording balance. Vacuum within the furnace is controlled about an order of 1 torr.

to determine the blocking temperature by ThD because of an explosive nature of the rocks. More than 90% of the phonolite specimens have exploded itself on the course of ThD at the temperature around 300°C. After each ThD step, an initial susceptibility value (χ) was measured to detect the change of magnetic property of specimen caused by heating. There are no significant change of the χ value for this case. The cooling curve of thermomagnetic analysis approximately retraces the heating curve, and indicates a single Curie temperature (T_c) which is identical with that of magnetite. Under a microscopic observation of the polished surface, microphenocrysts of magnetite possessing ilmenite lamellae are visible. This fact suggests a high temperature oxidation occurred in situ. It is possibly interpreted that this type of rocks has been preserving primary NRM.

Fig. 3 shows the other type which represents the majority of the rest

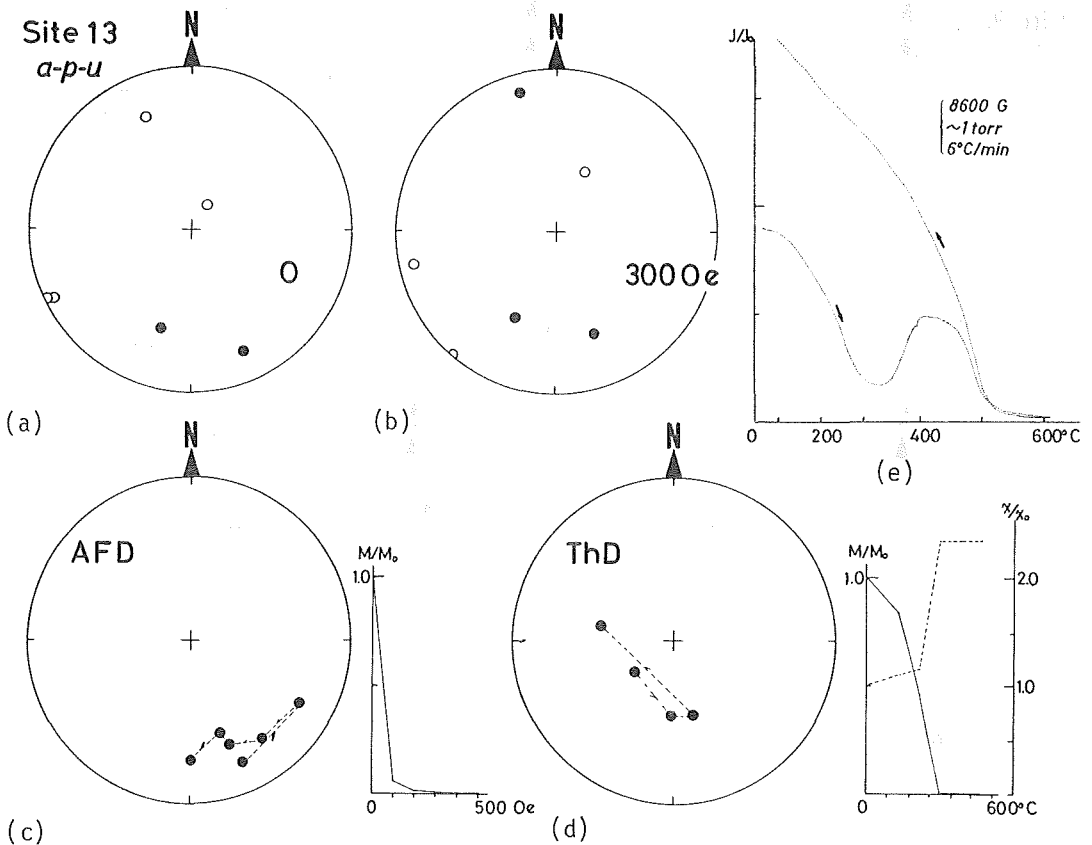


Fig. 3. Typical results of unsuccessful site. See Fig. 2 for explanation. An abrupt change of χ value by progressive ThD, and irreversibility of thermomagnetic curve are notable.

sites. Most of this type are not successful to give paleomagnetic data with a few exceptions. The result of progressive AFD of Fig. 3(c) shows a very low MDF value (~ 50 Oe), and random flips of remanent direction. It seems very difficult to find a stable end point of remanent vector before getting spurious magnetization by AFD. ThD is also not effective in removing secondary component. And an abrupt increase of χ value commonly occurs at the temperature higher than 250°C. Thermomagnetic curve of heating process shows that T_c is within range of 250°C to 350°C, and then there appears a hump around 400°C. Cooling curve is quite unlike with the heating curve. Intensity of magnetization recovers almost twice as large as the initial value. Such an irreversibility of the thermomagnetic curve may be caused by the high temperature oxidation of unoxidized titanomagnetite during the heating process of the experiment (Ozima and Larson, 1970), because our thermomagnetic balance could not attain enough vacuum to suppress an unexpected oxidation of the specimen within the furnace. Under reflective microscope, large opaque minerals with highly oxidized rim of pseudobrookite (partly rutile) are commonly observed. We could not find any ilmenite lamellae on such magnetic minerals. It may be supposed that the titanomagnetites of large grain size ($T_c \sim 300^\circ\text{C}$) are

only responsible to the NRM and also are the cause of instability mentioned above. These characters of instability have been also discussed by Grommé et al. (1970), and Patel and Gacii (1972) for the volcanic rocks of Tanzania and Kenya. For the case of titaniferous rock like a phonolite which had no chance of in situ oxidation, such an instability may be quite natural.

Table 1. Summary of paleomagnetic data of successful sites which have smaller α_{95} than 30° .

SITE	ROCK	Jst	N	D	I	A_{95}	k	AFD	VLAT	VLON	dp	dm
3	p-p	ir	6	144.8	-34.9	24.5	8.4	300 Oe	-50.9	157.2	16.3	28.3
8	p-p	r	4	-27.3	-16.8	26.7	12.8	400 Oe	61.2	287.3	14.2	27.6
26	p-p	ir	5	3.0	-1.0	28.4	8.2	200 Oe	86.8	149.3	14.2	28.4
28	p-p	r	5	-5.2	-8.3	21.5	13.6	200 Oe	82.9	263.2	10.9	21.7
30	p-p	r	5	-1.7	-0.6	5.5	194.3	200 Oe	88.0	275.9	2.8	5.5
12	a-p-l	ir	5	21.6	-1.3	13.7	32.2	200 Oe	68.3	131.0	6.9	13.7

Explanation: ROCK, rock type, see the text. Jst, r(ir), reversible(ir-reversible). N, number of specimens. D, declination. I, inclination. A_{95} and k, Fisher's statistical parameter. AFD, level of partial AFD. VLAT, latitude of VGP. VLON, longitude of VGP. dp and dm, error angles of VGP.

Paleomagnetic data of successful sites are listed in the Table 1. These sites are tentatively selected to have a smaller α_{95} than 30° . Only six sites can be approved by this rather loose criterion among 33 sites. Samples from the p-p phonolite show normal polarity except Site 3. This site is located on the top of isolated small hill which has been parted by dry valley from the main part of plateau phonolite. Though the rock from Site 3 is petrographically identical with the p-p phonolite, there remains a possibility of mis-correlation of rock.

VGPs of the six sites seem to be randomly distributed around the present geographical pole. Block (1981) has summarized paleomagnetic data from African Continent. He found that the most of Cenozoic VGPs were distributed closely around the present geographic pole. And he has also mentioned about the small but significant deviation of the VGPs from the present pole, which was firstly pointed out by Wilson (1970). Unfortunately, our data are too poor to make a discussion in detail, and further experiments of more sophisticated demagnetization are required.

References:

- Baker, B.H., L.A.J. Williams, J.A. Miller and F.J. Fitch (1971) *Tectonophys.*, 11, 191.
- Block, A. (1981) *Paleoreconstruction of the continents*, Geodynamic Ser., vol. 2, ed. by M.W. McElhinny and D.A. Valencio, ppl 77 (Agu, Washington, D. C. and GSA, Colorado) p. 65.
- Grommé, C.S., T.A. Reilly, A.E. Mussett and R.L. Hay (1970) *Geophys. J. Roy. astr. Soc.*, 22, 101.
- Ishida, S., M. Torii, T. Matsuda, K. Koizumi, Y. Kawamura, and H. Ishida (1981) in preparation
- Ozima, M and E.E. Larson (1970) *J. Geophys Res.*, 75, 1003.
- Patel, J.P. and P. Gacii (1972) *Earth Planet. Sci. Lett.*, 16, 213.
- Shackleton, R.M. (1946) *Geological Survey of Kenya*, Report No. 11.
- Steiger, R.H. and E. Jäger (1977) *Earth Planet. Sci. Lett.*, 36, 359.
- Wilson, R.L. (1970) *Geophys. J. Roy. astr. Soc.*, 19, 417.

A PROGRESS REPORT ON PALEOMAGNETIC STUDY ON CRETACEOUS ROCKS
OF WEST JAPAN.

Haruo DOMEN and Hiroshi MUNEOKA

Institute of Physical Sciences, Faculty of Education,
Yamaguchi University, 753 Japan.

In the area of the west end of Japanese Main Island, the Cretaceous rocks are widely distributed. One of the present authors (H.D.) has reported some results of the paleomagnetic works on these rocks previously (Domen 1966, 1971, 1975, 1979). Recently, several districts within Yamaguchi Prefecture and one district in Shimane Prefecture, west Japan were attacked and some tens of samples were collected from these respective district and the samples have now been submitted to the paleomagnetic study. Most of all samples collected were measured thier NRM up to the present day. And thier stability and Js-T analysis of the ferromagnetic rock forming minerals have now been examined.

Those localities are as follows;

1. Yamaguchi Prefecture.

1-1. Yoshimi district (Locality A in Fig. 1).

Rock type of this district submitted to this study is inkstone. Samples were taken from two separated sites; Kojuku and Kushimoto-zaki, near by Shimonoseki City. The Kojuku samples had once been sampled previously (Domen 1966, 1971, 1975, 1979).

1-2. Zuiko district (Loc. B).

Dioritic rocks were sampled at Zuiko district, Asa, Sanyo Township.

1-3. East-Atsu district (Loc. C).

Volcanic and/or tuff breccias were sampled at Yamanaka, East-Atsu, Mine City. Some samples were taken within a tunnel which is now under construction.

1-4. Misumi district (Loc. D).

Porphyritic and andesitic rocks were collected from Misumi district, Nagato City. Two sites closely located were attacked. One of these is the same site at where some rock samples were previously taken (Domen 1971, 1975, 1979), and the other site has newly excavated by the road construction after the former sampling mentioned above.

1-5. Taika-zan district (Loc. E).

At the skirt of small mountain, Taika-zan, vicinity of Tokuyama City, two sites are selected for the sampling. The rock samples from one of those are rather weakly magnetized so that the NRM is very difficult to be determined.

2. Shimane Prefecture.

2-1. Hikimi district (Loc. F).

Granodioritic rocks were collected from Hikimi district, Shimane Prefecture, near by the border to Yamaguchi Prefecture, several years ago and this time thier NRM was measured.

References;

- Domen, H. (1966) 1965 Annu. Prog. Rep. Rock Mag. Res. Group in Japan, 151.
---- (1971) Bull. Fa. Educ., Yamaguchi Univ., 19(Part 2), 27.
---- (1975) *ibid*, 25(2), 63.
---- (1979) *ibid*, 29(2), 11.

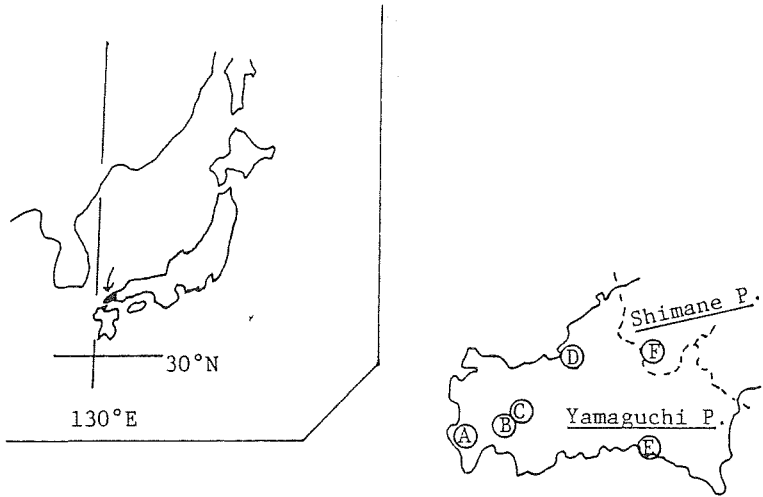


Fig. 1. Sampling localities of Cretaceous rocks, west Japan.

PALEOMAGNETIC RESULTS OF CRETACEOUS GRANITIC ROCKS
IN EASTERN CHUGOKU, SOUTHWEST JAPAN

Haruaki ITO, Katsuyasu TOKIEDA
and
Yukio NOTSU

(Department of Physics, Shimane University, Matsue 690)

1. Introduction

The Chugoku district of Southwest Japan is one of the sites of violent acidic igneous activity in the Japanese Islands during the late Cretaceous to Paleogene. K-Ar age data of granitic rocks in the Chugoku district suggest that the major igneous activities were in the range from 90 to 35 Ma (Nozawa, 1975; Shibata, 1979). K-Ar dates on granitic rocks exposed south of Tsuyama, Okayama Prefecture, have been obtained by Shibata (1979). The ages of Myoken-zan, Nibori and Tsuyama granitic masses range mainly from 80 to 76 Ma. On the other hand, the K-Ar ages of the Ibaragi complex by Shibata (1971) were 76 to 74 Ma and the Rb-Sr ages by Ishizaka (1971) were 83 to 76 Ma. Moreover, the available paleomagnetic data of the Ibaragi complex indicate that the complex has recorded both normal and reversed polarity and NRM directions of normal samples were significantly easterly (Ito and Tokieda, 1978).

Part of granitic rocks exposed in Yokota-cho, Mitoya-cho and Daito-cho, Shimane Prefecture, and Neu-cho and Misasa-cho, Tottori Prefecture, were reversely magnetized (Ito and Tokieda, 1972). K-Ar ages of these granitic rocks having reversed polarity fall within the range of 65-35 Ma (Nozawa, 1975). As a general rule, granitic masses in which the reversed NRM was partly observed would be expected to have both normal and reversed polarity in a single body, but it is not so easy to present abundant evidences to indicate that a granitic mass has recorded both normal and reversed magnetizations because we can seldom encounter with successive outcrops exposed over a few hundred meters within the mass.

The K-Ar ages of granitic rocks exposed south of Tsuyama are 80-76 Ma and correspond to those of the Ibaragi complex dated at 76-74 Ma by K-Ar method (Shibata, 1971) and 83-76 Ma by Rb-Sr method (Ishizaka, 1971) as mentioned above. This suggests that some of these granitic rocks have recorded both normal and reversed polarity in a single body or are reversely magnetized. The present investigation was undertaken to examine whether granitic complex and masses dated at 80-76 Ma have both normal and reversed polarity in a body and NRM directions of them are consistent with those of the Ibaragi complex or Cretaceous rocks in Southwest Japan.

2. Geological setting

Geological or petrological investigations in eastern Chugoku, Southwest Japan, have been reported by many workers. Granitic rocks exposed in the vicinity of Susai, Okayama Prefecture, have been investigated by Mitsuno and Omori (1965) or Shirakawa (1975). In this area, the largest mass is the Nibori granite with 10 km long and 7 km in width and the smallest one

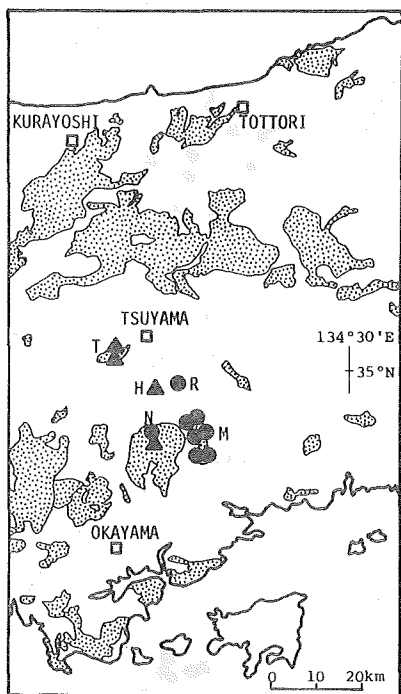


Fig. 1. Sampling sites and granitic rocks in eastern Chugoku. Dots represent stably magnetized sites and triangles represent unstably magnetized sites. H: Honzanji granodiorite, M: Myoken-zan granodioritic complex, N: Nibori granite, R: Renjaku quartzdiorite, T: Tsuyama granite.

in the seven. The sampling sites are three in the rock type (1), one in the rock type (3) and two in the rock type (7). One or two core samples with 2.5 cm in diameter and 2.4 cm long were drilled from a hand sample in the laboratory.

4. Results of measurements

The NRM of all core samples have been measured with a spinner magnetometer having a background noise of $<10^{-7}$ emu. Thermal demagnetization was done for a few core samples at each sampling site and the remaining core samples were subjected to stepwise alternating field demagnetization in order to get the stable component of magnetization. After demagnetization treatments, sites where samples with the stable and consistent NRM directions were taken are as follows: all sites in the Myoken-zan complex, one site in the Nibori mass and one site in the Renjaku mass. In the Myoken-zan complex, sites M-1, M-2 and M-3 were located in the rock type (1), site M-4 in the rock type (3) and sites M-5 and M-6 in the rock type (7).

is the Honzanji granodiorite with 1 km long and 0.5 km in width (Mitsuno and Omori, 1965). The Myoken-zan granodioritic complex is a small stock-like mass with 9 km long and 3 km in width according to Shirakawa (1975). It seems that the complex was formed by magmatic differentiation and emplaced at the shallow levels of the crust. The Myoken-zan complex is divided into seven rock types from the field occurrences and petrographic features, but it is apparently classified in two bodies of the north and south. Boundary between the seven rock types is generally sharp and the mode of occurrence of the rock types (1) to (5), which form the north body, is like a concentric ellipse.

3. Sampling

About one hundred eighty hand samples were collected from 12 sites of road cut or quarries in the Myoken-zan, Nibori, Renjaku, Honzanji and Tsuyama masses. Sampling sites are shown by numbered dots and triangles in Fig. 1. Oriented hand samples were taken from two sites in the Tsuyama granitic mass, two sites in the Nibori granitic mass and one site in the Honzanji granodioritic mass and Renjaku quartzdioritic mass. In the Myoken-zan complex, we collected hand samples only from three rock types

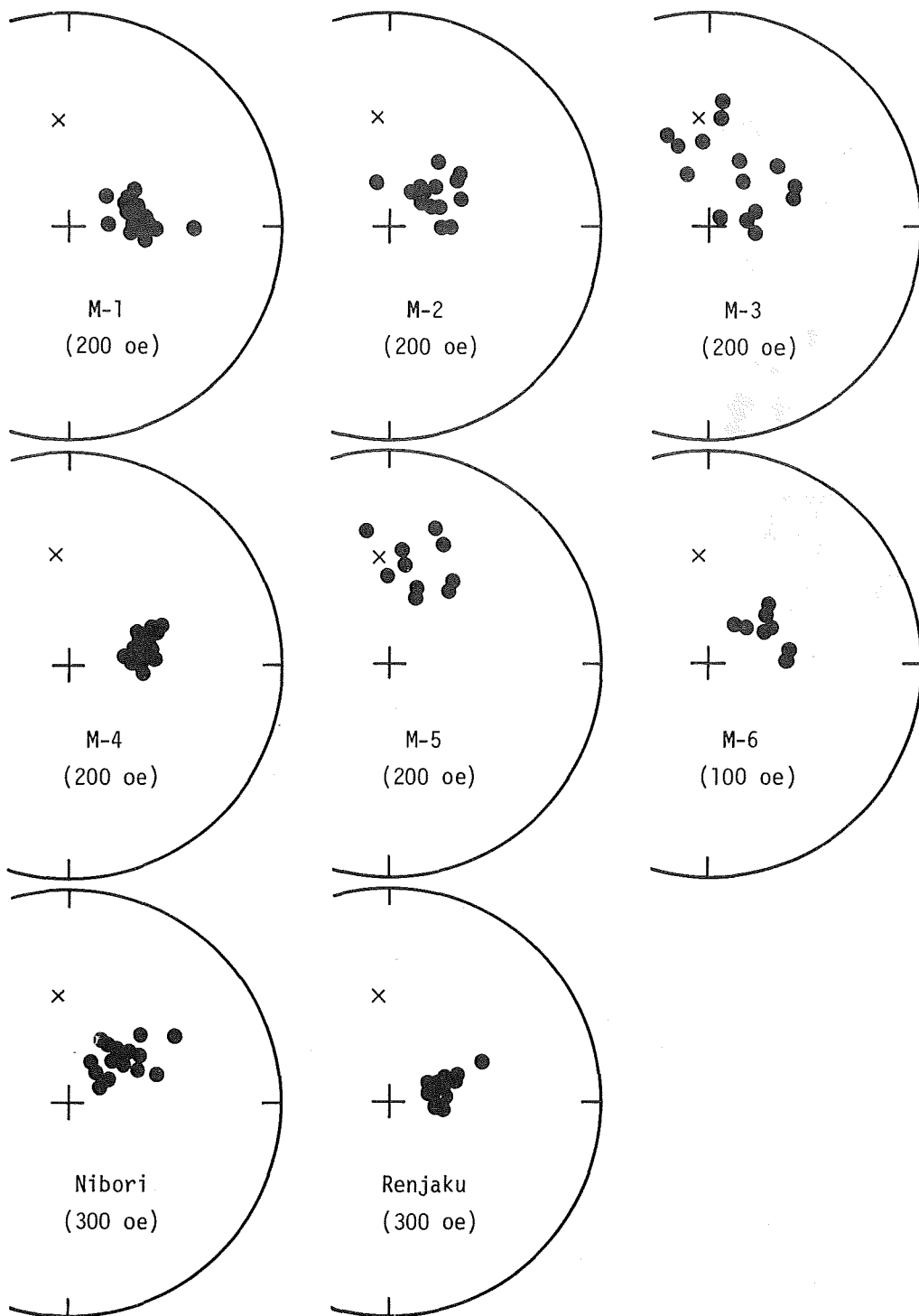


Fig. 2. NRM directions after alternating field demagnetization. Cross mark denotes present-day geomagnetic field direction at sampling site.

Results of measurements after alternating field demagnetization are listed in Table 1 and NRM directions of the eight sites having stable component of magnetization are shown in Fig. 2. The NRM directions indicate well agreement between the sites and their declinations of magnetization are evidently easterly as first presented by Kawai et al. (1961). The easterly NRM directions are wholly consistent with those of normal samples in the Ibaragi complex. Although many reversed samples were taken from the Ibaragi complex, we unfortunately were unable to encounter with reversed samples within the Myoken-zan complex. It should be, however, noted that part of the oldest rocks and most of the youngest ones in the Ibaragi complex were normally magnetized and the directions of NRM are clearly antipodal to those of reversed samples.

5. Discussion

Eight sites from the Myoken-zan, Nibori and Renjaku masses gave a VGP at 49°N , 170°W and the pole is close to that for Cretaceous rocks in Southwest Japan as seen in Fig. 3. The VGP is also located near those for the Ibaragi complex (76-74 Ma) and for Cretaceous granitic rocks (125-110 Ma) in the Oshima

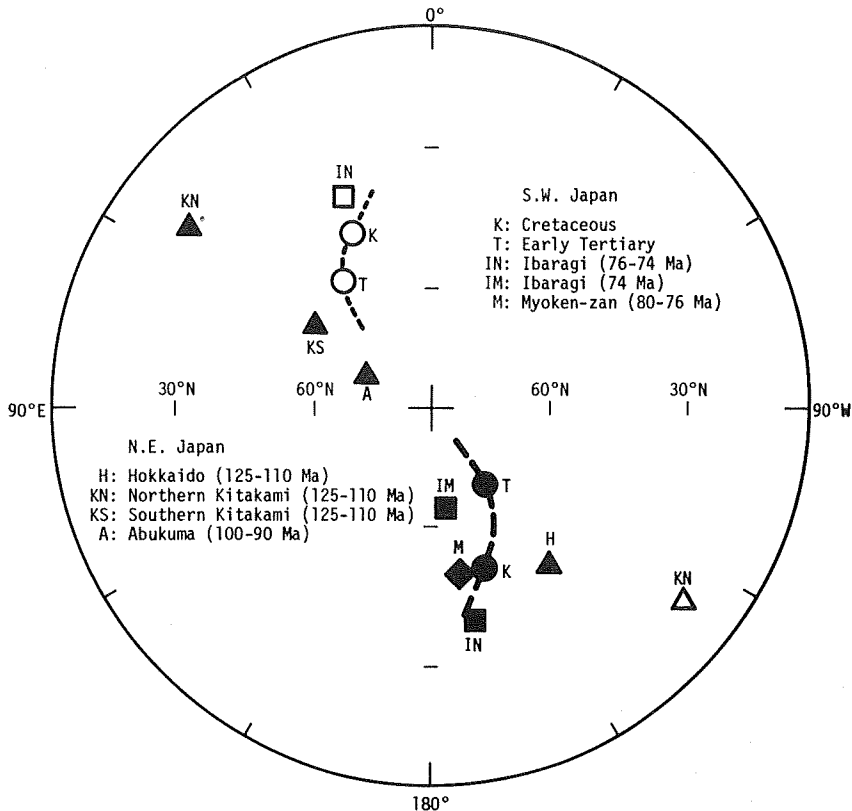


Fig. 3. Virtual geomagnetic poles. Map is stereographic projection centered on north pole. Closed symbols denote to be the Northern Hemisphere and open symbols denote to be the Southern Hemisphere.

peninsula of Hokkaido. Normal samples (30 sites) taken from Cretaceous rocks in Southwest Japan give a VGP at 49°N , 160°W and a mean pole calculated from reversed samples (9 sites) is 44°S , 25°E . On the other hand, NRM directions of Cretaceous granitic rocks in Northeast Japan were almost westerly (Kawai et al., 1971; Ito et al., 1980) and VGPs obtained from granitic rocks (125-110 Ma) in the northern and southern Kitakami mountains and Abukuma granitic rocks (100-90 Ma) are situated at remarkably different positions from that for Southwest Japan or the Oshima peninsula of Hokkaido.

The Myoken-zan complex are exposed west of about 130 km away from the Ibaragi complex. However, these two complexes are known to have the nearly same age at 76 Ma by Shibata (1971, 1979) and normal samples from both the complexes resemble each other in the NRM directions. Moreover, the NRM directions of these normal samples are almost easterly and they are in accord with those from Cretaceous rocks in Southwest Japan as reported by many workers (e.g. Sasajima, 1981).

At present available paleomagnetic data from Cretaceous rocks in various regions of the Japanese Islands show that VGP positions for each region are not always consistent. In particular, a typical example of inconsistencies in VGP positions between the regions are observed from Northeast Japan as seen in Fig. 3. The VGPs for the four regions of the Oshima peninsula of Hokkaido, northern Kitakami, southern Kitakami and Abukuma are distinctly different from each other (Ito et al., 1980). This would indicate that original magnetic vectors of rocks are affected by some local tectonic phenomena occurred in Northeast Japan. On the other hand, the VGPs for various regions of Southwest Japan are well grouped and their mean pole is 49°N , 160°W . This fact suggests that magnetic vectors of rocks are not markedly changed by local tectonic movements since the rocks were formed. Therefore, a VGP for Cretaceous rocks in Southwest Japan would be one of the most reliable Cretaceous poles for the Japanese Islands.

References

- Ishizaka, K. (1971) *J. Geol. Soc. Japan*, 77, 731.
Ito, H. and K. Tokieda (1972) *Mem. Fac. Lit. Sci., Shimane Univ.*, 5, 23.
Ito, H. and K. Tokieda (1978) *Mem. Fac. Sci., Shimane Univ.*, 12, 33.
Ito, H., K. Tokieda and Y. Notsu (1980) *Rock Mag. Paleogeophys.* 7, 113.
Kawai, N., H. Ito and S. Kume (1961) *J. R. Astro. Soc.*, 6, 124.
Kawai, N., T. Nakajima and K. Hirooka (1971) *J. Geomag. Geoelectr.*, 23, 267.
Mitsuno, C. and N. Omori (1965) "Susai" Scale 1:50000, *Geol. Surv. Japan*.
Nozawa, T. (1970) *J. Geol. Soc. Japan*, 76, 493.
Sasajima, S. (1981) *Am. Geophys. Union*, 115.
Shibata, K. (1971) *Chikyū Kagaku*, 25, 268.
Shibata, K. (1979) *Mem. Geol. Soc. Japan*, 17, 69.
Shirakawa, Y. (1975) *J. Japan. Assoc. Min. Petrol. Econ. Geol.*, 70, 107.

Table 1. Summary of results

Locality	Lat.	Long.	Age (Ma)	N	D	I	K	α_{95}	VGP		dp	dm	Cleaning field(Oe)
									Lat.	Long.			
M-1	34°54'N	134°07'E	75.7	16	82.6°	64.6°	69.9	4.4°	29.2°N	174.5°W	5.7	7.1	200
M-2	34°54'N	134°07'E	75.7	14	53.4°	69.5°	55.1	5.4°	48.7°N	179.2°W	7.9	9.2	200
M-3	34°53'N	134°07'E	75.7	15	23.7°	66.3°	14.4	10.5°	67.7°N	178.5°E	14.1	17.2	200
M-4	34°53'N	134°08'E	75.7	15	76.6°	59.4°	239.5	2.5°	31.0°N	165.8°W	2.8	3.7	200
M-5	34°51'N	134°09'E	75.7	10	17.5°	48.3°	30.9	8.8°	74.2°N	120.0°W	7.6	11.6	200
M-6	34°51'N	134°10'E	75.7	8	61.0°	63.3°	73.4	6.5°	43.3°N	167.4°W	8.1	10.3	100
Nibori	34°52'N	134°01'E	79.9	16	51.9°	63.3°	55.1	5.0°	49.6°N	166.4°W	6.2	7.9	300
Renjaku	34°58'N	134°04'E	-	11	78.0°	69.0°	233.2	3.0°	34.0°N	180.0°E	4.3	5.1	300

N: Number of samples.

D: Declination, degrees east of north.

I: Inclination.

K: Fisher's precision parameter.

α_{95} : Semi-angle of cone of 95 % confidence for the site mean direction.

dp, dm: Semi-axes of ovals of 95 % confidence.

PALEOMAGNETISM AND K-Ar AGE OF CRETACEOUS ROCKS FROM
KOREAN PENINSULA
-- GYEONGSANG SUPERGROUP IN SOUTH KOREA --

Yo-ichiro OTOFUJI*, Jin Yong OH**, Takao HIRAJIMA*
Kyung Duck MIN** and Sadao SASAJIMA*

* Department of Geology and Mineralogy, Faculty of Science,
Kyoto University, Kyoto, Japan

** Department of Geology, Yonsei University, Seoul, Korea

Introduction

Gyeongsang Basin is located in the southeastern part of the Korean Peninsula (Fig. 1). The upper Cretaceous strata of the Gyeongsang Basin are very suitable for paleomagnetic study, because the remanent magnetizations of both sedimentary and volcanic rocks from the basin are magnetically stable and the bedding planes of the strata are clearly recognized. The work presented here is the attempt to obtain the relative movement between the Korean Peninsula and Asian continent from the viewpoint of paleomagnetism.

Geology and sampling

The Gyeongsang Basin consists of thick sequence of fluviolacustrine sediments intercalated with lavas and volcanoclastic rocks of Cretaceous age. These strata constitute the Gyeongsang Supergroup. According to the definition of Chang (1975), the Gyeongsang Supergroup is divided into three groups of the Sindong, Hayang and Yuchon Groups in ascending order (see Table 1); the Sindong Group consisting of sediments of the pre-volcanic

phase, the Hayang Group comprising non-volcanic sediments with some volcanic horizons and the Yuchon Group consisting of volcanic formations.

The Sindong Group, the lowest Gyeongsang Supergroup, is extensively fossiliferous, and it is documented as lowest Cretaceous in age (Yabe, 1905; Kawasaki, 1929; Um and Reedman, 1975). The K-Ar data for granitic plutons intruding the Yuchon volcanics range from 62 to 88 Ma (Chang, 1975; Lee, 1980) which put the end of Cretaceous as the upper limit of the Supergroup. These indicate that the Gyeongsang Supergroup

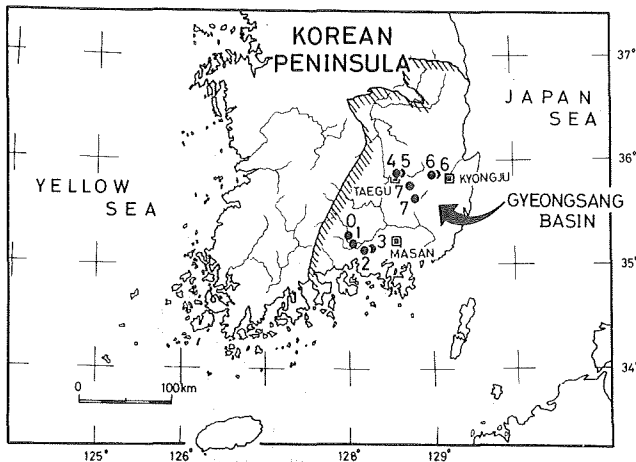


Fig. 1 Sampling localities in Gyeongsang Basin. Site 0 = Nagdong Fm.; Site 1 = Hasandong Fm.; Site 2 = Jinju Fm.; Site 3 = Chilgog Fm.; Site 4 & 5 = Hagbong Volcanic Members; Site 6 = Chaeyagsan Fm.; Site 7 = Yuchon Group.

Table 1. Stratigraphy of Gyeongsang Supergroup in Gyeongsang Basin (after Chang, 1975) and the stratigraphic horizons of sampling sites

GYEONGSANG SUPERGROUP	YUCHON GROUP		---- Site 7.	
		Jindong Subgroup	Geoncheonri Fm. Chaeyagsan Fm. Songnaedong Fm. Banyaweol Fm.	---- Site 6.
	HAYANG GROUP	Uiryong Subgroup	Haman Fm. Hagbong Volcanic Member Silla Conglomerate	---- Site 5 & 4.
		Chilgog Subgroup	Chilgog Fm.	---- Site 3.
	SINDONG GROUP		Jinju Fm. Hasandong Fm. Nagdong Fm.	---- Site 2. ---- Site 1. ---- Site 0.

was formed during Cretaceous.

More than 120 samples were obtained from widely spaced ten locations in Gyeongsang Basin. Fig. 1 shows the distribution of sampling sites. The samples of sites 0~2 are from the Sindong Group, those of sites 3~6 are from the Hayang Group, and those of site 7 are from the Yuchon Group. The bedding planes were clearly recognizable at all sampling localities except for site 5 of basaltic lavas. Detailed stratigraphic horizons of sampling sites and the rock types are given in Table 1 and Table 2. The basaltic rock samples were collected for K-Ar age determination from the Hagbong Volcanic Member of the site 4 in the Hayang Group.

Paleomagnetic data

The block samples collected were drilled into 2.4 cm-diameter cores and cut into individual specimens 2.4 cm-long; most cores were long enough to yield two or three specimens.

Natural remanent magnetization (NRM) of all specimens were measured on a Schonstedt SSM-1A spinner magnetometer. Three or more specimens from independently oriented samples in each site were stepwise demagnetized as pilots by both alternating field (AF) cleaning and thermal cleaning techniques. The remainder of each site was treated by the optimum field and/or temperature. The optimum demagnetization level for each site was chosen as the value for which more than three directions of pilots were most clustered. When little direction changes of NRMs for the pilots were observed in response to the AF and thermal demagnetizations, the optimum demagnetization was confined to the AF method only.

Pilot specimens from site 1 (Hasandong Formation), site 3 (Chilgog Formation), site 4 and 5 (Hagbong Volcanic Member), and site 7 (Yuchon Group) showed only small changes of direction during magnetic cleaning by both AF and thermal methods. There appear, however, little evidences that the primary magnetization has been masked by the secondary one after demagnetization up to high field or temperature. The NRMs after cleaning by optimum demagnetization fields are drawn in Fig. 2.

Remanent magnetizations of specimens of site 2 (Jinju Formation) showed

a different behaviour in response to AF and thermal demagnetizations. Specimens were cleaned either by AF demagnetization in peak field of 300 Oe or by thermal demagnetization at 150 °C.

Specimens from site 0 (Nagdong Formation) had a remanent intensity of less than 10^{-8} emu/gr. These specimens were rejected to avoid the introduction of errors through instrumental noise on measurements. Pilot specimens from site 6 (Chaeyagsan Formation) showed a stable remanent magnetization in response to both AF and thermal demagnetization. However, precision parameter k (Fisher, 1953) of three pilots specimens was less than 2.0 at any demagnetization level. The directions of all specimens ($N=44$) demagnetized after 300 Oe were also highly scattered: Precision parameter was only 1.2. It is possibly that the block samples from this site may have been subjected individually to arbitrary rotation or movement after they had acquired the stable remanent magnetization. Data from this site were, therefore, omitted from further paleomagnetic considerations.

Table 2 represents a summary of the paleomagnetic results after corrected for geological dip. The largest dip correction was 15°; most were in the range of 11°. Gyeongsang Supergroup yields a mean direction of $D = 26.6^\circ$, $I = 62.3^\circ$ and $\alpha_{95} = 8.3^\circ$, which is that at the representative point of the Korean Peninsula ($128^\circ E$, $37^\circ N$): The mean declination and inclination values were calculated from five directions into which the directions at five sites in Gyeongsang Basin were converted at the representative point.

The characteristic NRM direction of specimens from site 5 of Hagbong Volcanic Member ($D = -19.0^\circ$, $I = 78.9^\circ$ and $\alpha_{95} = 6.9^\circ$) deviates by

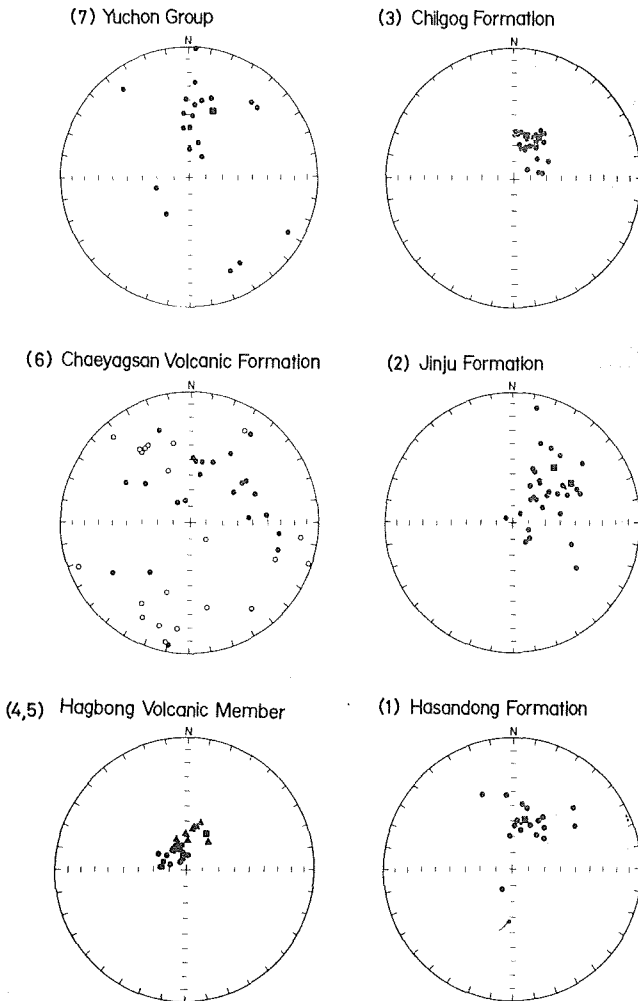


Fig. 2 Equal-area projections showing cleaned directions of remanent magnetization. Remanent magnetization after AF demagnetization at the optimum field intensity and after thermal demagnetization at 400 °C are shown with circle (or triangle) and square symbols, respectively. The remanent directions of site 4 after tilting correction in Hagbong Volcanic Members are shown with triangle symbols. Solid symbols on the lower hemisphere, open symbols on the upper hemisphere.

Table 2. Results of paleomagnetic measurement

Site	Locality		Rock type	N	Level of Demag.	D	I	α_{95}	K	Lat.	Long.	δp	δm
Site 7	Yuchon Group	35.72°N 128.74°E	Andesite	22	200 Oe	20.8'	57.7°	19.4°	3.5	73.2°N	203.6°E	20.9°	28.5°
Site 4.	Hagbong Volcanic Member	35.89 129.03	Basalt	6	300 Oe	6.6	66.3	5.1	142.8	76.3	147.3	8.4	8.4
Site 3	Chilgog Fm.	35.17 128.16	Shale	27	200 Oe	27.8	58.7	1.9	210.8	67.5	198.8	2.1	2.8
Site 2	Jinju Fm.	35.16 128.10	Sandstone	7	150 °C	53.1	60.1	7.5	12.9	48.4	193.2	8.6	11.4
Site 1	Hasandong Fm.	35.17 128.03	Sandstone	24	300 Oe	18.8	58.8	7.5	19.8	74.5	196.1	8.3	11.2
Mean		37. 128.		5		26.6	62.3	8.3	85.0	68.9	191.2	10.1	12.9

N = number of specimens, D = declination, I = inclination, α_{95} = radius of 95 % confidence circle, K = precision parameter, Lat. & Long. = VGP north pole, δp & δm = semi-axes of ovals of 95 % confidence.

22.2 degree from the mean of the Gyeongsang Supergroup, while the deviation of the NRM direction of site 4 from the same volcanic member is only 9.9 degree from the mean. The large deviation of site 5 may be ascribed to the lack of the dip correction for the direction. The data after treatments of magnetic cleaning (both AF and thermal methods) and dip correction would show the reliable paleomagnetic direction of Gyeongsang Supergroup, although no specimens with reversed polarity were observed. The agreement of directions between the lava flow and sediments confirms the reliability.

K-Ar age of basalts from Hagbong Member

K-Ar whole rock age of basalt from Hagbong Volcanic Members in Hayang Group was determined by the Geochronometry Section of Teledyne Isotopes. Prior to request for K-Ar dating, thin section of samples was examined. The rock is composed of phenocrysts of olivine and clinopyroxene, and groundmass of clinopyroxene, plagioclase, opaque mineral, biotite, and glass. All olivine crystals and glass are completely altered to talc (sometimes idding-site) and chlorite, respectively. The other constituents of rock, however, remain unaltered.

Results of K-Ar dating are given in Table 3, confirming the latest of the Cretaceous period. The obtained age 68.1 ± 3.4 Ma lends strong support to the geological estimation (Chang, 1975) that the Gyeongsang Supergroup

Table 3. Results of K-Ar dating for volcanics from Hagbong Volcanic Members

Sample No.	Locality		Isotope Age (Ma)	Sec Ar ^{40Rad} /gm x 10 ⁻⁵	% Ar ^{40Rad}	% K
PG 35	129.03°E	35.90°N	68.1 ± 3.4	0.295 0.298	74.8 69.8	1.10 1.10

The constants for the age calculation are : $\lambda_{\beta} = 4.962 \times 10^{-10} \text{ yr}^{-1}$, $\lambda_{\epsilon} = 0.581 \times 10^{-10} \text{ yr}^{-1}$, $k^{40} = 1.167 \times 10^{-4}$ atom per atom of natural potassium (Steiger & Jager, 1977).

The error indicated to the ages consists of a summation of all analytic errors (5%).

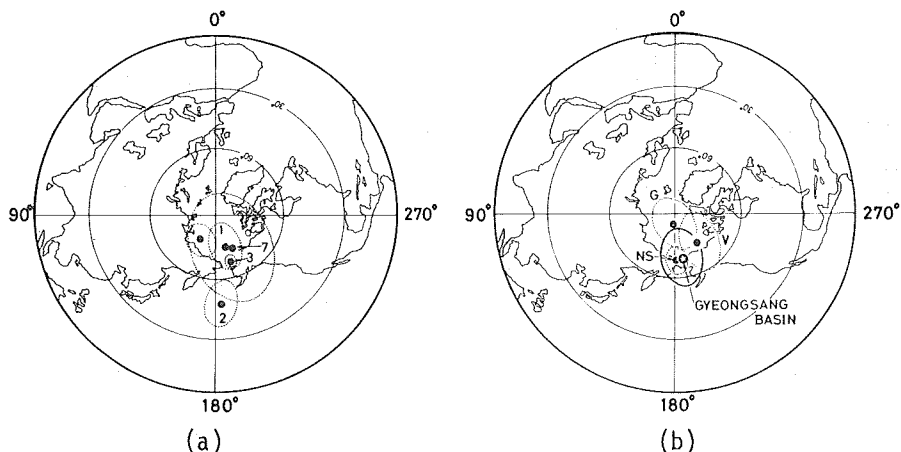


Fig. 3 (a) Pole positions and 95 % cones of confidence for Gyeongsang Basin. Site number as in Table 2. (b) Cretaceous pole positions and 95 % cones of confidence for Korean Peninsula. Pole V = Volcanic rocks (Kienzle & Scharon, 1966); Pole NS = North Korean sediments (Grarii et al., 1966); Pole G = Granitic rocks (Ito & Tokieda, 1980).

was formed during Cretaceous.

Discussion

The most striking results from this work are the great predominance of normally magnetized rocks. The question arises whether this predominance of normal polarity is primary, or due to overprinting by the later heat of the intrusion of the plutons known as the Bulgugsa Granite Serieese (Um and Reedman, 1975). The thermal demagnetization tests strongly suggest that no significant thermal overprinting has occurred and the magnetization is primary. The radiometric data support this implication: Since the age determination shows that the Gyeongsang Supergroup was formed during the Cretaceous, rocks could acquire the magnetization with normal polarity which was dominant in the middle to upper Cretaceous age (Larson and Hilde, 1975; LaBrecque et al., 1977; Lowrie and Alvarez, 1981).

No systematic movements are observed in the distribution of virtual geomagnetic pole positions for five acceptable sites as shown in Fig. 3. Radiometric data and stratigraphic sequence suggest that the rock units sampled covered nearly the entirely range of Cretaceous time. It seems reasonable, therefore, to assume that the obtained mean pole position (191°E and 69°N) averages over enough time to eliminate secular variation effects and gives a reliable estimate of the Cretaceous paleomagnetic pole position.

Comparison of the pole position with other Cretaceous pole positions from the Korean Peninsula is made in Fig. 3. Overlapping circles of 95 per cent confidence indicate that the Gyeongsang Supergroup pole and other poles from volcanics (Kienzle and Scharon, 1966), granites (Ito and Tokieda, 1980) and North Korean sediments (Grarii et al., 1966) are not significantly different and probably represent much the same position of the Cretaceous pole. While the Gyeongsang Basin pole is in excellent agreement with the poles from the sediments of North Korea, others from igneous rocks are rather far removed from the Gyeongsang Basin pole. The cause of these deviations may be attributed, in part, to the lack of dip correction for data from the volcanic

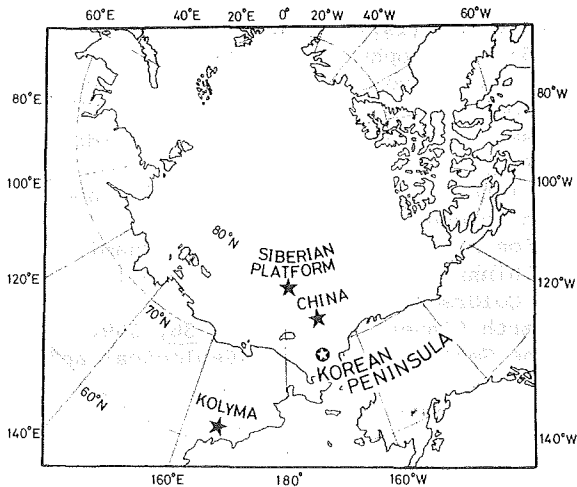


Fig. 4 Cretaceous pole positions for Korean Peninsula and neighboring regions. The Korean Peninsula pole calculated from both data of the present study and North Korean sediments is 189.5°E and 68.9°N . Poles of neighboring regions are a compilation from data of McElhinny (1973), Sasajima (1981), Khramov et al. (1981) and Nishida et al. (1980): Siberian Platform pole = $(180.9^{\circ}\text{E}, 75.4^{\circ}\text{N})$; Kolyma pole = $(166.1^{\circ}\text{E}, 61.3^{\circ}\text{N})$; China pole = $(190.0^{\circ}\text{E}, 72.4^{\circ}\text{N})$; Southwest Japan pole = $(196.1^{\circ}\text{E}, 45.9^{\circ}\text{N})$.

west Japan from the Asian continent (Hilde and Wageman, 1973; Yaskawa, 1975). The agreement between the Korean pole and those from the neighboring regions excepting Southwest Japan, on the contrary, draws the following conclusion that the Korean Peninsula has been a part of Asian continent at least since Cretaceous and that the peninsula was not subjected to the rotational movement relative to the continent.

References

- Chang, K. H. (1975) *Jour. Geol. Soc. Korea*, 11, 1.
 Fisher, R. (1953) *Proc. R. Soc. London, Ser. A*, 217, 295.
 Grarii, G. Z., P. N. Kropotokin, M. A. Pevzner, R. S. Von and V. M. Trubikhin, *Izv. Earth Phys.*, 11, 128.
 Hilde, T. W. C. and J. M. Wageman (1973) *The Western Pacific*, P. J. Coleman, ed. (University of Western Australia Press, Perth, W.A.) p. 415.
 Ito, H. and K. Tokieda (1980) *J. Geomag. Geoelectr.*, 32, 275.
 Kawasaki, S. (1928) General geological map of Chosen (1: 1,000,000) *Geol. Surv. Chosen*.
 Khramov, A. N., G. N. Petrova and D. M. Pechersky (1981) Paleoreconstruction of the continents, *Geodynamic Ser.*, vol. 2, edited by M. W. McElhinny and D. A. Valencio, pp 177 (AGU, Washington, D. C. and GSA, Colorado) p. 194.

and granite samples, because the strata of Gyeongsang Supergroup where the granites intruded and the volcanics overlies, are in southward dip with low angles of about $10\sim 30$ degrees. Thus, it seems likely that the paleomagnetic pole (Long = 190°E , Lat = 69°N) calculated from data of Gyeongsang Supergroup and North Korean sediments represents a true Cretaceous pole.

In Fig. 4 are shown the Cretaceous poles for neighboring regions of Korean Peninsula (McElhinny, 1973; Nishida et al., 1980; Sasajima, 1981; Khramov et al., 1981). The obtained Korean pole is in excellent agreement with poles from China, Kolyma and Siberian Platform: The polar distances between Korean pole and others are less than 13° . However, two circles of 95 per cent confidence for the Korean pole and Southwest Japan pole fail to overlap. Polar distance between them is larger than 23° . The cause of this separation is explained by the southward drifting accompanied with the clockwise rotation of South-

- Kienzle, J. and L. Scharon (1966) *J. Geomag. Geoelectr.*, 18, 413.
- LaBrecque, J. L., D. V. Kent and S. C. Cande (1977) *Geology*, 5, 330.
- Larson, R. L. and T. W. C. Hilde (1975) *J. Geophys. Res.*, 80, 2586.
- Lee, Y. J. (1980) *Jour. Japan Assoc. Min. Petrol. Econ. Geol.*, 75, 105.
- Lowrie, W. and W. Alvarez (1981) *Geology*, 9, 392.
- McElhinny, M. W. (1973) *Paleomagnetism and Plate Tectonics*, (Cambridge University Press, London) p. 358.
- Nishida, J., C. L. So, K. Maenaka, T. Ikeda, O. Tamada, S. Sasajima and T. Yokoyama (1980) *Tsukumo Earth Science*, 15, 27.
- Sasajima, S. (1981) *Paleoreconstruction of the continents*, *Geodynamic Ser. Vol. 2*, edited by M. W. McElhinny and D. A. Valencio, pp 115 (AGU, Washington, D. C. and GSA, Colorado) p. 194.
- Steiger, R. H. and E. Jager (1977) *Earth Planet. Sci. Lett.*, 36, 359.
- Um, S. H. and A. J. Reedman (1975) *The Geology of Korea* (Geological and Mineral Institute of Korea, Seoul).
- Yabe, H. (1905) *J. Sci. Coll. Imp. Univ. Tokyo*, 20, Art. 8.
- Yaskawa, K. (1975) *Geophys. J. R. astr. Soc.*, 43, 835.

(Submitted to *Geophys. Monogr. Ser.*, edited by D. E. Hayes, entitled " The Tectonic and Geologic Evolution of Southeast Asian Seas and Islands, Volume II ")

A PALEOMAGNETIC STUDY ON SILURIAN-DEVONIAN SYSTEM
IN KUROSEGAWA TECTONIC ZONE, SOUTHWEST JAPAN

Hidetoshi SHIBUYA and Sadao SASAJIMA

Department of Geology and Mineralogy, Kyoto University, Kyoto, 606

The paleoposition of Southwest Japan is important for reconstructing its evolution. In order to add to the knowledge of the Paleozoic paleoposition of Southwest Japan, a paleomagnetic study on Silurian to Devonian strata in Kurosegawa Tectonic Zone, one of Outer Zones in Southwest Japan was performed.

Samples were collected from Yokokurayama area, east of Kochi city and Konomori area, northern part of Kochi city, Central Shikoku Island (Fig.1). In Yokokurayama area, 25 oriented hand samples were collected from three different horizons apart several tens of meters each other in a Silurian sequence described as G_1 - G_2 and G_3 by Yoshikura and Sato (1976). Rock types of these horizons were acidic tuff (site 3), acidic welded tuff (site 4) and limestone (site 5) from lower to upper. The welded tuff and limestone were too massive to measure the strike and the dip of the bedding plane. Thus these were measured at site 3 were used for bedding correction of this rock body, because this sequence has rather simple homoclinal structure (Hamada 1959). In Konomori area, there appears Silurian to

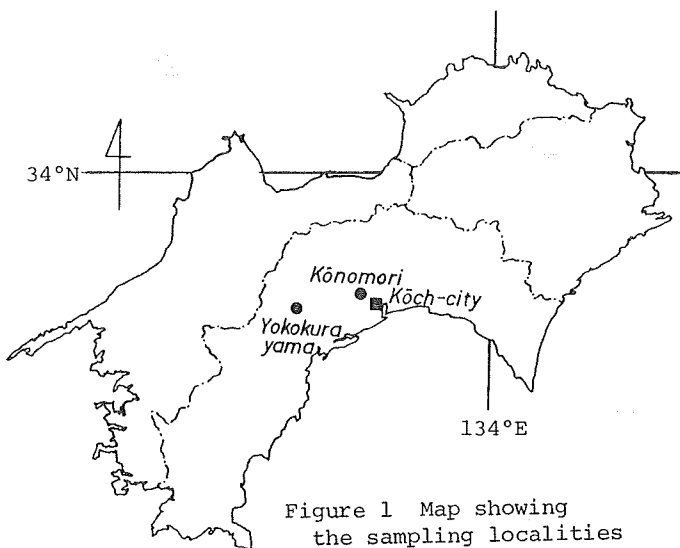


Figure 1 Map showing the sampling localities

Devonian deposits consisting of shales and acidic tuffs (Katto et al. 1976). Seventeen hand samples were collected at two localities (site 1 and 7) in this sequence. Stratigraphic relation of these two sites was not so clear.

A few core specimens with the same diameter and length of 24mm were drilled from each hand sample. Thermal demagnetization was adopted for removing the secondary magnetization. All heating treatments were carried out in an electric furnace with a quasi-zero magnetic field (less than 10 gammas) insulated by three layered permalloy cylinder which was demagnetized by alternating field once in every week. Remanent magnetizations were measured with Schonstedt SSM-1A spinner magnetometer.

Except for site 5, more than three pilot specimens for each site were subjected to progressive thermal demagnetization from room temperature up to 600°C, in order to determine an appropriate demagnetization temperature. Basically, the temperature which gave a good "stable end point" of magnetic direction was chosen as the optimum. Then, all other specimens were demagnetized in this temperature. However, when the end point was not distinct, all other specimens were demagnetized progressively. And the

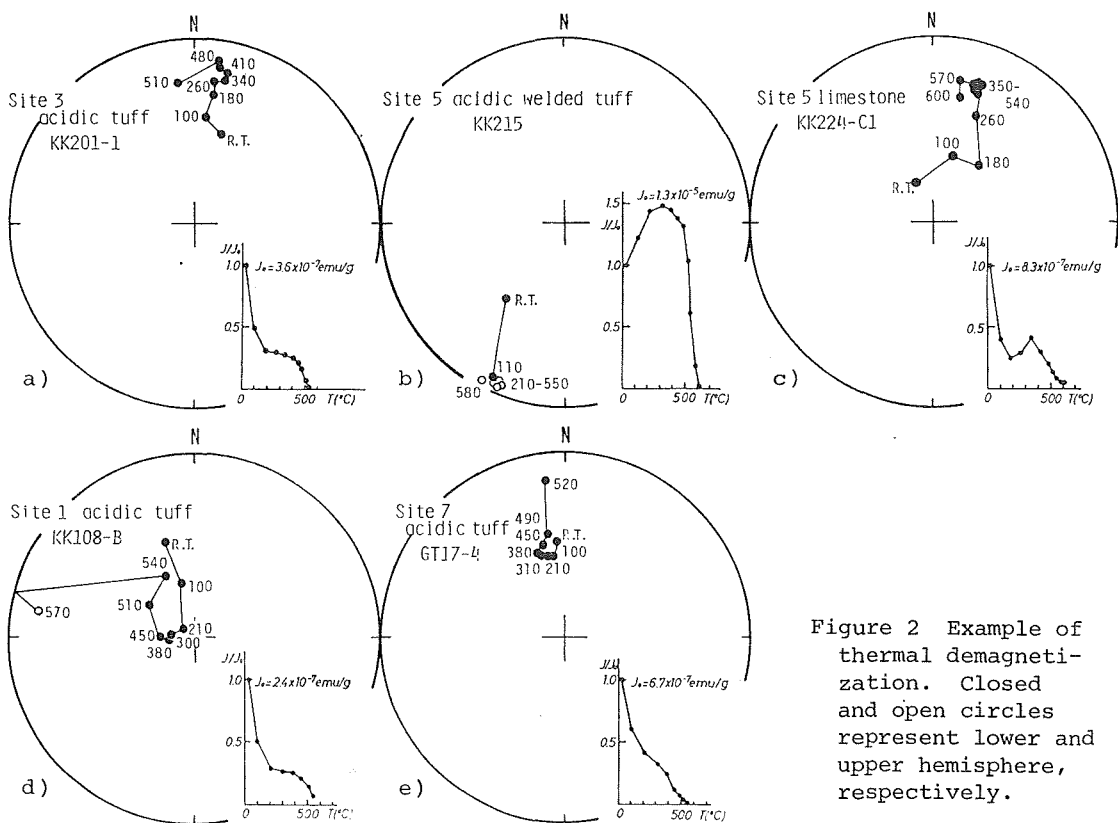


Figure 2 Example of thermal demagnetization. Closed and open circles represent lower and upper hemisphere, respectively.

demagnetization level which gave the largest Fisher's precision parameter (k) was adopted.

Response of the magnetization of each site to the heating treatment was as follows (Fig.2)

Site 3; The direction of six pilot specimens did not show a definite stable end point, although it moved less than 30° by heating treatment of over 300°C where an initial intensity drop stopped. As the appropriate demagnetization temperature was not able to determined only by a few pilot specimens, nine other specimens were demagnetized progressively from 200°C up to 500°C . And 420°C was adopted because of largest k .

Site 4; A demagnetization at 300°C gave a distinct end point on pilot specimens. Other specimens were demagnetized at the same temperature.

Site 5; Only one specimen was successful to measure its reliable remanence, but the others were too weak to measure with our spinner magnetometer. The magnetic direction of the former attained a stable end point at 350°C .

Site 1; The direction seemed to reach a end point at about 300°C in Fig. 2d, but another pilot specimen did not show a distinct end point. Then other specimens were demagnetized progressively. The maximum k was obtained at 280°C .

Site 7; The direction showed very little movement until 490°C , but the maximum k was obtained at about 300°C .

Major blocking temperature of the component adopted in this study was between 450°C and 580°C. It is supposed that the major magnetic mineral carrying stable component is magnetite or titan poor titanomagnetite.

Magnetic direction of entire specimens at the adopted demagnetization level are illustrated in Fig. 3. In Yokokurayama sites, directions of site 3 and 5 are close to each other and both are almost antipodal (apart about 160°) to that of site 4. As the stratigraphic order of these layers are from site 3 through 4 to 5 from the lower to the upper, it is evidenced that this sequence has recorded at least two polarity reversals. It could be safe to conclude that these direction cannot be taken as neither indication of a excursion nor a transition of reversal.

Site 7 shows a very close direction to the present magnetic field. It might be a completely over-printed magnetization, thus it was thought to be safe not to be used in the later discussion.

Mean magnetic directions after bedding correction are shown in Fig. 4

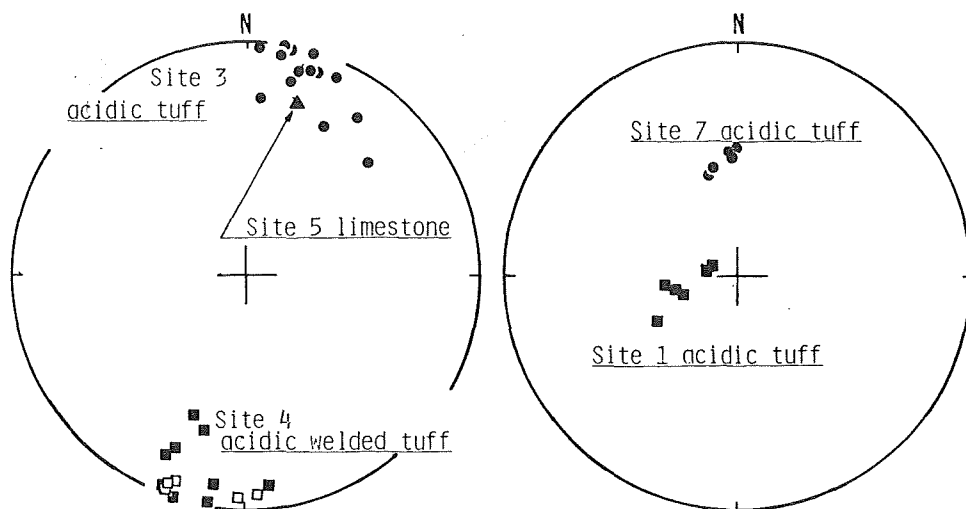


Figure 3 Directions of magnetization after thermal demagnetization at the temperature described in the text. The directions are not corrected for bedding. Closed and open symbols are represent lower and upper hemisphere, respectively.

Locality	Site	Material	N	D	I	Dc	Ic	α_{95}	k	T	P.Lat.
Yokokurayama	3	acidic tuff	15	18.0	10.1	-40.5	20.2	8.5	21.3	420	10.4
	4	acidic welded tuff	14	-165.7	7.6	157.5	-27.3	8.8	21.5	300	14.5
	5	limestone	1	18.0	25.8	-52.7	9.8	—	—	350	4.9
Konomori	1	acidic tuff	6	-101.9	70.8	-175.9	-39.3	8.6	61.6	280	22.3
	7	acidic tuff	5	-6.5	48.9	125.1	-0.3	5.1	225.0	300	0.2

Table 1 Mean direction for each site.

N number of specimens; D and I declination and inclination before bedding correction (°); Dc and Ic declination and inclination after bedding correction (°); α_{95} semi-angle of the cone of confidence (°); k precision parameter; T temperature of treatment (°C); P.Lat. paleolatitude corresponding to the inclination (°).

and Table 1. As tectonic movements of Yokokurayama and Konomori blocks are not known, any particular significance can not be attached for absolute declination. The characteristic of this result is ascribed to the low paleo-inclination of them. The mean inclination of these sites except for site 7 was 24° , which corresponded to 14° in paleolatitude. Sasajima (1981) summarized paleomagnetic data in Southwest Japan and concluded that the paleolatitude was low from the Carboniferous to the Jurassic. This tendency seems to have been kept since the Silurian.

Another area where pre-Carboniferous rocks are distributed in Southwest Japan is the Hida terrain. To establish the evolutionary history of Southwest Japan, it is important to know whether Hida terrain and Kurosegawa Tectonic Zone were formed in a single land block or as separate land blocks. Paleomagnetic studies in Hida Terrain is necessary to solve the current problem.

Only one paleomagnetic result obtained so far from Silurian to Devonian strata in Japan and its vicinity is published by Minato and Fujiwara (1965) who studied on a middle Devonian basaltic tuff in Kitakami district, Northeast Honshu Island. It gave an inclination of 64° which is much steeper than this result, even taking the present difference of latitude into account. It might be suggested that the paleoposition where they occupied was separated at least a few thousand kilometers in each other.

References

- Hamada, T. (1959) *J. Geol. Soc. Japan*, 65, 688. (in Japanese)
 Katto, J., I. Obata, S. Yoshikura, N. Tsutiya, K. Handa, Y. Ogawa and T. Sasaki (1976) *Res. Rep. Kochi Univ.*, 25, 1. (in Japanese)
 Minato, M. and Y. Fujiwara (1965) *J. Assoc. Geol. Collaboration Japan*, 78, 21.
 Sasajima, S. (1981) *Paleoreconstruction of the Continents*, M.W. McElhiny and D.A. Valencio ed., *Geodynamic Ser.* 2, A.G.U. and G.S.A.
 Yoshikura, S. and K. Sato (1976) "Toukokiban" (basement of Japan), 3, 53. (in Japanese)

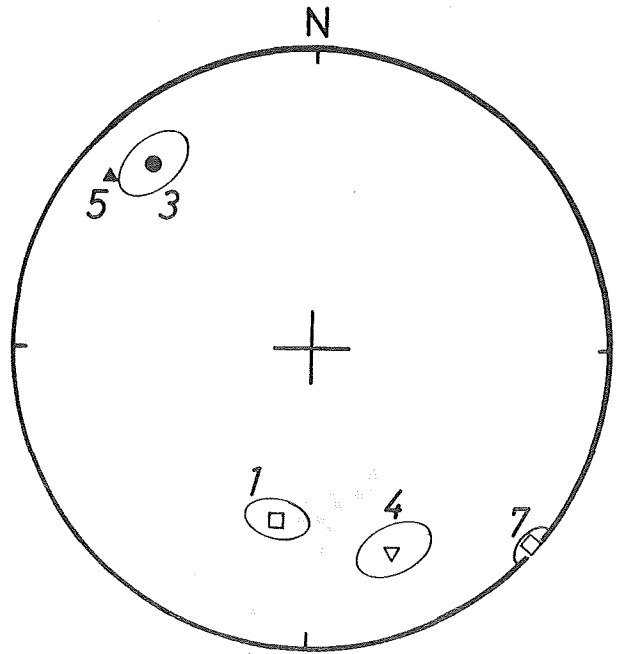


Figure 4 Mean direction of each site after bedding correction. Numbers represent site number.

PRELIMINARY REPORT ON THERMOMAGNETIC ANALYSIS OF VOLCANIC ASH ERUPTED
FROM MOUNT ST. HELENS, U.S.A., 1980.

Haruo DOMEN

Institute of Physical Sciences, Faculty of Education,
Yamaguchi University, 753 Japan.

It was May 18, 1980, the gleaming white peak of Mount St. Helens in the Cascades of northwestern U.S.A. had blasted away the top and tremendous amount of volcanic ash was thrown out widely spreading by this eruption. Only a portion of the ash mentioned above; a handful ash sample was sampled at about 10 km northwest of the mountain soon after of this eruption occurred and was offered to the present author by the courtesy of an NHK (Japan) TV reporter.

On the ash sample thus obtained, a thermo-magnetic analysis has now been under performance by means of a thermomagnetic balance; Naruse Kagaku Co. Ltd., Japan (Type; MB-2). Questioned ash sample was analyzed little by little submitting two kinds of the sample such as that bulk ash specimen and ferromagnetics extracted from the bulk specimen by a hand-magnet at the room temperature, and also under different evacuated atmospheric conditions, say 10^{-3} and 10^{-6} Torr and in open air. Different magnetic field intensities are supplied by an electromagnet. Several different rates of heating speed and cooling are employed.

A concentration of the ferromagnetics extracted from the bulk ash specimen is about 18 wt% so far as the above-mentioned magnetic separation. A hundred and several ten mg of the ash specimen was submitted to the analysis at one time.

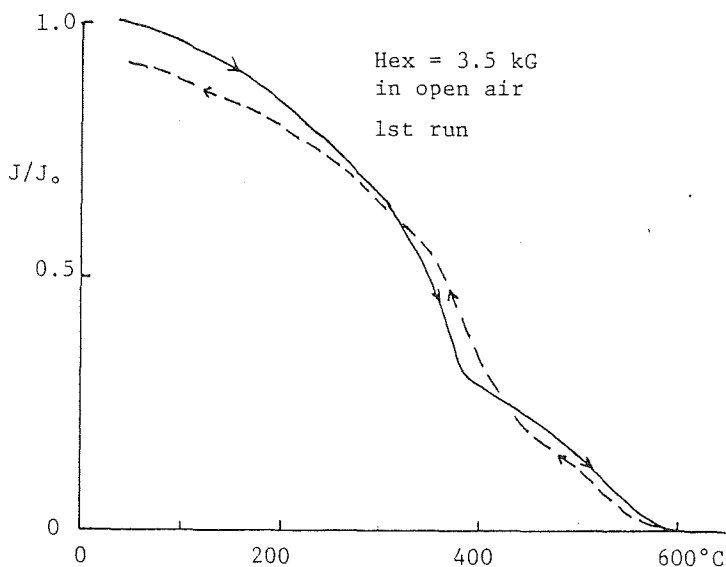


Fig. 1. J_s -T curve for bulk ash from Mt. St. Helens.

Typical example of thermo-magnetic curves (Js-T curve) thus obtained is illustrated in Fig. 1. As far as the analysis has been carried out by this time, it seems that the test specimens, both the bulk ash and ferromagnetics extracted have two different kinds of ferromagnetic solid phases. One of them shows its Curie point at around 400°C and the other 580°C. It seems that these ferromagnetic phases are rather stable during heat treatments, not only the 1st run but also 2nd run and so on, even in the open air. However, it could not to clarify whether the single ferromagnetic grain contains those two solid phases within or two different kinds of grains having different Curie points exist respectively in the basketfull (~100 mg) test specimen. It is also not obvious to recognize that the submitted ash sample is a part of the mountain herself or newly born from the magma underneath at Mount St. Helens.

ON THERMOMAGNETIC PROPERTY OF AN ICELANDIC MATUYAMA REVERSED ROCK.

Haruo DOMEN

Institute of Physical Sciences, Faculty of Education,
Yamaguchi University, 753 Japan.

1)Sample:- A basaltic lava sample of Matuyama Reversed Epoch from Iceland has now been submitted to thermomagnetic analysis. One fist-sized basaltic sample was taken at about 100 km north of Reykjavik, Iceland on late summer of 1979. The sample shows entirely reversed of NRM. A part of this sample was clashed into flakes and several pieces thus obtained are now under examination by means of an automatic thermomagnetic balance; Naruse-Kagaku Co. Ltd., Sendai, Japan (MB-2).

2)Preliminary result:- The analysis has been carried out under several different conditions such as that the different atmospheric pressures, say in open air, 10^{-3} and 10^{-6} Torr and different magnetic fields; some thousands up to 10^4 Gauss, and also different thermal agitation rates. Figs.1 & 2 show typical examples of thermomagnetic curves (J_s -T curve) thus obtained about the several flakes of the bulk specimen. Mode of the initial heating curve seems likely to that of N-type ferri-magnetics. The magnetization has once disappeared at around 350°C , then recovered its magnetization again when the specimen was heated up over this compensation temperature and falls down the magnetization to zero at higher temperature, about 500°C . Such a decay mode during the initial heating is irreversible. The cooling curves of 1st run and 2nd and more runs did not show such the extraordinary mode any more as has been shown in the figure, and could not be prevented even by highly evacuated condition such as 10^{-6} Torr.

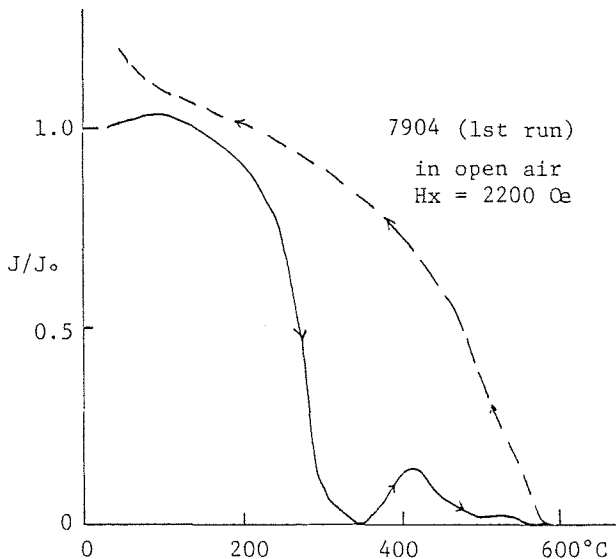


Fig. 1. J_s -T curve of bulk specimen from Icelandic Matuyama Reversed basalt.

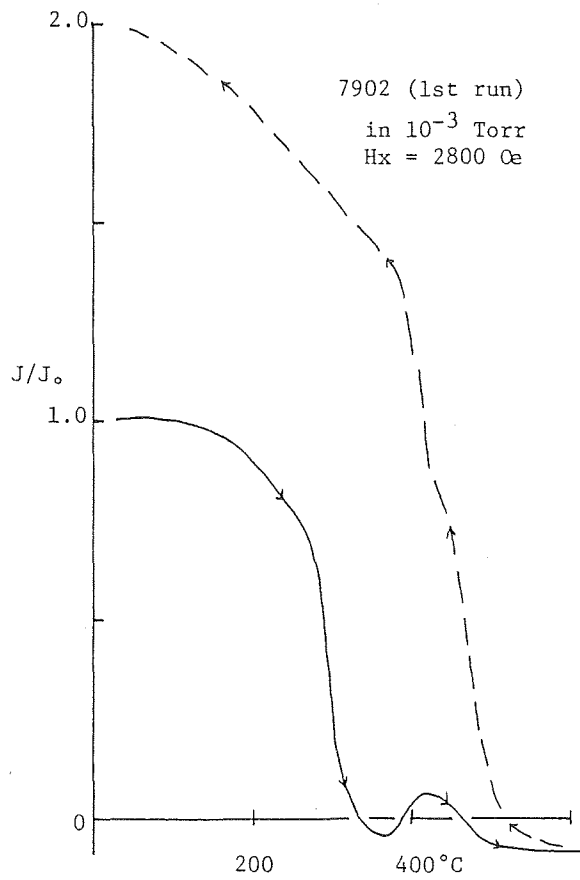


Fig. 2. A J_s -T curve for Icelandic Matuyama Reversed basalt (bulk specimen).

ORIGIN OF DECAY OF A POST-DEPOSITIONAL REMANENT MAGNETIZATION IN WET SEDIMENTS DURING DESICCATION

Yo-ichiro OTOFUJI, Ikuo KATSURA
and
Sadao SASAJIMA

Department of Geology and Mineralogy, Faculty of Science,
Kyoto University, Kyoto, Japan

Introduction

The magnetic effects associated with drying have been recently reported in both deep-sea sediment core (Johnson et al., 1975) and the lake sediments (Shuey et al., 1977; Stober and Thompson, 1977). The effects of drying under the presence of magnetic field are (1) decay in natural remanent magnetization (NRM) in intensity and (2) acquisition of a magnetization parallel to the applied magnetic field (Johnson et al, 1975; Henshaw and Merrill, 1979; Verosub et al., 1979). When sediments are allowed to dry in a magnetic field free space, only decay is observed.

The work presented here is the attempt to study the origin of the decay of the post-depositional remanent magnetization (post-DRM) in wet sediments through a series of experiments. The experiments show that the decay of more than 80 % of the post-DRM during desiccation in magnetic field free space is due to the physical random rotation of the magnetic particles trapped in shallow energy wells which are overcome by the torques caused by the application of the alternating magnetic field less than 200 Oe.

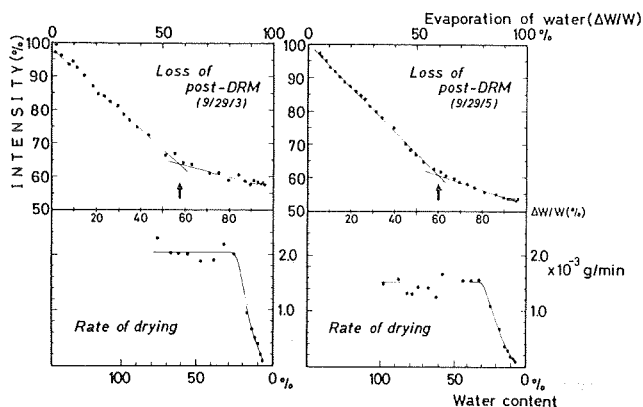


Fig. 1 Changes in the intensity of the post-DRM and rate of drying. The intensity is normalized by the remanent intensity before desiccation. The abscissa indicates both the drying stage $\Delta W/W$ and the water content on the dry basis. The drying stage is defined as the ratio of the weight of the evaporation loss of ΔW and the weight of water W before desiccation in specimen. Initial water contents on the dry basis of specimens of 9/29/3 and 9/29/5 are 145.4 % and 150.9 %, respectively.

Decay of post-DRM during desiccation

Compacted sediments in a specimen holder (25 mm in both diameter and length) with post-DRM was produced by the centrifuge method from the slurries of deep-sea and lake sediments with density of 1.12 g/cm³ and 1.21 g/cm³. The apparatus and experimental procedure were the same as those described by Otofujii and Sasajima (1981). The compacted wet specimens were allowed to dry at room temperature within quasi field free space where the geomagnetic field was reduced to less than 200 Gamma. The remanent magnetization of specimen was measured at intervals on Schonstedt SSM-1A spinner magneto-

meter. The weight of specimen was also measured at the same time within an accuracy of ± 0.002 g.

The loss of remanent magnetization of wet specimens produced from the lake sediments is shown as a function of the evaporation of the water in

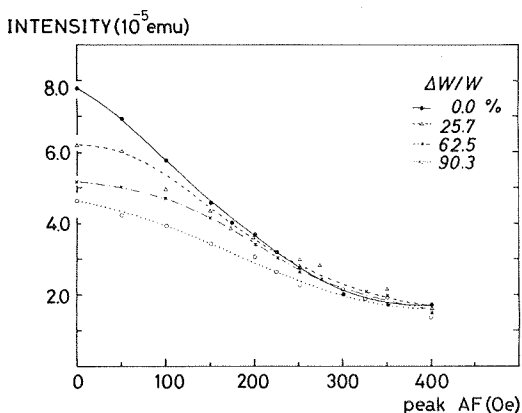


Fig. 2 Variation in the intensity of the post-DRM during progressive AF demagnetization for specimens at the different drying stage $\Delta W/W$. All specimens have the same remanent intensity of 7.81×10^{-5} emu/g before desiccation.

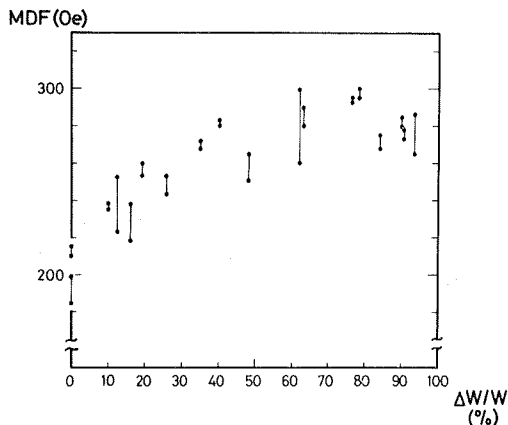


Fig. 3 Median destructive fields (MDFs) of AF demagnetization for the post-DRM of specimens at the different drying stage $\Delta W/W$. Three values of MDF are estimated from the demagnetization curves of orthogonal three components of the post-DRM. The MDF of the post-DRM is defined to lie within a field interval of each vertical bar which is made by the highest and lowest values in the three values of MDFs.

the evaporation of the water in Fig. 1, together with the rate of the drying. There appears the critical drying stage at which the rate of decay changes: The swift decay of the post-DRM terminated at the drying stage of about 60 % (about 60 % in water content on the dry basis) (indicated by arrows in Fig. 1), and after that period a slow decay of remanence was observed. More than 80 % of the total loss of remanence was lost until the critical drying stage. The critical drying stage was also observed at about 60 % during the drying process for specimens from deep-sea sediments. The critical drying stage was clearly prior to the falling rate period of drying (see lower diagram of Fig. 1). The following experiments will indicate that the swift decay of remanence before the critical drying stage is ascribed to the physically random rotation of magnetic particles which can be subjected to a physical rotation under the alternating magnetic field.

Experiments and results

(i) AF demagnetization curves of post-DRM of wet sediments

A total eighteen specimens with almost similar water content (104 % ~ 126 % on dry basis) were prepared from deep-sea sediments. Stepwise AF demagnetization was carried out using a three-axes tumbler system for specimens which attained a certain drying stage after evaporation in the quasi field free space. The demagnetization curves for specimens at various drying stages are shown in Fig. 2. The wet specimen has a low stability in response to AF demagnetization. This property is clearly indicated by the median destructive fields (MDFs) (Fig. 3): Before the desiccation proceeds to about 60 % in drying stage, the

MDF values increases but later tends to level off at saturation value. This implies that wetness of the specimen before the critical drying stage of about 60 % plays an important role in the remanent stability. The low stability of wet specimen is not, however, attributed to the mechanical deformation by tumbling during demagnetization, because no decrease in remanence was observed when the wet specimen was tumbled without applying the alternating field for more than 10 min.

(ii) Acquisition of anhysteretic remanent magnetization (ARM)

After stability test up to 700 Oe was performed, ten specimens were stepwise given an ARM by peak alternating field between 100 Oe and 1500 Oe (0.44 Oe steady field). Fig. 4 is a plot of the ARM acquisition for specimens of different drying

ARM INTENSITY (10^4 emu)

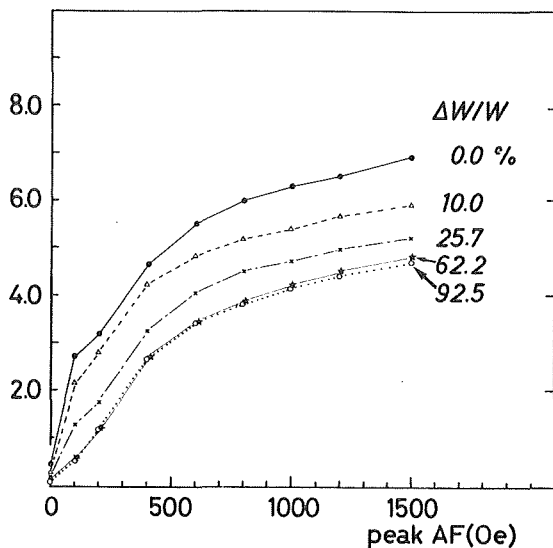


Fig. 4 Intensity of ARM as a function of the drying stage $\Delta W/W$ and the peak alternating field.

stage. As the evident from the figure, wetter specimen acquires stronger ARM. The ARM acquisition curve of specimen at drying stage above about 60 % matched that of completely dry specimen. These results are explained as follows: The dry specimen at the drying stage less than 60 % acquired the apparent ARM which consisted of the ordinary ARM and addition remanence probably due to a physical rotation of magnetic particles.

It should be noted that the addition remanence was acquired by 200 Oe in peak field. This implies that all the magnetic particles which are carrying the addition remanence have been controlled by forces caused by the application of magnetic field less than 200 Oe.

(iii) Demagnetization curve of apparent ARM

The specimens given the apparent ARM was subsequently demagnetized by AF increasing steps. Fig. 5 is a relation between the MDF and the drying stage. The MDFs of specimens at the drying stage of greater than 60 % tend to level off at saturation values.

The demagnetization curves (Fig. 6) show that there is no substantial difference above 200 Oe in demagnetization field among demagnetization curves for specimens at different stages of drying. The low MDF of wet specimen is attributed to large destruction of remanence at lower demagnetization field less than 200 Oe.

Physical random rotation of magnetic particles

The critical drying stage of wet sediments points out the stage at which all the changes occurs in rate of decay in post-DRM intensity during

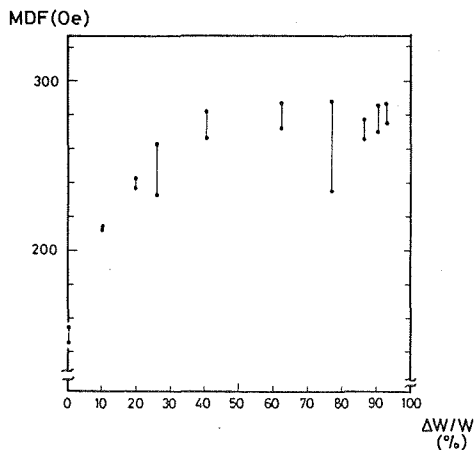


Fig. 5 Median destructive fields (MDFs) of AF demagnetization for ARMs of specimens at the different drying stage $\Delta W/W$. Three values of MDF are estimated from the demagnetization curves of orthogonal three components of ARM. The MDF of the ARM is defined to lie within a field interval of each vertical bar which is made by the highest and lowest values in the three values of MDFs.

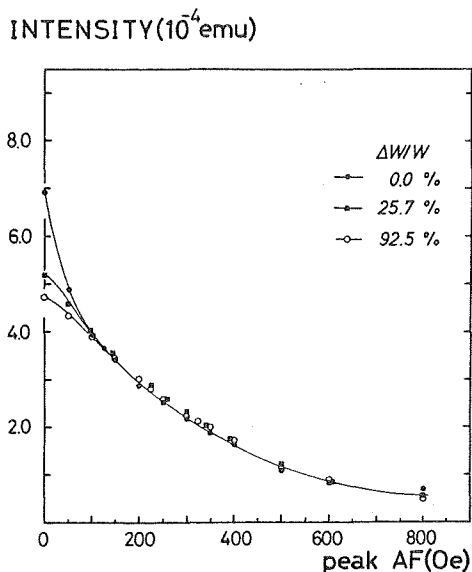


Fig. 6 Variation in the intensity of ARM during progressive AF demagnetization for specimens at the different drying stage $\Delta W/W$.

drying, acquisition of ARM and stabilities of post-DRM and ARM in response to AF demagnetization. These changes are explained by the assumption that there are many mobile particles in the wet specimen before the critical drying stage.

The addition remanence in the apparent ARM is ascribed to the physical rotational remanent magnetization postulated by Stober and Thompson (1979). The alternating magnetic field imparts a vibratory motion to the mobile particles, when the wet specimens are given an ARM. This motion facilitates the rotation for particles to align to the direct field. These mobile particles are carrying the addition remanence superimposed on the ordinary ARM.

Comparison with the acquisition curve and demagnetization curve of the apparent ARM (Fig. 4 and Fig. 6), the addition remanence in the apparent ARM is not only acquired but also demagnetized by the alternating field less than 200 Oe. From this result it appears that the addition remanence is erased by physical random rotation of magnetic particles which contributes to the acquisition of addition remanence. We conclude that the mobile magnetic particles within wet sediments play an important role in demagnetization as well as in the acquisition of remanence in alternating field. The low stability of post-DRM of wet specimen is also explained due to the effect of random rotation of mobile magnetic particles.

The critical drying stage seems to be characterized as a vanishing point of mobile particles or particle units which can be dynamically responsible to the alternating field less than 200 Oe. This inference is supported by the facts (see Fig. 2) that above 200 Oe in alternating field the demagnetization curves of wet specimens before the critical drying stage matched that of specimens at about the critical stage of 62.2%. The magnitude of torques is estimated to be less than 3.5×10^{-12} dyne·cm for the multidomain magnetic particles with radius of 2×10^{-5} cm

to start rotation within wet sediments before the critical stage, where the intensity of magnetization is assumed to be 1/1000 of saturation magnetization (100 emu/g) (Collinson, 1965). After the critical stage magnetic particles have been already settled in so stable positions that they cannot be rotated by the forces caused by the application of alternating field less than 1500 Oe. The energy well in which magnetic particles or units are trapped (Tucker, 1980), in the dry sediments after the critical stage, is presumably more than seven times as deep as that before the critical one.

Torques more than 3.5×10^{-12} dyne·cm are likely caused during drying of wet sediments before the critical stage, because observation of shrinkage during the drying process has shown the major part of shrinkage occurs during the constant rate period (Fig. 1). And it is commonly believed, in the study of the clay and ceramics (Grimshaw, 1971; Ford, 1964), that during a constant rate period of drying each particle is separated from its neighbours by film of water and liquid water is drawn to the surface of the sediments by capillary action. The water film also reduces the resistivity for particles or units to rotate. The physically random rotation is, therefore, the dominant in the wet sediments before the critical drying stage laid down within field free space during drying. The swift decay of the remanence is concluded to be due to the random rotation of the particles in shallow energy wells which are overcome by the torques caused by the application of the alternating field less than 200 Oe.

Since the torques more than 3.5×10^{-12} dyne·cm to magnetic particles arises from the mechanical vibration and deformation, the decay in remanent magnetization would also be observed under these conditions (Barton et al., 1980; Kodama and Cox, 1978).

Discussion

It is now possible to consider the physical origins of decay of remanent intensity during desiccation. The clues to the origins are the inferences that the randomization mechanism may change at the critical drying stage during drying process.

Recently, electron microscopic work (Yong and Warkentin, 1975) indicated the presence of hierarchical fabric systems in soils. They noted that the aggregation of particles formed a unit termed as cluster (or ped) within which the microscopic fabric is recognized. The geometrical arrangement of the cluster units constitutes a macroscopic fabric. Scanning electron microscope photomicrograph of lake sediments showed also the cluster of micron and submicron size particles (Barton et al., 1980).

The fabric systems infer, from the viewpoint of the dynamics, that single particles action hardly occurs in the microscopic fabric even when the magnetic fields are applied. The most important forces are bonds due to the London-Van der Waals force and electrical force in the microscopic fabric, while the forces holding cluster units are chemical bonds. The frictional torques around the particles with radius of 2×10^{-5} cm in the microscopic fabric is estimated to be 2×10^{-8} dyne·cm, where the London-Van der Waals force of 2×10^{-3} dyne and coefficient of static friction of 1, measured for quartz on quartz, are used (Yong and Warkentin, 1975; Weast, 1973). The frictional torques clearly exceed the magnetic torques of 3.5×10^{-12} dyne·cm. On the other hand, since a cluster unit has fairly small surface area relatively to its volume, the cluster units are easily moved by its own gravitational force or forces caused by the application of magnetic field against the chemical forces due to nonclay and inorganic bonding to surface of the cluster unit. It is inferred that the swift decay of the remanence is due to the random rotation of the cluster units within which magnetic particles are also constituents of microscopic fabric.

Slow decay of the post-DRM in the dry specimen after the critical drying stage may be explained by the random rotation of the magnetic particles within the cluster units. These particles are trapped in deeper energy well than the cluster units. The decrease in the rate of the drying is ascribed to the difficulty of rotation of the magnetic particles in the microscopic fabric. The rotation of particles, by the surface tension, caused by the gas/liquid menisci (Noël, 1980) may become important at a much drier stage when the water content is less than the critical moisture content of 30 % on dry basis as shown in Fig. 1.

References

- Barton, C. E., M. W. McElhinny and D. J. Edward (1980) *Geophys. J. R. astr. Soc.*, 61, 355.
- Collinson, D. W. (1965) *J. Geophys. Res.*, 70, 4663.
- Ford, R. W. (1964) *Drying*, Inst. Ceramic. Textbook No.3 (McLaren & Sons Ltd, London) p. 62.
- Grimshaw, R. W. (1971) *The chemistry and physics of clays* (Ernest Benn Ltd, London) p. 1024.
- Henshaw, P. C. and R. T. Merrill (1979) *Earth Planet. Sci. Lett.*, 43, 315.
- Johnson, H. P., H. Kinoshita and R. T. Merrill (1975) *Geol. Soc. Am. Bull.*, 86, 412.
- Kodama, K. P. and A. Cox (1978) *Earth Planet. Sci. Lett.*, 38, 436.
- Noël, M. (1980) *Geophys. J. R. astr. Soc.*, 62, 15.
- Otofujii, Y. and S. Sasajima (1981) *Geophys. J. R. astr. Soc.*, 66, 241.
- Shuey, R. T., R. O. Uglund and C. R. Schmit (1977) *J. Geophys. Res.*, 82, 3739.
- Stober, J. C. and R. Thompson (1977) *Earth Planet. Sci. Lett.*, 37, 139.
- Stober, J. C. and R. Thompson (1979) *Geophys. J. R. astr. Soc.*, 57, 727.
- Tucker, P. (1980) *Geophys. J. R. astr. Soc.*, 63, 149.
- Verosub, K. L., R. A. Ensley and J. S. Ulrick (1979) *Geophys. Res. Lett.*, 6, 226.
- Weast, R. C. (ed.) (1973) *Handbook of chemistry and physics*, 53rd ed. (Chemical Rubber Co., Cleveland).
- Yong, R. N. and B. P. Warkentin (1975) *Soil properties and behaviour* (Elsevier Scientific Publishing Company, Amsterdam) p. 449.

(Submitted to *Geophys. J. R. astr. Soc.*)

NOTE ON THE EXPERIMENTAL ACQUISITION OF REMANENCE
IN SEDIMENT DURING A FIELD REVERSAL

Ikuo KATSURA and Sadao SASAJIMA

Department of Geology and Mineralogy, Kyoto University, Kyoto 606

Introduction

Paleomagnetic records during geomagnetic field transitions show that the reversal in polarity is accompanied by a decrease in intensity of the field and that is taken as the best indication of the time of the reversal in polarity from sediment records (Fuller et al., 1979). These features may not always be seen, they are common to most records. Recent re-depositional experiments have demonstrated the process of post-depositional remanent magnetization (post-DRM) (Irving and Major, 1964; Kent, 1973). This mechanism yields a time lag of the magnetization from the deposition (Løvlie, 1974) and a time lag could be caused by a difference of the blocking depth of the magnetic grains (Løvlie, 1976). The grain mobility is determined by the degree of the compaction and the field intensity (Tucker, 1980). This phenomenon introduces the difference of the magnetic carriers at various compaction stages. For the discovery of the true geomagnetic field change, the additive property of partial post-DRM under the same polarity (Otofujii and Sasajima, 1981) relates to an interpretation of intensity change of remanences during

the transitional zone in sediments. This report shows an experimental result of the acquisition of remanence in centrifuged sediment under given conditions that simulate geomagnetic field reversal and excursion.

Experimental Procedure

A centrifuge type apparatus was set to study the post-DRM acquired during a field transition (Fig.1). The applied field generated in solenoid coils is changeable in sense and intensity within an accuracy of $\pm 5\%$.

Reddish brown marine clays dredged at ST446 off Japan Trench (GH76-2 Cruise of Geological Survey of Japan; Honza, 1977) were used. The clays

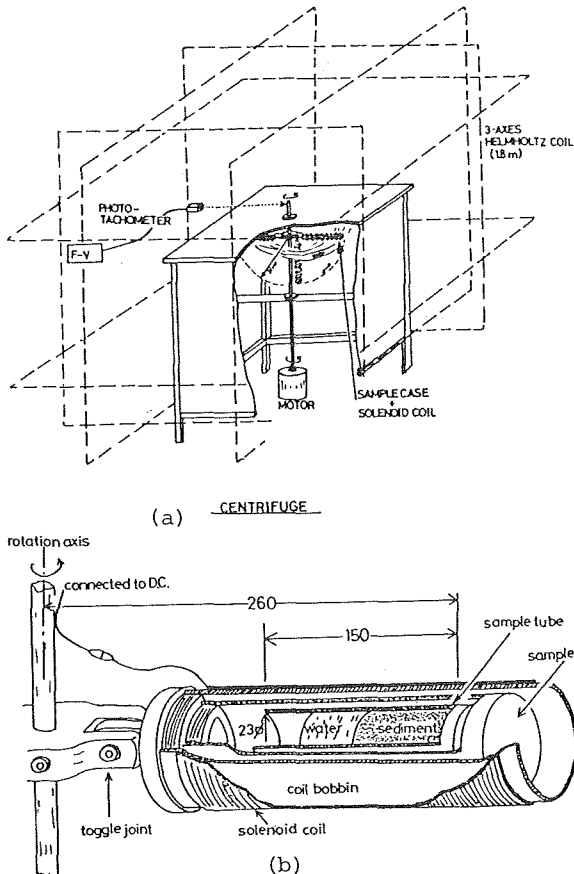


Fig.1 a) Schematic view of the whole apparatus. The geomagnetic field within the rotary space of the samples is canceled less than 1000 gamma. b) Schematic cross section of sample container. Numerals are in millimeter.

were sieved down to 74 μm diameter. The finer sediments were disaggregated with a dispersant "sodium hexametaphosphate" and stirred in distilled water using ultrasonic agitator. The suspensions called "slurry", which were about 4:1 water to solid, were stored in bottles for the experimental runs. Before each run, the slurry was treated in ultrasonic bath for 5 min. Next, the slurry was poured into sample tubes within field free space. The sample tubes were placed in sample holders and a magnetic field was applied while centrifuging. Each run was performed under the rotation at 600 r.p.m. for 300 min.

Immediately after the compaction for 300 min., the core sample was pushed out from tube and cut off its rim kept contact with tube wall. Thus, specimens, each with a tetragonal prism shape, 15 mm \times 15 mm in horizontal section and 5 mm in thickness, were prepared for magnetic measurement. The remanence was measured with a Schonstedt SSM-1A spinner magnetometer.

The natural density of sliced specimen is used as a parameter indicating the degree of compaction throughout this experiment. The natural density (ρ) is estimated from water content (dry basis) with assuming the mean density of solid particles (2.45 g/cm^3 in this study).

Description of Centrifuged Core Sediment

The sediment core sample was compacted to about 4 cm in height from the starting slurry of 9 cm in height. While the rotation was continued at 600 r.p.m., the density change of the core is shown in Fig.2 with respect to the duration of the compaction. These densities are estimated at various duration

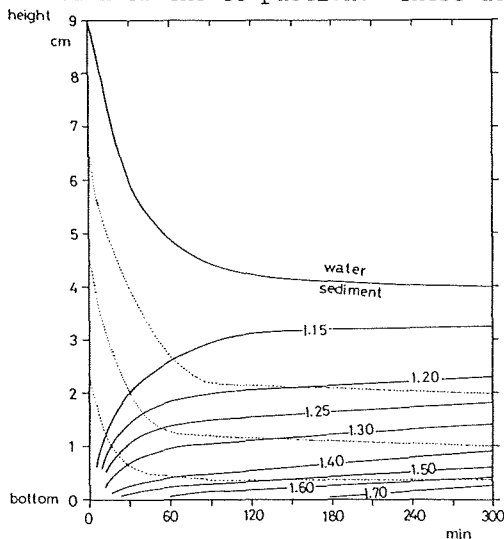


Fig.2 Contours of equal density (g/cm^3) (solid line) and lines of descendings of mean particles (dotted line) in a core during the process of the compaction at 600 r.p.m. for 300 min. Starting slurry is homogenized in the density of 1.13 g/cm^3 . Density (ρ) is calculated from water content (w) (dry basis), as follows;

$$\rho = (w + 1) / (w + 1/\rho_s)$$
 where ρ_s is mean density of solid particles (2.45 g/cm^3 assumed).

of the compaction by the measurement of weights of sliced specimens. This figure shows the distinct increase in density at near the bottom until 30 min. The concentration of coarser grains near the bottom, about 0.5 cm thick, accounts well for this density change.

Ideal movements of mean particles, which is estimated on the basis of the concentration of mean particles producing those density patterns without vertical mixing, are also shown in dotted curves of Fig.2. It reflects clearly that the settling of the particles occurs rapidly before about 60 min. followed by a gradual increase of density.

Experimental Results

(1) preliminary experiment in constant magnetic field; "normal"

A constant polarity, "normal" field ("normal" means the direction toward sample bottom) was applied. For each run, the intensity of the ambient field was varied from 0.20 Oe to 0.95 Oe.

The acquired remanences of specimens subsampled from one core made a tight cluster in remanent directions around the direction of

the applied field ($I=+90^\circ$) with an error angle $\alpha_{95}=2\sim 5^\circ$. The remanent intensities showed an increase with increase in field intensity (Fig.3a). The gradual increase of remanent intensity was observed in the sediment core according to the descending order (Fig.3b).

First, these remanences were progressively demagnetized by alternating field (AF). The results showed no considerable difference in coercivity with different depths of specimens and also no directional change from initial directions. Median destructive field (MDF) was all about 280 Oe.

Next, the acquisition experiment of ARM (anhysteretic remanent magnetization) for the specimens from various depths except the bottom most specimen showed a similar increase in intensity and saturation remanence at the same peak AF level of about 800 Oe. The bottom specimen acquired a stronger intensity. Lastly, the AF demagnetization of these ARMs revealed similar behavior to the initial remanences (post-DRM) in coercivity spectrum. The MDF was about 260 Oe.

These results suggest that the magnetic carriers appear to be made of the same constituents in both post-DRM and ARM according to Amerigian (1977). The bottom specimen should be excluded for further post-DRM studies, because the abundance and size distribution of magnetic particles, and the sedimentary fabric seem to be clearly different from the other parts.

The remanences acquired during compaction process are post-DRM and have following characters. The acquired intensity is proportional to the intensity of the applied field (Fig.3a). The fact is consistent with the results of former studies (Kent, 1973; Otofujii and Sasajima, 1981) and correspondent to the result of the concentrated slurries of Barton et al.(1980). Furthermore, the acquired intensity of post-DRM depends on the density change of sediment (Fig.3b). The acquired intensity of post-DRM of sediments, which underwent a large increase in density due to the rapid compaction, is larger than the intensity of the other post-DRM which is acquired during little increase in density for same time duration of compaction from the same state. These two points are accepted as the fundamental properties of post-DRM acquisition.

(2) experiments under field patterns with "normal/free" and "free/normal"

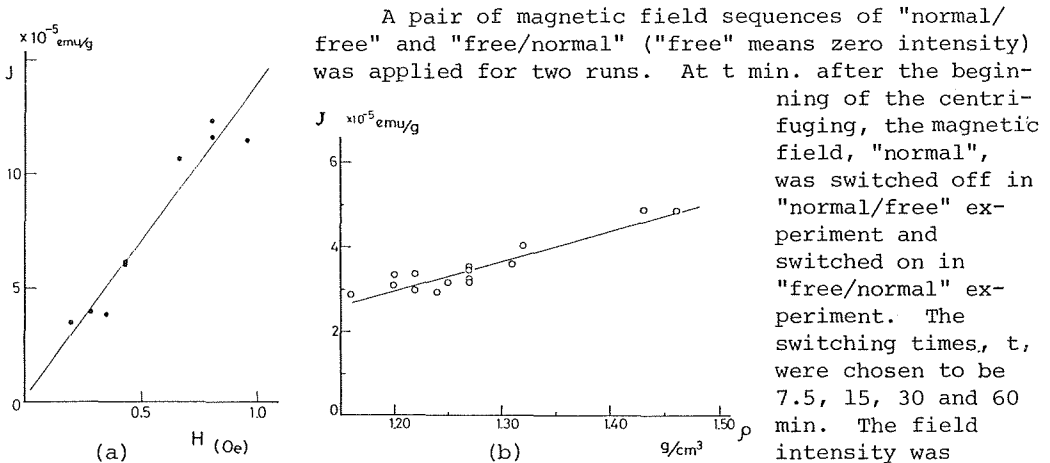


Fig.3 a) Field intensity dependence of remanent intensity. Sediments were compacted by 600 r.p.m. for 300 min. from starting density of 1.13 g/cm^3 . Specimens were selected from cores on the condition that the final density of sediment was 1.22 g/cm^3 . b) Linear proportional increase of the remanent intensity to the increase of natural density. Samples were compacted by 600 r.p.m. for 300 min. in "normal" field with 0.30 Oe in intensity.

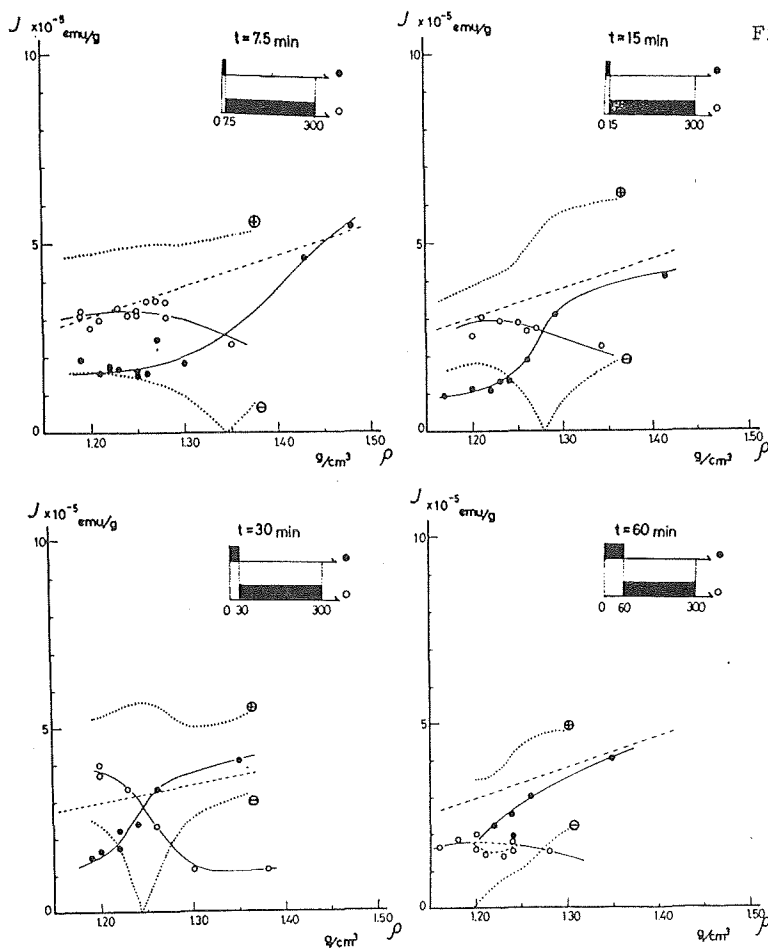


Fig.4 Remanent intensities acquired in "normal/free" (solid circle) and "free/normal" (open circle) fields with respect to the specimen densities. Switching times of the field were 7.5, 15, 30 and 60 min. Broken lines represent the standard intensity as Fig.3b. Intensity of "normal" field was 0.30 Oe. Furthermore, the addition intensity and the difference intensity from "normal/free" and "free/normal" results are shown in dotted lines with plus (+) and minus (-) marks.

preserved in 0.30 Oe during "normal" field. The changes of the remanent intensity are shown in Fig.4 with respect to the density of the specimens.

Two kinds of post-DRMs acquired in "normal/free" and "free/normal" field sequences, which are both switched at time t , reveal distinct changes in intensity at about same density zone. It appears that the zone representing distinct intensity change shifts upward to the lower density horizon as a function of the field switching time (t). The zone is varied from about $\rho=1.35 \text{ g/cm}^3$ at $t=7.5 \text{ min.}$ to about $\rho=1.20 \text{ g/cm}^3$ at $t=60 \text{ min.}$

We attempted to interpret our experimental results in terms of the additive property (Otofujii and Sasajima, 1981). If the additivity of partial post-DRM holds good during this compaction process, the resultant post-DRM acquired in "normal" field experiment should be represented by following expression;

$$J_N(J_{O,H}^{300}) = J_{N/O}(J_{O,H}^t + J_{t,O}^{300}) + J_{O/N}(J_{O,O}^t + J_{t,H}^{300}) \quad \dots (1),$$

where J_N , $J_{N/O}$ and $J_{O/N}$ are total post-DRM acquired in "normal", "normal/free" and "free/normal" experiments, respectively, and the other J in bracket represents partial post-DRM acquired in various field conditions; $J_{t_1,H}^{t_2}$ means a partial post-DRM acquired in the constant magnetic field (H Oe) during the compaction stages from t_1 to t_2 . It is noted that the partial post-DRM acquired in null field is equal to zero. However, the results of experiment (see Fig.4) imply the relation, $J_{O,H}^{300} < J_{O,H}^t + J_{t,H}^{300}$. This fact

means that there is a difference from the additive manner (Otofujii and Sasajima, 1981) in this compaction process. The difference could mostly be resulted from the experimental technique using thin slice specimen.

(3) field reversal experiment; "normal/reverse"

A magnetic field sequence of "normal/reverse" was applied. At t min. after the start, the polarity of the field was switched from normal to reverse. The switching times, t , were chosen to be 7.5, 15, 30, 45 and 60 min. The field intensity was preserved always in 0.30 Oe irrespective of "normal" and "reverse" fields.

A result unexpected of this step was a gradual decrease and gradual recovery of remanent intensity in transitional zone, of which remanences were acquired during an instantaneous applied field reversal. The directional changes of remanences with different field switching times are shown on the equal area projection (Fig.5a). The reversal cannot be recorded over $t=45$ min. Changes in remanent intensity and inclination are plotted on Fig. 5b with respect to the specimen depth. These results show that the transitional level to reversed polarity shifts upward in accordance with the increase of the field switching time, t . These transitional zones accompany the decrease in intensities. It is, of course, confirmed that the remanent directions in transitional zone are stable to AF demagnetization treatment. In spite of a weak initial intensity of boundary specimen, the MDF is about 270 Oe.

Suppose that every partial post-DRM, $J_{t1,H}^{t2}$, represents the net acquired increment of remanent intensity as like as the resultant intensity of "normal/free" and "free/normal" experiments. The additivity of partial post-DRM during a field reversal could be rewritten by a modified expression of eq.(1), as follows;

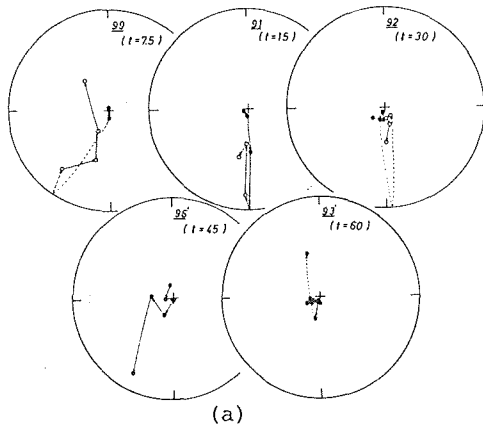
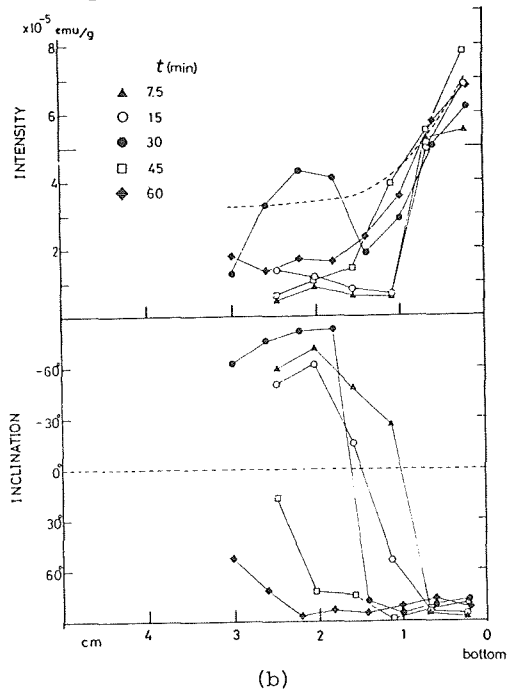


Fig.5 Results of "normal/reverse" experiment. a) Directional changes from normal to reverse plotted on equal area projection. Solid circle and open circle represent on lower and upper hemispheres, respectively. Switching times of the field were 7.5, 15, 30, 45 and 60 min. Both "normal" and "reverse" fields were 0.30 Oe.



b) Remanent intensities and inclinations plotted on specimen depths. Symbols in figures represent various field switching times. Broken line in intensity plot represents the standard remanent intensity of "normal" field of 0.30 Oe.

$$J_{N/R} (J_{0,H}^t + J_{t,H}^{300}) = J_{N/O} (J_{0,H}^t + J_{t,O}^{300}) - J_{O/N} (J_{0,O}^t + J_{t,H}^{300}) \quad \dots (2),$$

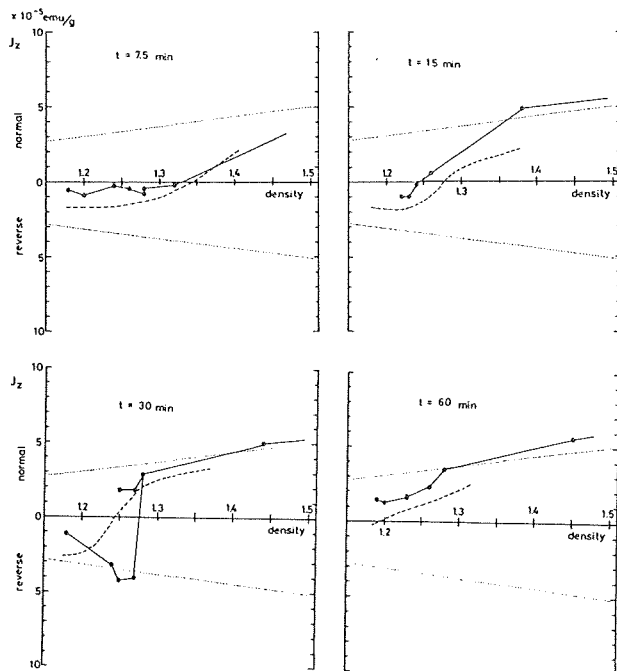
where \bar{H} is an intensity of the reversed field as same as H in normal field. The left term of the formula means that the total post-DRM ($J_{N/R}$) is divided into two components of partial post-DRMs.

It follows to compare the actual results of field reversal experiment with expected ones based on eq.(2). Fig.6 shows remanent intensities, $J_{N/R}$, acquired in a "normal/reverse" experiment, with respect to density. In the diagrams, the expected intensity values, $J_{N/O} - J_{O/N}$ ($J_{O/N} = -J_{O/R}$), calculated by eq.(2) are plotted. The results of $J_{N/R}$ show a similar trend with the expected intensity change. It is noticeable that the normal/reverse boundary shown by the intersections of both actual $J_{N/R}$ and expected $J_{N/O} - J_{O/N}$ with the abscissa (zero intensity) shifts to the lower density horizon in accordance with the delay of the switching time of the field.

There is a linear relationship between the logarithm of the field switching time (t) and the natural density of expected intensities intersecting the abscissa of Fig.6 (Fig.7). The plots of the relation between final density and log-t of the actual intensities intersecting the abscissa of Fig.6 are also shown in Fig.7 as cross marks. This diagram means that the layer of remanence showing the normal/reverse boundary could be estimated from the field switching time.

The sediment particles which carry the normal/reverse boundary can be inferred to come down from an upper horizon along the line of grain descensions depicted in Fig.2. These boundary particles have lain in the lower density zones (about $\rho = 1.15 \text{ g/cm}^3$) at the field switching time. In "normal/reverse" experiment, the sediments acquired reverse records only when they were not compacted larger than $\rho = 1.16 \text{ g/cm}^3$ from initial slurry ($\rho = 1.13 \text{ g/cm}^3$) before the field switching time (t). The sediments experienced a large increase in density (larger than 1.16 g/cm^3) before the application of the reverse field.

The remanent intensity and polarity of total post-DRM in all horizons



of the sediment core are determined by the difference of normal ($J_{0,H}^t$) and reverse

Fig.6 Intensity - density relations obtained from "normal/reverse" field experiment (solid circle with solid line). Expected intensities are also shown in broken lines. These expected intensities are estimated from the results of "normal/free" and "free/normal" experiments based on eq.(2). The broken line consists with the "minus" results of Fig.4. Switching times of the field were 7.5, 15, 30 and 60 min., respectively. Dotted line represents the standard intensity curve due to "normal" field of 0.30 Oe.

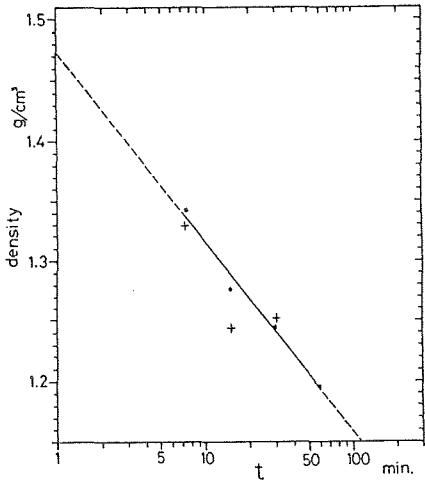


Fig.7 Linear relation between the logarithm of the switching time of the field and the natural density of normal/reverse boundary specimens finished the through compaction. Solid circle and cross symbol represent the actual result of "normal/reverse" experiment and the expected result based on eq.(2), respectively. Normal/reverse boundary specimens are shown as the intersections of the results with the abscissa in Fig.6.

($J_{t,H}^{300}$) fractions of partial post-DRMs. Fig.7 represents the relation between $\log t$ and final density of the sediments representing normal/reverse boundary ($|J_{0,H}^t| = |J_{t,H}^{300}|$). In this figure, the lower density area from the line carries reversed post-DRM ($|J_{0,H}^t| < |J_{t,H}^{300}|$), and the higher density area from the line carries normal post-DRM ($|J_{0,H}^t| > |J_{t,H}^{300}|$).

area from the line carries normal post-DRM

(4) field excursion experiment; "normal/reverse/normal"

An applied magnetic field was controlled as simulating the geomagnetic excursion with a "normal/reverse/normal" field sequence for each run. The field excursion was set in at 15 or 20 min. after the start. The duration of the reverse field was varied from 5 min. to 60 min. The field intensity was preserved always 0.43 Oe in both "normal" and "reverse" fields.

Diagrams in Fig.8 show the changes of intensity and inclination in the remanence with respect to the specimen depth.

The reversed duration plays an important role in post-DRM acquisition. The reversed inclinations are only recorded in the cores which have experi-

enced the reverse field for a longer duration than 30 min. The remanent intensities produced by the field excursion show the minimum at reversed zone or two minima at transitional zones. The range of the intensity decrease

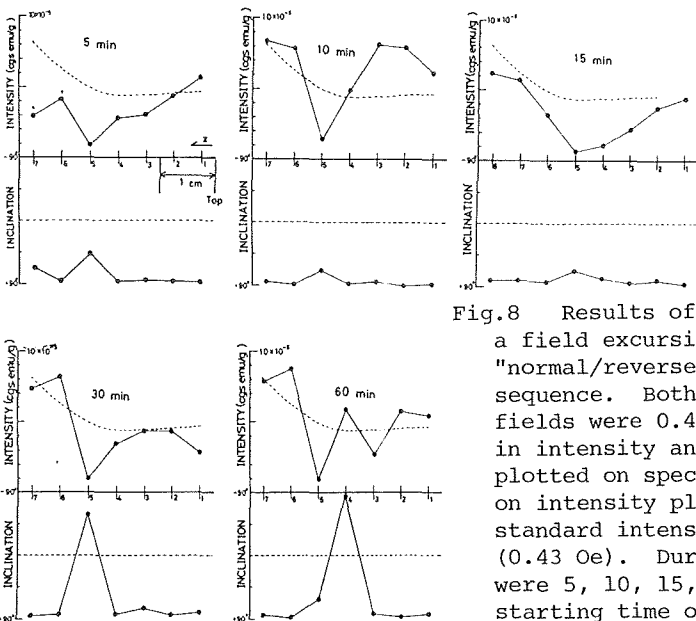


Fig.8 Results of experiment simulating a field excursion as a manner of "normal/reverse/normal" applied field sequence. Both "normal" and "reverse" fields were 0.43 Oe. Remanent changes in intensity and inclination are plotted on specimen depth. Dotted line on intensity plot represents the standard intensity of "normal" field (0.43 Oe). Durations of reverse fields were 5, 10, 15, 30 and 60 min. The starting time of reverse field was 15 min. (for reverse durations of 5, 10, and 60 min.) and 20 min. (for reverse durations of 15 and 30 min.) after the start of centrifuging.

includes the range of the directional transition. Since the compaction process of core sediment is previously established to be reproducible by repeated runs of the experiment, it can be stated that the recorded range of a field reversal reflects the duration of each excursion, and that a very short excursion could not be discovered.

Discussion

The range of the decrease in remanent intensity accompanied with a significant directional change under field excursion experiment (see Fig.8) may be a confession of the true existence of additive property in the acquisition of post-DRM. Detailed measurement of field transition zone of deep-sea sediments have shown that the intensity of remanences begins to drop prior to and posterior to the directional change (Hammond et al., 1979), or to say the least, that the drop in intensity is coincident with the directional change (Opdyke et al., 1973). The intensity decrease associated with reversals appears to be longer than the time duration of directional transition in other records with the exception of that in deep-sea sediments (Hillhouse and Cox, 1976; Dodson et al., 1978). This phenomenon could be caused by the existence of two opposed polarity components of post-DRM (Kobayashi et al., 1971; Løvlie, 1976). Furthermore, we obtained experimental indication of field reversal and excursion, which showed the decrease in remanent intensity with instantaneous polarity transition. These facts should afford some constraints on the interpretation of ancient geomagnetic behaviors recorded in sediments. They are that the possible decrease of the geomagnetic dipole moment during transition (Cox et al., 1975; Fuller et al., 1979) is dubious in its time duration, and that the more quick geomagnetic pulse or excursion, if existed in nature, it cannot possibly be observed in sediments as fossil remanences (total post-DRM). Two opposed components of partial post-DRMs contribute to a measurable total post-DRM in accordance with the additive property.

References

- Amerigian, C. (1977) *Earth Planet. Sci. Lett.*, 36, 434.
Barton, C.E., M.W. McElhinny and D.J. Edwards (1980) *Geophys. J. R. astr. Soc.*, 61, 355.
Cox, A., J. Hillhouse and M. Fuller (1975) *Rev. Geophys. Space Phys.*, 13, 185.
Dodson, R., J.R. Dunn, M. Fuller, I. Williams, H. Ito, V.A. Schmidt and Y.M. Wu (1978) *Geophys. J. R. astr. Soc.*, 53, 373.
Fuller, M., I. Williams and K.A. Hoffman (1979) *Rev. Geophys. Space Phys.*, 17, 179.
Hammond, S.R., S.M. Seyb and F. Theyer (1979) *Earth Planet. Sci. Lett.*, 44, 167.
Hillhouse, J. and A. Cox (1976) *Earth Planet. Sci. Lett.*, 29, 51.
Honza, E. (1977) in Honza ed. *Geol. Surv. Japan Cruise Report, No.7*, 1.
Irving, E. and A. Major (1964) *Sedimentology*, 3, 135.
Kent, D.V. (1973) *Nature*, 246, 32.
Kobayashi, K., K. Kitazawa, T. Kanaya and T. Sakai (1971) *Deep-Sea Res.*, 18, 1045.
Løvlie, R. (1974) *Earth Planet. Sci. Lett.*, 21, 315.
Løvlie, R. (1976) *Earth Planet. Sci. Lett.*, 30, 209.
Opdyke, N.D., D.V. Kent and W. Lowrie (1973) *Earth Planet. Sci. Lett.*, 20, 315.
Otofujii, Y. and S. Sasajima (1981) *Geophys. J. R. astr. Soc.*, 66, 241.
Tucker, P. (1980) *Geophys. J. R. astr. Soc.*, 63, 149.

(To be published in *Mem. Fac. Sci., Kyoto Univ., Geol. Min.*)

MAGNETIC SUSCEPTIBILITY ANISOTROPY OF CHONDRITIC METEORITES

Yozo HAMANO and Kiyoshi YOMOGIDA

Geophysical Institute, Faculty of Science, University of Tokyo
Bunkyo-ku, Tokyo 113, JAPAN

Introduction

It is widely known that the chondrites have strong magnetic anisotropies. Stacey et al. (1961) measured the magnetic anisotropy of some chondrites by means of a torque meter, and found a good correlation between magnetic grain elongations, which can be estimated from the anisotropy measurements, and the degree of compaction of the chondrites as reflected in their porosities (cf. Fig. 2). Their observation indicates a potential usefulness of the magnetic anisotropy measurements for studying the formation process of meteorites. However, their measurements are with only eight chondrites, and it is too early to draw any conclusion from the measurements. Other problem of their measurements is that they observed the magnetic anisotropy in one plane. Hence, the obtained anisotropy gives a minimum value for each chondrite, and the shape of the anisotropy ellipsoid can not be inferred from their measurements. The shape is a good indicator for the cause of the anisotropy.

In the present paper, we will show the results of the magnetic susceptibility measurements and discuss the inference derived from the anisotropy measurements.

Samples and experiments

For the present measurements, we used eleven Antarctic meteorites, which have been collected and distributed by Natl Polar Res. Inst. All the meteorites are ordinary chondrites with rock types of H and L. The samples have a rectangular shape with a volume of more than 1 cc. Before the magnetic measurements, physical properties of these chondrites were observed. The properties are bulk density, intrinsic density, and porosity. The intrinsic density was measured by a helium pycnometer, and the bulk volume of each sample was observed with a standard immersion technique. The bulk density and the porosity were calculated from the above results. Table 1 summarizes the observed properties for the present samples. The properties are the fundamental parameters for the discussion of the origin of chondrites.

The magnetic susceptibility anisotropy was measured with a SSM-1A Schonstedt spinner magnetometer and a Bison susceptibility bridge. The spinner gives five independent values in the anisotropy matrix, that is, (K22-K11), (K33-K22), K23, K31, K12. In order to determine the full anisotropy matrix, one more independent measurement is necessary. For the purpose we used the Bison susceptibility bridge to measure K33.

The theory and the operation of the anisotropy measurement with a spinner are explained by Noltimier (1971). We employed a 6-spin measurement so that the effect of the sample inhomogeneity was minimized. The duplicate measurement indicated that the accuracy of the measurement was about 3%. Repeated measurement with a Bison susceptibility bridge indicated that the accuracy of the measurement was also about 3%. For the determination of the susceptibility matrix, susceptibility in one direction is sufficient. However, since the absolute value of the susceptibility observed by the Bison bridge essentially

TABLE 1. Physical properties of the chondrites

Sample name	Rock type	Volume (cc)	Intrinsic density (g/cc)	Bulk density (g/cc)	Porosity (vol.%)
Y 74191	L3	3.14	3.60	3.23	10.3
Y 75097	L4	3.77	3.65	3.27	10.3
ALH769	L6	2.44	3.59	2.89	19.4
ALH78103	L6	3.52	3.73	3.23	13.4
ALH78251	L6	3.56	3.70	3.21	13.2
MET78003	L6	1.92	3.61	3.33	7.8
ALH77231	L6	1.28	3.58	3.07	14.3
Y 74156	H4	5.20	3.80	3.45	9.2
Y 74647	H45	3.25	3.83	3.48	9.1
ALH77294	H5	2.20	3.84	3.34	12.9
ALH77288	H6	2.81	3.77	3.69	2.0

determines the degree of the anisotropy, a conversion factor between the two apparatuses has been calculated by measuring the susceptibilities in three mutually perpendicular directions.

From the above measurements, three eigen values and eigen vectors of the susceptibility matrix were calculated with a standard technique. The results gives three principal susceptibilities and their directions. The obtained directions do not coincide with the directions of the sides of the sample rectangular, suggesting that the effect of the sample shape on the susceptibility anisotropy is relatively small. But for a detailed discussion, the effect should be considered.

TABLE 2. Results of the susceptibility measurements

Sample name	Principal susceptibilities			Mean K	Anisotropy parameters		Mean grain elongation (1 - c/a)
	K1	K2	K3		A	B	
	(0.001 G/oe)						
Y 74191	14.9	14.6	10.3	12.9	1.02	1.43	0.254
Y 75097	19.8	18.7	14.1	17.1	1.06	1.33	0.192
ALH769	13.1	13.0	10.0	11.9	1.01	1.29	0.188
ALH78103	15.2	13.9	11.4	13.3	1.09	1.22	0.123
ALH78251	14.7	14.4	11.5	13.3	1.02	1.25	0.163
MET78003	20.5	19.8	14.2	17.7	1.04	1.39	0.230
ALH77231	18.0	17.4	14.2	16.4	1.03	1.22	0.145
Y 74156	47.5	46.0	32.3	40.7	1.03	1.42	0.248
Y 74647	60.5	57.2	47.0	54.2	1.06	1.22	0.134
ALH77294	44.3	43.3	31.0	38.5	1.02	1.40	0.241
ALH77288	39.4	39.3	37.6	38.7	1.01	1.05	0.032

Results

The results of the susceptibility measurements are summarized in Table 2. K_1 , K_2 , and K_3 are the maximum, the intermediate, and the minimum principal susceptibility respectively, and the mean susceptibility, K , is calculated by

$$(1/K) = (1/K_1) + (1/K_2) + (1/K_3) .$$

The susceptibilities in the chondrites are generally high compared to those in terrestrial rocks (for example, see Lindsley et al., 1966), and the H chondrites have larger susceptibilities than L chondrites. These can be attributed to the facts that the magnetism in the chondrites is carried by Fe-Ni alloys, the content of which ranges from about 3% to 25%, and the iron content in H chondrites is much higher than that in L chondrites.

For the description of the anisotropy, various kinds of parameters have been used (cf. Kligfield et al., 1977). In Table 2 the anisotropy parameters, A and B , are listed, where the parameters are defined by

$$A = (K_1/K_2) , \quad B = (K_2/K_3) .$$

From the two parameters, the flattening parameter, F , can be calculated by

$$F = (A - 1) / (B - 1) .$$

Since F varies from 0 to 1 for oblate ellipsoids and from 1 to infinity for prolate ellipsoids, it is a quantitative parameter for describing the relative shape of the susceptibility ellipsoid.

As evident from Table 2, the susceptibility anisotropy in the chondrite is very large compared to that in the usual terrestrial rocks. This is probably due to the difference of the shape between iron, which is the dominant magnetic mineral in ordinary chondrites, and magnetite, which is common magnetic phase in terrestrial rocks.

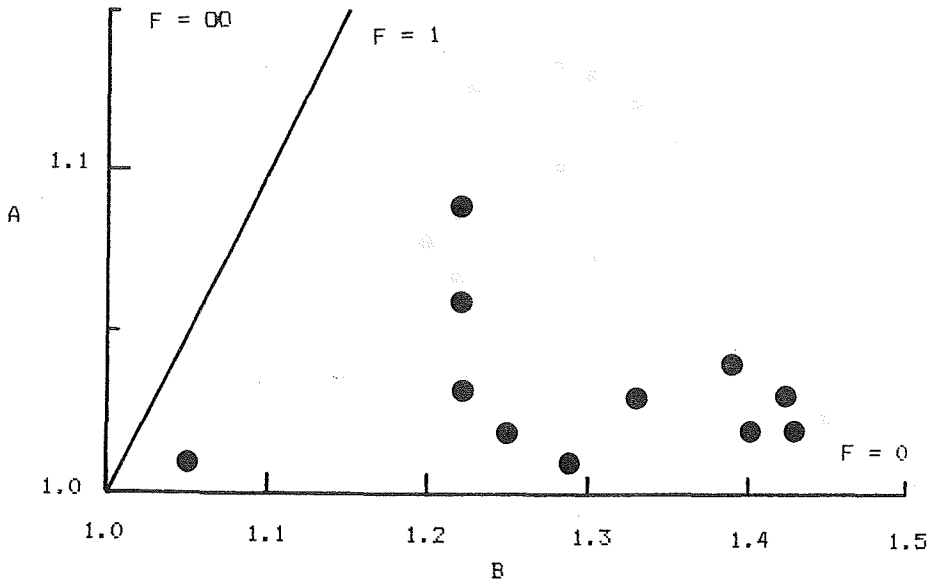


Fig. 1 Susceptibility plot for the present chondrites. The parameters A , B , and F are defined in the text.

In order to investigate the type of the anisotropy, we plotted the anisotropy parameters A and B in Fig.1. This susceptibility plot indicates the shape of the susceptibility ellipsoid. As shown in the plot, the flattening parameter F, is very small (less than about 0.4), which indicates that the shape of the susceptibility ellipsoid is oblate. And the oblate shape suggests that the stress system, which caused the anisotropy, is uni-axial compression type. This observation must be useful to investigate the origin of the susceptibility anisotropy and the origin of the chondrites.

In their experiments, Stacey et al.(1961) observed a torque curve under a high magnetic field (14 kG), and calculated the mean magnetic grain elongation. In the present case, we observed weak field magnetic susceptibilities. In order to compare the present results with the previous work, we calculated the mean grain elongation from the observed susceptibilities. Because iron grains in chondrites are large, it is reasonable to assume that the demagnetizing field in the magnetic grains determines the observed susceptibility. Then, the susceptibility of the sample is inversely proportional to the demagnetizing coefficient in the direction, and the ratio of the susceptibilities in two perpendicular directions gives the ratio of the respective demagnetizing coefficients. Assuming the grain shape of the oblate spheroid, the above statement can be expressed by equation

$$\frac{K_3}{(K_1 \times K_2)^{1/2}} = N / (1-2N)$$

where N is the demagnetizing coefficient in the plane perpendicular to the minimum susceptibility axis. The grain elongation can be calculated from the demagnetizing coefficient by a standard formula (Bozorth, 1951). The results of the calculation is given in Table 2, and Fig.2 shows the relation between the grain elongation and the porosity observed for each sample

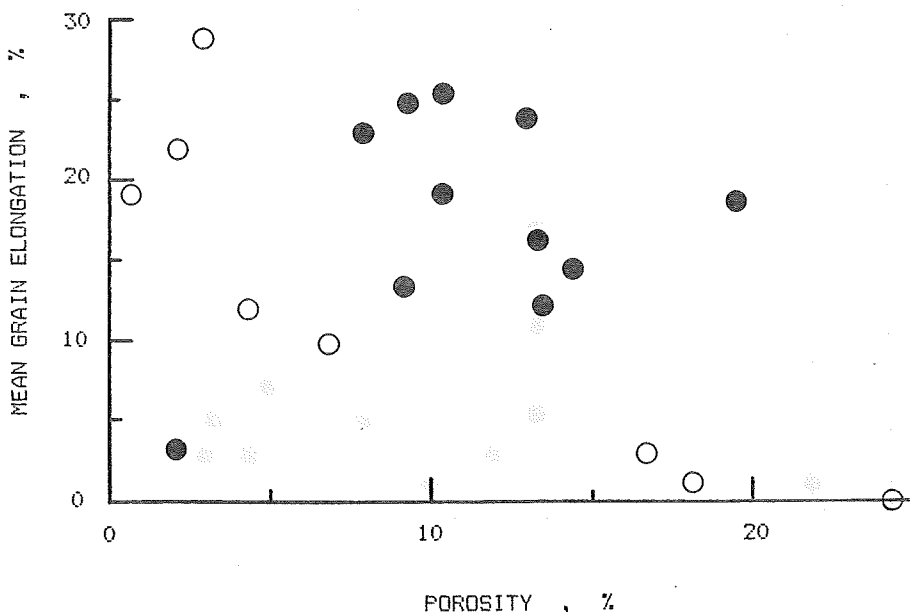


Fig. 2 Mean magnetic grain elongation vs. porosity. ○; Stacey et al.(1961), ●; present work.

In Fig.2 both the present results and the results by Stacey et al. (1961) are plotted. Although Stacey et al. noted a strong correlation between the porosity and the grain elongation, the relation is not obvious for the present data. This fact suggests that more than two factors control the porosity and the grain elongation.

Before closing this section, it is worth while to examine the meaning of the "magnetic mean grain elongation". This value shows the real grain shape only when these grains are perfectly allined in the sample. If elongated grains are randomly distributed in the sample, the sample will not show an anisotropy. Therefore, the "mean grain elongation" obtained from the susceptibility measurements gives a minimum value for the magnetic grain shape. Both the directional distribution of the grains and the grain shape affect the observed anisotropy. This is important for the interpretation of the magnetic anisotropy measurements.

Discussions

From the magnetic anisotropy measurements it is evident that the chondrites have a large magnetic anisotropy. Origin of the anisotropy might be a useful clue for the early evolution of the solar system. Chondrites had been experienced many events before they were found on the earth's surface. The process must have affected the physical and the chemical properties of the chondrites.

Evidently chondrites have been formed in their parent bodies. The evolutionary process can be conveniently divided into two periods at the time of the chondrite formation. During the post-formation process, the parent bodies were destructed. This event and the later collision give large compressional stress on the chondrites, which may cause the uni-axial anisotropy in the chondrites. Very large deformation of the chondrites is necessary to account for the observed anisotropy. However, based on the physical property data on the chondrites (Wood, 1963), it is unreasonable to assume that the chondrites have deformed such a large amount and still keep their cohesivity. Therefore, this later stage of the evolution can not play a dominant role for developing the anisotropy.

Two stages can be considered for the pre-formation process. Initially the proto-planetary materials were non-cohesive and had a powder-like structure. The aggregate of powder suffered a compaction due to the shock compression at the surface of the parent body and the static compression exerted by overlying materials. Besides this compaction stage, the proto-meteorite materials became sintered and metamorphosed by the effect of temperature and pressure inside a parent body. In the later discussion, we call the latter stage as a consolidation stage. Combined effects of the two stages formed the present chondrites. Relative importance of the two stages may be different in each chondrite.

During the compaction process, flattening of iron grains by shock compression and reorientation of the grains would develop the anisotropy. The observed uni-axial compression type anisotropy would be caused by these processes. During the consolidation stage, diffusion type deformation of iron grains may occur if non-hydrostatic stress is operative. But the type of the anisotropy depends on the stress system. Relative importance between the two stages for developing the anisotropy is not obvious. However, some clues can be drawn from the present results shown in Fig. 2. First, the fact that the low metamorphosed chondrites (Type 3 or 4) show very large anisotropy indicates the importance of the compaction stage for enhancing the anisotropy. Second, the highly metamorphosed chondrites (Type 6) have various degrees of anisotropy. This fact also supports the above interpretation.

These two stages are also responsible for varying the porosity of the chondrites. Simply minded, both the processes decrease the porosity. From the previous sintering experiments, the compaction process has dominant effect for decreasing the porosity during the high porosity range and the consolidation process is important in the low porosity range. Contrary to the anisotropy case, the later collision process may also affect the porosity.

The anisotropy-porosity diagram shown in Fig.2 reflects the effects of the above processes. Even if the anisotropy and the porosity has a strong correlation, the later stage may obscure the relation. It can be said that the later stages affect largely on the porosity. In the consolidation process, grain size, chemical composition of the grains, and environmental condition may affect the porosity change. For future study, it is important to investigate whether the orientation of the magnetic grains controls the anisotropy, or the grain shape effect is dominant. Discrimination of pores into the shock-generated cracks and the pores survived during the pre-formation process is also helpful. If these observations can explain the apparent diversity of the data in Fig.2, the anisotropy, porosity, and other physical property measurement can help for studying the early evolution of the solar system.

References

- Bozorth, R.M. (1951) *Ferromagnetism*, D. van Nostrand Co., Princeton N.J.
Kligfield, R., Lowlie, W., and Dalziel, I.W.D. (1977) *Tectonophysics*, 40, 287
Lindsley, D.H., Andreasen, G.E., and Balsley, J.R. (1966) *Handbook of Physical Constants*, Geol. Soc. Am.
Nalimier, H.C. (1971) *J. Geophys. Res.*, 76, 4849
Stacey, F.D., Lovering, J.F., and Parry, L.G. (1961) *J. Geophys. Res.*, 66, 1523
Wood, J.A. (1963) in *Solar System IV*, University of Chicago Press, Chicago

MAGNETIC SURVEYING OF ARCHEOLOGICAL SITES

Hidefumi TANAKA

Department of Applied Physics, Tokyo Institute of Technology
Ookayama 2-12-1, Meguro-ku Tokyo 152, Japan

Archeologists often use geophysical methods for detecting archeological sites (Rainey and Ralph, 1966). Of these, magnetic surveying by proton magnetometer is very simple and easy. In Japan, several authors applied this method to the detection of archeological sites and at the same time studied about basic problems such as noise reduction (e.g., Torii et al., 1974; Iwamoto, 1974). Recently, T. Tanaka (1979) improved on the display method of results and developed an automatical recording system at the site.

Ozaki-Maeyama is an archeological site on a small hill containing several ironmaking furnaces and associated dwelling sites of ninth century which were excavated together by Yachiyo Town and the Research Group of Ironmaking History in Tokyo Institute of Technology (Committee of Education in Yachiyo Town, 1981; Takatsuka et al., 1981; Takatsuka et al., 1979). We made magnetic surveying on this site before the beginning of excavation in order not to really detect sites but rather to know the efficiency of this method by comparing the obtained geomagnetic anomaly map with the real position of detected sites.

We must consider the noise of period longer than five or ten minutes most of which comes from electric trains and the geomagnetic daily variation other than the ordinary noise of very short periods. But we can perfectly exclude the noise of this type by operating two magnetometers at the same time. This is just the same method as is used in the earthquake prediction study at Izu Peninsula, Japan in which one of two magnetometers is used for continuous measurement at a stationary point and the differences of the total force value at each measuring point from that of stationary point are monitored (Rikitake et al., 1981). Another problem is how to set the height of the sensor of proton magnetometer. Height of 1.5 m is usually selected but we had better set the sensor as low as possible within the limitation of not largely suffering from the effect of inhomogeneous magnetization near ground surface.

The area investigated by magnetic surveying is rectangular of about 50 m by 30, and is located on the southern edge of a small hill. Northern flat cultivated field is the area which is already excavated and again filled up in summer, 1979. The noise of geomagnetic field in this area was within $\pm 1 \gamma$ when measured every six seconds for one minutes. In fact, the area had an ideal condition for magnetic surveying without any noise source such as a factory or high voltage line around there. The gradient of variation of total force with vertical direction was smaller than $1 \gamma/m$ in the flat cultivated field and in most cases even the sensor setted just on the ground surface gave a signal good enough to measure total force, so that we adopted 50 cm as a height of the sensor. One of two magnetometers was fixed in the bush near the area to



Fig.1. Total force anomaly and locations of archeological sites.

continuously measure total force every 30 seconds.

The geomagnetic anomaly map (Fig.1) shows differences of the total force on each mesh point of 1m by 1m from that of the stationary point at the same time. Fig. 1 also shows locations of excavated archeological sites. Five sites were discovered from the northern field. Hatched portion shows a furnace. From this map we can know low correlation of total force anomaly with the location of the dwelling site. Careful observation of this map makes it clear that the line of equal total force deflect a little around the furnace in the dwelling site. This anomaly, less than 5 γ , is too small to detect the furnace site, because there are many other small geomagnetic anomalies not related to any archeological sites. The long and slender anomaly to the E-W direction just south of the dwelling site D is caused by the topographic effect of step like land. Some of the very strong anomaly are clearly due to magnetization of a pile made of ferroconcrete.

Three iron-making furnace sites in the southern area were found in the previous excavation. The anomaly of about -40 γ near the furnace site G may be concerned with the magnetization of baked earth in the furnace, but we can't find good correlation between them. Oshiman and Tanaka(1979) already made magnetic surveying in this area by almost the same method but with the sensor of 150 cm height. Their result showed the anomaly pattern similar to that of this report but with less amplitude. The anomaly of about 40 γ in the southwestern part caused by the furnace for baking tile in the Edo period is much emphasized in the anomaly map in this study than that of Oshiman and Tanaka(1979) due to short height of the sensor, but unknown anomaly probably caused by the effect of topography is also much intensified. This suggests that it is not always good idea to make magnetic surveying with low height of the sensor in an area of complicated topography.

This study gave rather pessimistic result for applying magnetic surveying to the detection of archeological sites. This is very natural when we calculate the expected geomagnetic anomaly from the magnetization of a small furnace site by approximating it with a uniformly magnetized sphere(Oshiman and Tanaka, 1979). The largest furnace was found in the dwelling site B and its size was 180 cm x 160 cm x 10 cm. The magnetization of baked earth contained in the furnace was not measured but we can reasonably suppose it as 5×10^{-4} emc/cc because Oshiman and Tanaka(1979) showed that the mean magnetization of the baked earth contained in the furnace site H was 2.26×10^{-4} emu/g. The total force anomaly of 3.2 γ caused by this furnace is expected when we approximate it with the sphere of 40 cm radius locating 1 m underneath the ground surface. The real observed anomaly caused by the furnace is comparable to the above estimated value. But most of the anomaly around 5 γ caused by the magnetization of furnace sites is too small to be distinguished from that by topographic effect.

This study revealed to our regret that magnetic surveying is not powerful to detect an archeological site of small size such as dwelling sites. This is very natural as an estimation of geomagnetic anomaly by a furnace in the dwelling site based on a simple theory comes to very small value of around 5 γ .

But this method will be applicable to the detection of a large scale furnace site as Iwamoto (1974) succeeded to detect an archeological furnace of 2 m x 8 m. As an excavation of archeological sites is very time and money consuming, it is worthwhile to refine this method by introducing new technique such as correction by topography.

References

- Committee of Education in Yachiyo Town (1981) (in Japanese)
- Iwamoto, K. (1974) *Archeology and Science*, 7, 31. (in Japanese)
- Oshiman, N. and H. Tanaka. *Rock mag. Geophys.*, 6, 7, 1979.
- Rainey, F. and E. K. Ralph (1966) *Science*, 153, 1481.
- Rikitake, T., Y. Honkura, H. Tanaka, N. Oshiman, Y. Sasai, Y. Ishikawa, S. Koyama, M. Kawamura, and K. Ohchi (1981) *J. Geomag. Geoelectr.*, 33, 721
- Takatsuka, H., T. Goto, H. Akutsu, M. Okamoto, K. Iida, T. Fukuda, and T. Doke (1978) *Humanities Review, Tokyo Inst. of Technology.*, 4, 147. (in Japanese)
- Takatsuka, J., T. Goto, H. Akutsu, W. Kawanobe, M. Okamoto, H. Tanaka, Y. Honkura, K. Iida, T. Fukuda, and T. Doke (1980) *Humanities Review, Tokyo Inst. of Technology.*, 6, 269. (in Japanese)
- Tanaka, T. (1979) *Archeology and Science*, 12, 128. (in Japanese)
- Torii, M., M. Otani, and H. Nakamura (1974) *Archeology and Science*, 7, 43. (in Japanese)

ELECTRON SPIN RESONANCE DATING OF CALCAREOUS MICROFOSSILS IN DEEP-SEA SEDIMENT

Takaharu SATO

Department of Physics, Faculty of Engineering Science,
Osaka University, Toyonaka, Japan

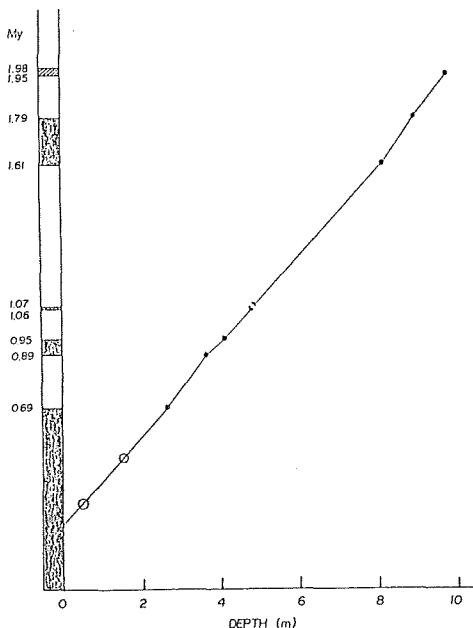
1. Introduction

The dating of deep-sea sediment composed of calcareous ooze is important in paleontology and paleoclimatology. It is also necessary in investigations of the variation in the paleomagnetic field intensity by use of deep-sea cores. Ages of deposition for deep-sea sediment have been estimated on the basis of various isotopic studies (Ku et al., 1968).

Electron Spin Resonance (ESR) of many types of samples has been studied for dating. The samples composed of CaCO_3 such as stalactite (Ikeya, 1975; Miki and Ikeya, 1978) and fossil shells (Ikeya and Ohmura, 1980) have been successfully used for ESR dating.

ESR dating has been made in following ways; (1) The density of radicals produced by natural radiation is measured by ESR. (2) The rate of production of radicals to radiation is estimated on the basis of measurements of ESR signals enhanced by the artificial irradiation. The dose of natural radiation received by the samples can be obtained by extrapolation. (3) One can calculate the age by dividing the dose by the annual dose of natural radiation.

In this paper, ESR of calcareous microfossils in deep-sea sediment whose sedimentation rates have already determined (Sato and Kobayashi, 1980) as shown in Fig. 1 is studied for dating.



2. Sample Preparations and Measurements

Grains 0.250 to 0.503 mm in diameter were selected with sieves from deep-sea sediment (KH 73-4-7 and KH 73-4-8) of cube samples prepared for paleomagnetic study (Kobayashi et al., 1980) and grains except microfossils were taken away under a microscope. ESR of

Fig. 1. Time versus depth plot for core KH 73-4-7 (Sato and Kobayashi, 1980). Depths and ages for two samples used in this study are indicated by open circles.

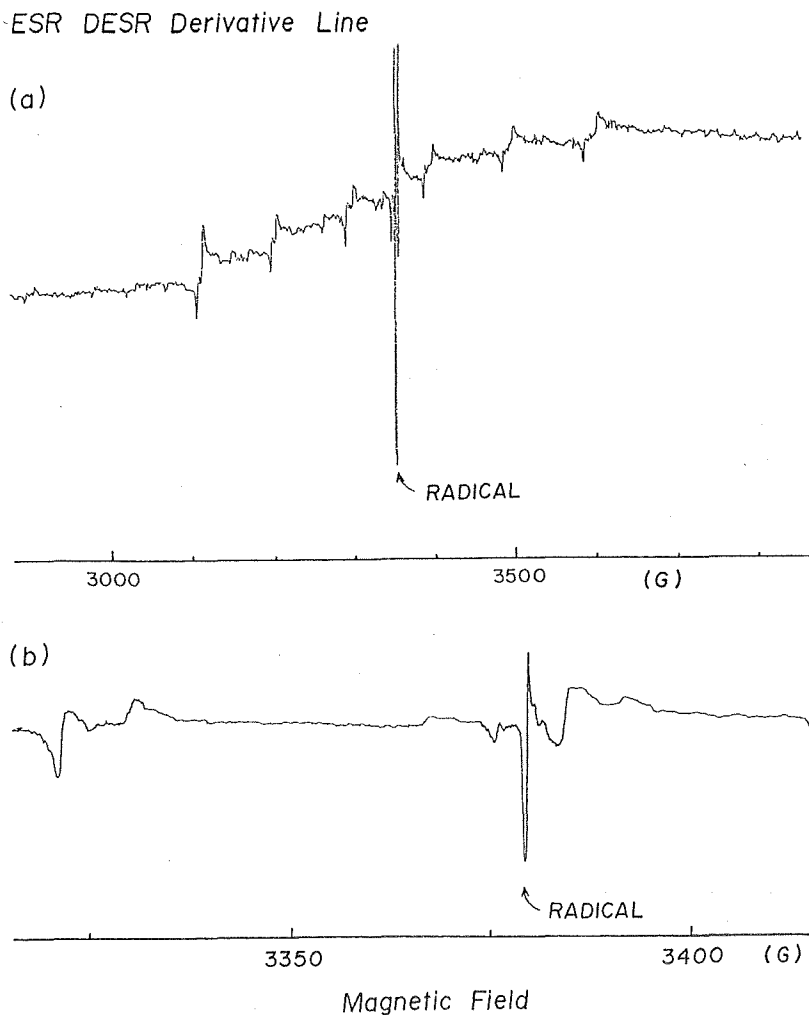


Fig. 2. Typical ESR spectra of calcareous microfossils from (a) core KH 73-4-8 and (b) core KH 73-4-7.

microfossils of 50 mg in weight was measured with JES-ME2X at room temperature. The field modulation at 100 kHz was 1 or 2 gauss. The amount of artificial irradiation received by samples for 1 hour is controlled by means of control of distance from the source of γ -ray.

3. Results and Discussion

Figs. 2a and 2b show typical ESR derivative lines of the microfossils. A signal with $g = 2.004$ is associated with the radicals produced by the natural radiation. The six lines associated with the hyperfine line of Mn^{2+} are observed as shown in Fig. 2a. In order to estimate the relative signal intensity of radicals, the signal intensity at $g = 2.004$ is divided by the signal intensity of Mn^{2+} in the sample or in the standard sample measured together.

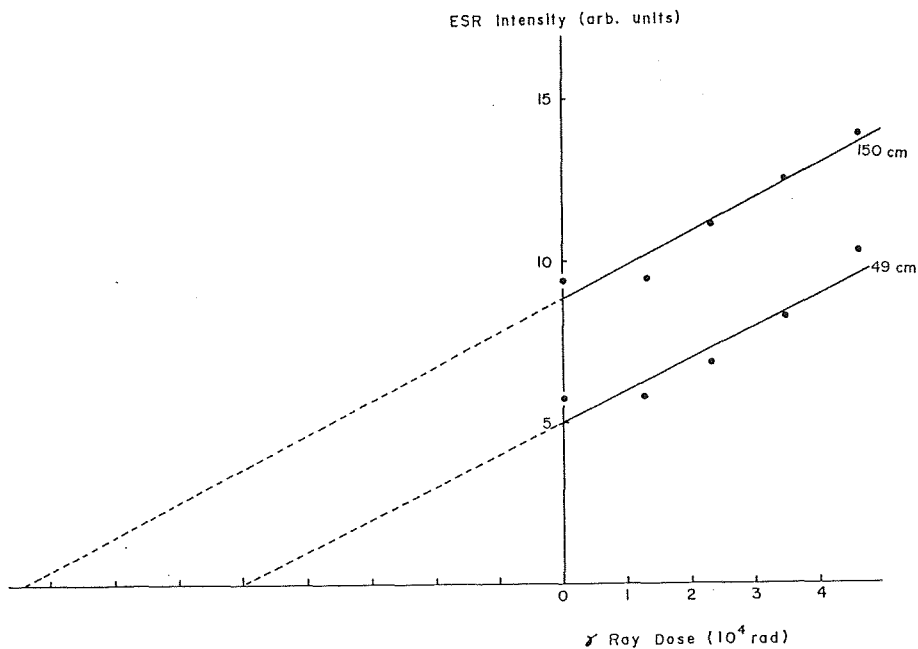


Fig. 3. Growth of the ESR signal of calcareous microfossils from core KH 73-4-7 with artificial γ irradiation.

Fig. 3 shows the enhancement of signal intensity of the microfossils in core KH 73-4-7 induced by ^{60}Co γ irradiation. The signal intensity increased as γ irradiation increased. If linear signal increase is assumed, the archeological doses of 5.0×10^4 and 8.4×10^4 rads for two samples are obtained by extrapolation. The archeological doses obtained here are the amounts of ^{60}Co γ irradiation which produce the same amounts of radicals as the natural radiation composed of α , β and γ -ray produced in the samples. The effect of α -ray is expected to be small, since the defects by α -ray seems only within a few μm of the surface of fossil shell (Ikeya and Ohmura, 1980).

The ages of two samples are estimated from Fig. 1 to be 0.35 and 0.51 Ma. Therefore, the annual radiation doses of two samples are estimated to be 0.14 and 0.16 rad/yr. These dose rates fit the data of about 0.1 to 0.2 rad/yr for cave formation such as stalactites and stalagmites (Ikeya, 1978) and for bones excavated from calcite caves (Ikeya and Miki, 1980). One can approximately estimate the sedimentation rate by assuming a constant annual dose, although the total content of radioactive elements must be accurately measured and estimate the annual radiation dose to investigate detailed variation in sedimentation rate.

Though more accurate estimations for archeological dose are necessary and many problems remain to be solved, it can be concluded that ESR dating is useful for calcareous microfossils in deep-sea sediment.

References

- Ikeya, M. (1975) *Nature*, 255, 48.
Ikeya, M. (1978) *Archaeometry*, 20, 149.
Ikeya, M. and T. Miki (1980) *Science*, 207, 977.
Ikeya, M. and K. Ohmura (1981) *J. Geol.*, 89, 247.
Kobayashi, K., S. Tonouchi, T. Furuta and M. Watanabe (1980)
Bull. Ocean Res. Inst. Univ. Tokyo.
Ku, T. L., W. S. Broecker and N. Opdyke (1968) *Earth Planet.*
Sci. Lett., 4, 1.
Miki, T. and M. Ikeya (1978) *Japan. J. Appl. Phys.*, 17, 1703.
Sato, T. and K. Kobayashi (1980) *Rock Mag. Paleogeophys.*,
7, 16.

MAGNETIC FIELD IN A CIRCULAR SYMMETRIC COIL

Masaru KONO

Department of Applied Physics, Tokyo Institute of Technology
 Okayama 2-12-1, Meguro-ku Tokyo 152, Japan

Magnetic Field on the Axis

A single loop at (z', r') carrying a current I induces at $(z, 0)$ an axial magnetic field $1/2 \mu_0 I r'^2 [(z'-z)^2 + r'^2]^{-3/2}$ where μ_0 is the permeability of vacuum. The magnetic field inside a coil is obtained by integrating this over the cross sectional area of the coil:

$$B_z = \frac{\mu_0 \epsilon I}{S} \int_0^h dz' \int_{r_1}^{r_2} \left[\frac{r'^2}{\{(z'-z)^2 + r'^2\}^{3/2}} + \frac{r'^2}{\{(z'+z)^2 + r'^2\}^{3/2}} \right] dr' \quad (1)$$

where S is the cross section of the conducting wire and ϵ is the packing factor which, in practice, takes a value between 0.7 and 0.8.

The integral in (1) cannot be expressed analytically when r_1 and r_2 are arbitrary functions of z . However, if we divide the coil into $2K$ equal parts and approximate each part by a rectangular coil such as is shown in Figure 1, the axial field can be expressed as

$$B_z(z, 0) = \frac{\mu_0 \epsilon I}{2S} \sum_{k=1}^K \sum_{i=1}^2 \sum_{j=1}^2 (-1)^{i+j} F(z_{k+i-2} - z, r_{jk}) + F(z_{k+i-2} + z, r_{jk}) \quad (2)$$

Where

$$z_k = hk/k$$

$$r_{jk} = r_j [z_{k-1} + \theta_{jk} (z_k - z_{k-1})], \quad 0 \leq \theta_{jk} < 1$$

and

$$F(z, r) = z \log(r = \sqrt{z^2 + r^2}) \quad (3)$$

In most AF coils, $r_1(z)$ and $r_2(z)$ are monotonically decreasing functions of $|z|$, i.e., the radius is broader at the center. For such coils, an upper bound for B_z is obtained by taking $\theta_{jk} = 2-j$, and a lower bound by $\theta_{jk} = j-1$.

Taylor Expansion

In order to calculate the field values at (z, r) , it is convenient to take the symmetry of the coils into consideration. Because of the cylindrical and mirror symmetries, the Taylor Expansion of B_z (B_r) near the origin contains only terms of

even (odd) powers of both z and r (Parry, 1967).

$$B_z = B_{z0} + \frac{z^2}{2!} \left(\frac{\partial^4 B_z}{\partial z^4} \right)_0 + \frac{z^4}{4!} \left(\frac{\partial^4 B_z}{\partial z^4} \right)_0 + \frac{z^2 r^2}{2!2!} \left(\frac{\partial^4 B_z}{\partial z^2 \partial r^2} \right)_0 + \frac{r^4}{4!} \left(\frac{\partial^4 B_z}{\partial r^4} \right)_0 + \dots \quad (4)$$

$$B_r = zr \left(\frac{\partial^2 B_r}{\partial z \partial r} \right)_0 + \frac{z^3 r}{3!} \left(\frac{\partial^4 B_r}{\partial z^3 \partial r} \right)_0 + \frac{zr^3}{3!} \left(\frac{\partial^4 B_r}{\partial z \partial r^3} \right)_0 + \dots$$

where the subscript 0 denotes the value at the origin. Using (4) the next relation can be obtained.

$$\begin{aligned} \frac{B_r}{r} + \frac{\partial B_r}{\partial z} + \frac{\partial B_z}{\partial r} \\ = 2z \left(\frac{\partial^2 B_r}{\partial z \partial r} \right)_0 + \frac{2z^3}{3!} \left(\frac{\partial^4 B_r}{\partial z^3 \partial r} \right)_0 + \frac{4zr^2}{3!} \left(\frac{\partial^4 B_r}{\partial z \partial r^3} \right)_0 + \dots \\ + z \left(\frac{\partial^2 B_z}{\partial z^2} \right)_0 + \frac{z^3}{3!} \left(\frac{\partial^4 B_z}{\partial z^4} \right)_0 + \frac{zr^2}{2} \left(\frac{\partial^4 B_z}{\partial z^2 \partial r^2} \right)_0 + \dots \end{aligned}$$

As the divergence and curl of the magnetic field vector are zero where no current flows, the next equations should hold everywhere inside the coil.

$$\frac{\partial B_r}{\partial r} + \frac{B_r}{r} + \frac{\partial B_z}{\partial z} = 0$$

$$\frac{\partial B_r}{\partial z} - \frac{\partial B_z}{\partial r} = 0$$

By combining these equations, we can easily show that

$$\begin{aligned} \left(\frac{\partial^{2n} B_z}{\partial z^{2n-2m} \partial r^{2m}} \right) &= \left(\frac{\partial^{2n} B_r}{\partial z^{2n-2m-1} \partial r^{2m-1}} \right) = - \frac{2m-1}{2m} \left(\frac{\partial^{2n} B_z}{\partial z^{2n-2m-2} \partial r^{2m-2}} \right)_0 \\ &= \dots = (-1)^m \frac{(2m-1)}{(2m)!!} \left(\frac{\partial^{2n} B_z}{\partial z^{2n}} \right)_0 \end{aligned}$$

Therefore, equations (4) can be rewritten as

$$\begin{aligned} B_z &= B_{z0} + \sum_{n=1}^{\infty} \sum_{m=0}^n \frac{z^{2n-2m} r^{2m}}{(2n-2m)! (2m)!} \frac{(-1)^m (2m-1)!!}{(2m)!!} \left(\frac{\partial^{2n} B_z}{\partial z^{2n}} \right)_0 \\ &= B_{z0} + \sum_{n=1}^{\infty} \sum_{m=1}^n U_n(z, r) \left(\frac{\partial^{2n} B_z}{\partial z^{2n}} \right)_0 \end{aligned} \quad (5)$$

$$\begin{aligned} B_r &= B_{z0} + \sum_{n=1}^{\infty} \sum_{m=1}^{\infty} \frac{z^{2n-2m+1} r^{2m-1}}{(2n-2m+1)! (2m-1)!} \frac{(-1)^m (2m-1)!!}{(2m)!!} \left(\frac{\partial^{2n} B_z}{\partial z^{2n}} \right)_0 \\ &= \sum_{n=1}^{\infty} \sum_{m=1}^{\infty} V_n(z, r) \left(\frac{\partial^{2n} B_z}{\partial z^{2n}} \right)_0 \end{aligned}$$

where

$$U_n(z, r) = \sum_{m=0}^n \frac{(-1)^m z^{2n-2m} r^{2m}}{2^{2m} (m!)^2 (2n-2m)!} \quad (6)$$

$$V_n(z, r) = \sum_{m=1}^n \frac{(-1)^m z^{2n-2m+1} r^{2m-1}}{2^{2m-1} m! (m-1)! (2n-2m+1)!}$$

Parry (1967) has already given the above expressions up to the order of $n=3$. It is now possible to calculate the field strengths inside a coil to any desired accuracies using only B_z and its z -derivatives at the origin.

Calculation of the z -derivatives

From equation (2),

$$\left(\frac{\partial^{2n} B_z}{\partial z^{2n}} \right) = \frac{\mu_0 \epsilon I k}{S} \sum_{k=1}^2 \sum_{i=1}^2 \sum_{j=1}^2 (-1)^{i+j} \frac{\partial^{2n} F(z, r)}{\partial z^{2n}} \Big|_{z=z_{k+i-2}} \quad (7)$$

To obtain the z -derivatives of $F(z, r)$, we first note that

$$\frac{\partial^2 F(z, r)}{\partial z^2} = \frac{z}{r + \sqrt{z^2 + r^2}} \left[\frac{1}{\sqrt{z^2 + r^2}} + \frac{r}{z^2 + r^2} + \frac{r^2}{(z^2 + r^2)^{3/2}} \right]$$

$$= f_{10}(z, r) + f_{11}(z, r) + f_{12}(z, r)$$

where

$$f_{nm}(z, r) = z r^m (r + \sqrt{z^2 + r^2})^{-n} (z^2 + r^2)^{-(n+m)/2} \quad (8)$$

Now, it can be shown that the second derivative of f_{nm} satisfies the relation

$$\frac{\partial^2 f_{nm}}{\partial z^2} = (2n+m)(2n+m-1) f_{m+1, m} + (2n+m)(m-1) f_{n+1, m+1}$$

$$- (3n^2 + 4nm + m^2 + 3n + 2m) f_{n+1, m+2} - (n+m)(n+m+2) f_{n+1, m+3}$$

Therefore, it is possible to write

$$\frac{\partial^{2n} F(z, r)}{\partial z^{2n}} = F^{(2n)}(z, r) = \sum_{m=0}^{3n-1} C_{nm} f_{nm}(z, r) \quad (9)$$

where the coefficients c_{nm} can be determined from the recurrence formula

$$C_{n+1,m} = (2n+m)(2n+m-1)C_{nm} + (2n+m-1)(m-2)C_{n,m-1} - (3n^2 + 4nm + m^2 - 5n - 2m)C_{n,m-2} - (n+m-3)(n+m-1)C_{n,m-3} \quad (10)$$

and

$$C_{10} = C_{11} = C_{12} = 1$$

$$C_{nm} = 0, \text{ for } m < 0 \quad \text{or} \quad m \geq 3n$$

Using equations (5)-(10), we can finally express the magnetic field inside the coil as

$$B_z(z,r) = \frac{\mu_0 \epsilon I \infty}{S} \sum_{n=0}^{\infty} A_n U_n(z,r) \quad (11)$$

$$B_r(z,r) = \frac{\mu_0 \epsilon I \infty}{S} \sum_{n=1}^{\infty} A_n V_n(z,r)$$

where U_n and V_n are defined by (6) and $U_0(z,r) = 1$, and

$$A_n = \sum_{k=1}^k \sum_{i=1}^2 \sum_{j=1}^2 (-1)^{i+j} F^{(2n)}(z_{k+i-2}, r_{jk})$$

$$= \sum_k \sum_i \sum_j (-1)^{i+j} F(z_{k+i-2}, r_{jk}), \quad n=0$$

$$= \sum_k \sum_i \sum_j (-1)^{i+j} \sum_{m=1}^{3n-1} C_{nm} f_{nm}(z_{k+i-z}, r_{jk}), \quad n>0$$

Equation (11) is very convenient for machine calculation because A_n depends only on the shape of the coil and not on the coordinates where the field value is to be calculated, whereas U_n and V_n are solely determined by the position (z,r) .

In equations (11) and (12), the magnitudes of U_n and V_n decreases monotonically while $F^{(2n)}$ increases with increasing n . The number of terms in the summation needed to obtain the magnetic field with a desired accuracy can be estimated by the following manner. The decrease of the magnitude of $U_n(z,r)$ and $V_n(z,r)$ is less rapid for points further from the origin. Usually, field uniformity is required within the sample space which is only a small part of the inner cavity, since sample holders and tumblers must also be fitted inside the coil. It is therefore more than enough if we calculate the field

uniformity in the space $-1/2 < z < 1/2$ and $0 < r < 1/2$, when the inner radius at the center (a) is taken as the unit of the length. Similarly, as $F^{(2n)}(z,r)$ increases with n more rapidly at points closer to the origin, $\lim_{z \rightarrow 0} |F^{(2n)}(z,1)/z|$

may be used as the fastest case of divergence. Such consideration show that terms up to $n=5$ are needed to obtain the field values with an accuracy of about 1%, while the summation must be extended to $n=10$ to obtain a 0.01% accuracy.

Reference

Parry, L.G., in *Methods in Paleomagnetism*, edited by D.W.Collinson et al., Elsevier, 1967.

(In press in *Journal of Geophysical Research*)

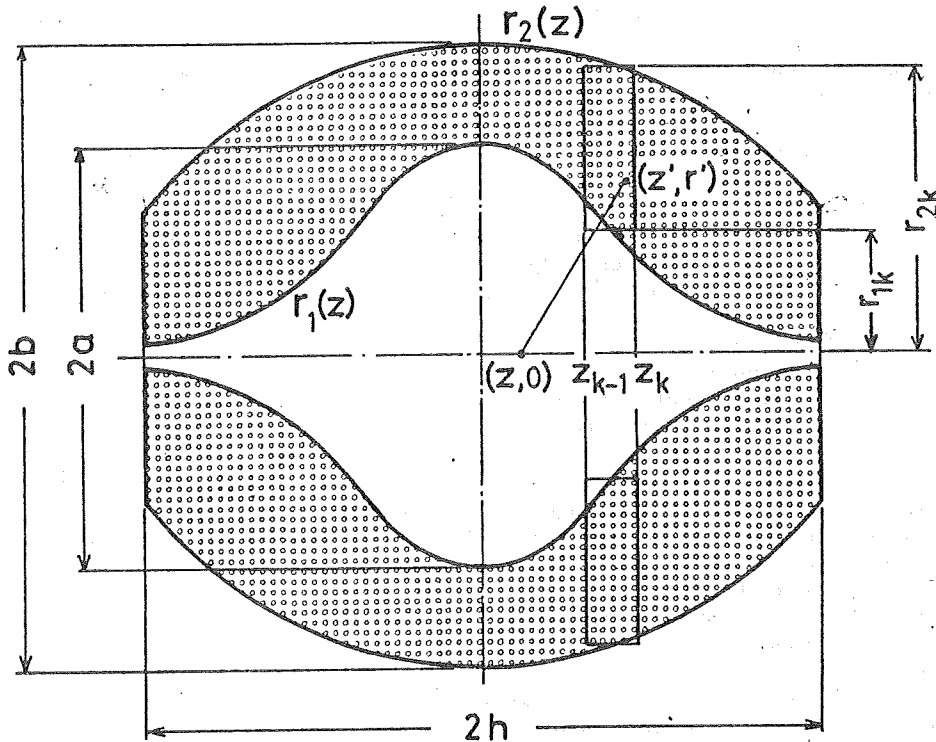


Fig. 1. Geometry of the coil.

NOBLE GAS CONSTRAINTS ON THE LAYERED STRUCTURE OF THE MANTLE

Ichiro KANEOKA

Geophysical Institute, Faculty of Science
University of Tokyo, Bunkyo-ku, Tokyo 113, Japan

1. Introduction

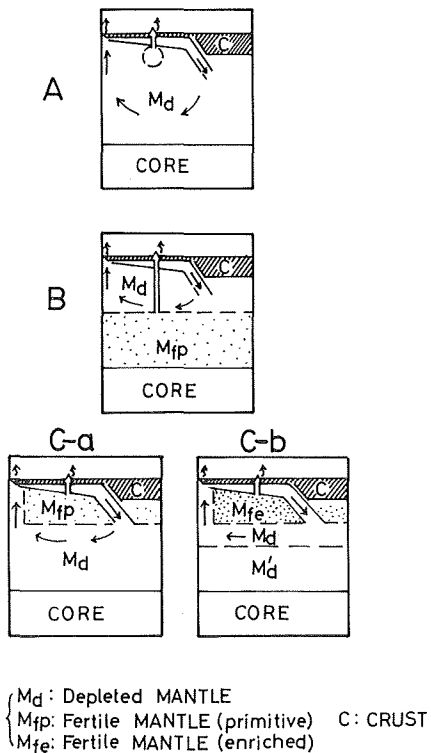
With the accumulation of isotopic data such as Sr, Nd and Pb volcanic rocks from various regions including both the oceanic and continental areas, it has become evident that MORB (Mid-Oceanic Ridge Basalt) does not always represent the characteristics of the source materials in the whole mantle. The combination of Nd and Sr isotopes has revealed that most volcanic rocks from the oceanic islands show lower $^{143}\text{Nd}/^{144}\text{Nd}$ and higher $^{87}\text{Sr}/^{86}\text{Sr}$ ratios compared with those of MORB (e.g. O'Nions et al., 1977). They locate mostly around a line which goes through the value for MORB and the value for the assumed bulk Earth. This line is called as "mantle array" (DePaolo and Wasserburg, 1976). To explain such a trend, there are two main interpretations. One of them is based on the mixing model between the MORB-type source material and the source material similar to that represented by the bulk Earth (e.g. DePaolo, 1980). The other one is that the trend represents the different degree of depletion from the bulk Earth as a function of ages since the time of depletion (e.g. Anderson, 1980).

In the Reykjanes Ridge - Iceland region, it has been observed that the concentration of LIL (large ion lithophile) elements in basalts increases along the Reykjanes Ridge toward Iceland (Schilling, 1973). Furthermore, $^{87}\text{Sr}/^{86}\text{Sr}$ and $^{206}\text{Pb}/^{204}\text{Pb}$ ratios increase from the typical MORB value to higher values along the Reykjanes Ridge toward Iceland in the same region (Sun et al., 1975). Based on the former, Schilling (1973) proposed that a mantle plume is arising from the lower mantle underneath Iceland. To explain such a trend in this region, a hypothesis of mantle heterogeneity is also raised (e.g. O'Nions and Pankhurst, 1973).

Although these examples do not always exclude the possibility of mantle heterogeneity to explain the observations stated above, the mixing between at least two different sources is required to explain the systematic change in the $^3\text{He}/^4\text{He}$ and $^{40}\text{Ar}/^{36}\text{Ar}$ ratios observed in large phenocrysts of volcanic rocks and ultramafic nodules from Hawaiian Islands (Kaneoka and Takaoka, 1980).

Based on these observations, the two chemically layered mantle model becomes more popular; one is the depleted mantle from which MORB is derived and the other is the fertile mantle from which a mantle plume may arise. In principle, it is not always necessary to assume the layered mantle. In effect, a mantle model is proposed where fertile parts are distributed like spots in the depleted mantle (Davies, 1981). Although this model may not always be incompatible with isotopic data on solid elements, it is difficult to explain the occurrence of relatively primordial components of noble gases in the fertile parts. Hence, such a model is not considered here.

Among the two layered mantle model, there are two essentially different ones. One assumes that the upper mantle is depleted, while the lower mantle is fertile (e.g. Jacobson and Wasserburg, 1979). The other assumes that the upper mantle is fertile and the lower mantle is depleted.



The latter is further divided into two alternatives : the fertile mantle is the remains of the primitive mantle (Tatsumoto, 1978) or the enriched one caused by mantle fractionation at some time in the earth's history (Anderson, 1980). These models are schematically shown in Fig. 1, where a model with only the depleted mantle is also included for comparison.

Although these models are proposed on the basis of chemical and isotopic data, the data on noble gases have been neglected to construct them. Since noble gases are considered to be lost from the solid earth when a large mantle fractionation occurs, the data on noble gases will give us different information on the structure of the mantle from that by solid elements. Hence, models shown in Fig. 1 are examined on the basis of noble gas data obtained for Hawaiian samples (Kaneoka and Takaoka, 1980).

Fig. 1. Models on the chemically layered structure of the mantle.

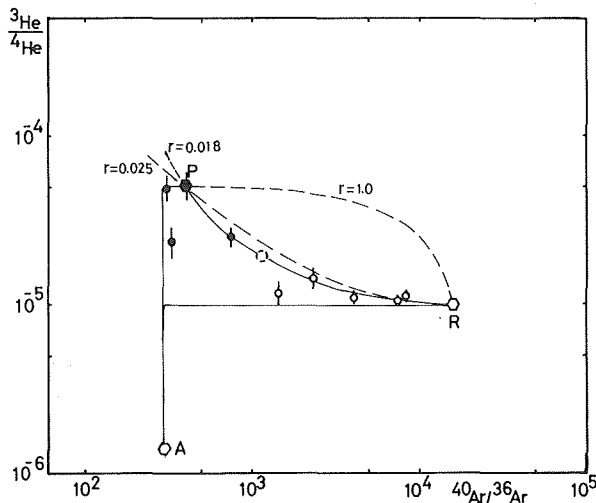


Fig. 2. The $^3\text{He}/^4\text{He} - ^{40}\text{Ar}/^{36}\text{Ar}$ plot for samples from Hawaiian Islands. Closed symbols : Ol and Cpx phenocrysts in volcanic rocks from Hawaii and Maui Islands.

Open symbols : ultramafic nodules from Hawaii and Oahu Islands. (Original data : Kaneoka and Takaoka, 1980).

P : P (plume) - type; R : R (ridge) - type; A : atmospheric.

$r \equiv (^4\text{He}/^{36}\text{Ar})_P / (^4\text{He}/^{36}\text{Ar})_R$.

2. Information based on the noble gas data for Hawaiian samples

By studying noble gas isotopes in large phenocrysts of volcanic rocks and ultramafic nodules from Hawaiian Islands, Kaneoka and Takaoka (1980) concluded that the source material of the Hawaiian volcanic rocks should be different from that of MORB. This conjecture is based on the observation that phenocrysts show systematically higher $^3\text{He}/^4\text{He}$ and lower $^{40}\text{Ar}/^{36}\text{Ar}$ ratios than those of MORB. In Fig. 2, the data reported in Kaneoka and Takaoka (1980) are plotted. In this figure, three mixing lines are calculated which go through P, R and A. In this calculation, P, R and A are assumed to represent typical values for the P (plume)-type source material ($^3\text{He}/^4\text{He} = 5 \times 10^{-5}$, $^{40}\text{Ar}/^{36}\text{Ar} = 400$), the R (ridge)-type (= MORB type) source material ($^3\text{He}/^4\text{He} = 1 \times 10^{-5}$, $^{40}\text{Ar}/^{36}\text{Ar} = 16000$) and the atmosphere ($^3\text{He}/^4\text{He} = 1.4 \times 10^{-6}$, $^{40}\text{Ar}/^{36}\text{Ar} = 295.5$), respectively. However, former two do not always mean the genuine extreme values which we have not yet known.

Fig. 2 shows that most data lie around the mixing line between P and R. The other data are still located in the area surrounded by the three mixing lines. When a relatively low $^{40}\text{Ar}/^{36}\text{Ar}$ ratio close to the value of the atmospheric Ar is observed in a sample, the low value is often attributed to the atmospheric contamination. In the case of Hawaiian samples, however, higher $^3\text{He}/^4\text{He}$ ratios than that of MORB are always accompanied with relatively lower $^{40}\text{Ar}/^{36}\text{Ar}$ ratios. Furthermore, most of them approximately lie on a mixing line which goes through the points P and R. Hence, the relatively low $^{40}\text{Ar}/^{36}\text{Ar}$ ratio observed in Hawaiian samples probably reflect the value of the source material. The intermediate values between P and R suggest that a mixing of such source materials should have occurred underneath the Hawaiian Islands. Such a mixing probably occurs when a mantle plume arises through the MORB-type source material.

In Fig. 2, r is a parameter defined as $(^4\text{He}/^{36}\text{Ar})_P / (^4\text{He}/^{36}\text{Ar})_R$, where the suffixes P and R represent the ratios for P and R, respectively. By adopting a value 0.018 ± 0.002 for r , most data can be fitted to the mixing line which goes through P and R. By combining the values of P and R with the value for r , we can get a following value: $(^4\text{He}/^{40}\text{Ar})_P / (^4\text{He}/^{40}\text{Ar})_R = 0.71 \pm 0.10$.

In Fig. 3, the relative abundance of primordial components ^3He and ^{36}Ar in the source materials for P and R is studied. This figure shows the relationship between the $(^3\text{He})_P / (^3\text{He})_R$ and the $(^{36}\text{Ar})_P / (^{36}\text{Ar})_R$ ratios.

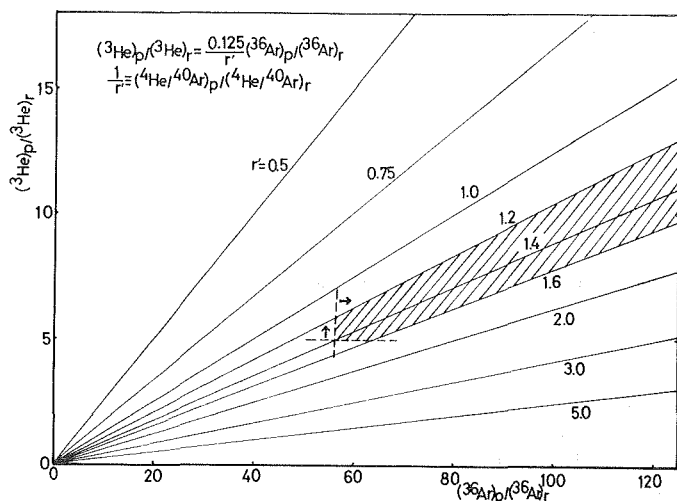


Fig. 3. The relationship between the $(^3\text{He})_P / (^3\text{He})_R$ and the $(^{36}\text{Ar})_P / (^{36}\text{Ar})_R$ ratios. The values in the shaded area are compatible with the data for Hawaiian samples.

Based on the result for r , the permitted range for r' ($\equiv 1/r$) is determined to be 1.4 ± 0.2 . Since the R-type source material is definitely depleted in incompatible elements including U and K compared with that of P-type source material, the concentrations of radiogenic components such as ^4He and ^{40}Ar in the P-type source material should be larger than those in the R-type source material. Hence, by assuming that P and R represent the values for the source materials for the P-type and the R-type, we can infer the minimum values for the $(^3\text{He})_p/(^3\text{He})_r$ and the $(^{36}\text{Ar})_p/(^{36}\text{Ar})_r$ ratios as 5 and 56, respectively. Hence, the P-type source material should contain larger amounts of primordial noble gas components compared with that of R-type. Only the values in the shaded area in Fig. 3 are compatible with the observed data for Hawaiian samples.

To calculate the mixing rate between the two source materials, we should know the isotopic ratios and relative concentrations for each end member. Although, P or R does not necessarily represent the end member, we assume tentatively that P and R approximate the values for each source material and the relative concentrations of noble gases are represented by the values as shown in Fig. 3. The result is shown in Fig. 4, where the case A represents the minimum mixing rate of the R-type source material with the P-type source material. Even in this case, however, if a sample shows a $^3\text{He}/^4\text{He}$ ratio of 2×10^{-5} as is the case for Kilauea samples, about 70% of the R-type source material might have mixed with 30% of the P-type source material. In general case, the mixing rate of the R-type should be larger than this estimate. This means that Kilauea samples were produced by mixing of larger amounts of R-type source material with lesser amounts of P-type source material, as long as noble gases are concerned.

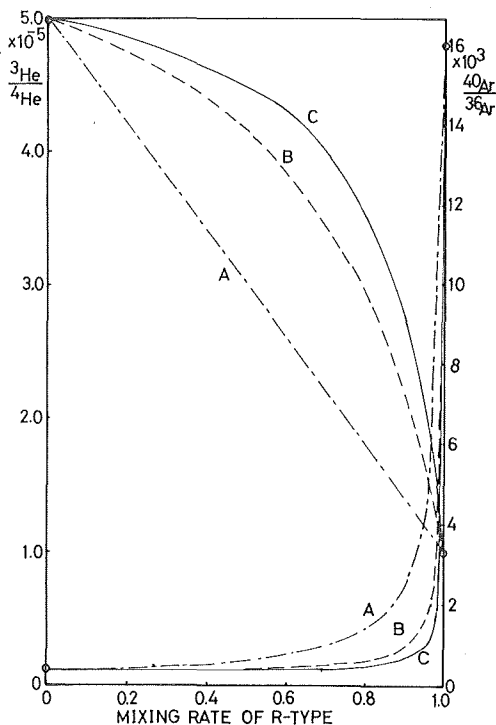


Fig. 4. The relationship between the observed $^3\text{He}/^4\text{He}$ and $^{40}\text{Ar}/^{36}\text{Ar}$ ratios and the mixing rate of R-type material with P-type material. For each end member, the following values are assumed.

$$\begin{aligned} \text{P} : & \quad (^3\text{He}/^4\text{He} = 5 \times 10^{-5}, \\ & \quad \quad \quad ^{40}\text{Ar}/^{36}\text{Ar} = 400) \\ \text{R} : & \quad (^3\text{He}/^4\text{He} = 1 \times 10^{-5}, \\ & \quad \quad \quad ^{40}\text{Ar}/^{36}\text{Ar} = 16000) \end{aligned}$$

$$\begin{aligned} \text{Model A} : & \quad (^3\text{He})_p/(^3\text{He})_r = 5, \\ & \quad \quad \quad (^{36}\text{Ar})_p/(^{36}\text{Ar})_r = 56, \\ \text{Model B} : & \quad (^3\text{He})_p/(^3\text{He})_r = 19, \\ & \quad \quad \quad (^{36}\text{Ar})_p/(^{36}\text{Ar})_r = 250, \\ \text{Model C} : & \quad (^3\text{He})_p/(^3\text{He})_r = 35, \\ & \quad \quad \quad (^{36}\text{Ar})_p/(^{36}\text{Ar})_r = 500. \end{aligned}$$

3. Discussion

As shown above, the source material for a mantle plume seems to be more abundant in primordial noble gas components than that for MORB. Furthermore, mixing between these source materials is quite likely at least for Hawaiian Islands and the mixing rate of the R-type material is much larger compared with that of the P-type material.

Since an oceanic plate is mainly composed of products by the P-type material, one may argue that the mixing occurs when a mantle plume arises from the asthenosphere through the plate. In this case, however, it seems very difficult to explain the mixing rate between the P-type and R-type source materials from the viewpoint of heat balance. Furthermore, if we assume that a mantle plume arises from the relatively shallow mantle, we must explain why larger amounts of primordial noble gases remain there, in spite of the depleted nature of the source material for MORB in the lower mantle. If one wants to explain it by the model C-b in Fig. 1, the primordial noble gas components should have been concentrated into the upper mantle without being lost to the atmosphere together with the incompatible elements. However, the observed data suggest that continental crust has surely lost most of primordial noble gases (e.g. Tolstikhin, 1978). Hence, it is not clear how to reconcile these requirements in the model C-b. In the case of the model C-a in Fig. 1, the primordial components are interpreted as the remains of primitive one. It is reported that the $^3\text{He}/^4\text{He}$ ratio for MORB is very uniform over Pacific, Atlantic and Indian Oceans (Lupton et al., 1977). To produce such a uniformity in the $^3\text{He}/^4\text{He}$ ratio, a uniform $^3\text{He}/(\text{U} + \text{Th})$ ratio or some homogenized process is required in the mantle. As a possibility for the latter, the role of the low velocity zone has been suggested (Kaneoka and Takaoka, 1980). Since He is mobile compared with other elements, it is not easy to conjecture that most primordial components remain at a relatively shallow depth in the mantle without being disturbed during the whole history of the earth.

These conjectures lead us to a conclusion that noble gas isotope data are most compatible with the model B among four models shown in Fig. 1. In this case, a mantle plume should arise from a relatively deeper mantle, though its depth cannot be designated from the present results. Although present noble gas data are only concerned with Hawaiian samples, preliminary results on samples from Iceland and Reunion Island seem to be compatible with the results as shown in Fig. 2. Furthermore, higher $^3\text{He}/^4\text{He}$ ratios than that of MORB are observed for samples from Yellowstone and Ethiopia where are classified as hot spot areas (e.g. Craig et al., 1978). Hence, the deeper part of the mantle seems to keep still primordial components of noble gases. In this connection, if excess ^{129}Xe , which is assumed to be the decay product of extinct nuclide ^{129}I , remains ubiquitously in the earth, it would be in the relatively deeper part of the mantle.

References

- Anderson, O.L. (1980) Preprint.
Craig, H., J.E. Lupton, J.A. Welhan and R. Poleda (1978) *Geophys. Res. Lett.*, 5, 891.
Davies, G.F. (1981) *Nature*, 290, 208.
DePaolo, D.J. (1981) *EOS*, 62, 137.
DePaolo, D.J. and G.J. Wasserburg (1976) *Geophys. Res. Lett.*, 3, 743.

- Jacobson, S.B. and G.J. Wasserburg (1979) Jour. Geophys. Res., 84, 7411.
Kaneoka, I. and N. Takaoka (1980) Science, 208, 1366.
Lupton, J.E., R.F. Weiss and H. Craig (1977) Nature, 266, 244.
O'Nions, R.K., P.J. Hamilton and N.M. Evensen (1977) Earth Planet. Sci. Lett., 34, 13.
O'Nions, R.K. and R.J. Pankhurst (1973) *ibid.* 21, 13.
Schilling, J.-G. (1973) Nature, 242, 565.
Sun, S.S., M. Tatsumoto and J.-G. Schilling (1975) Science, 190, 143.
Tatsumoto, M. (1978) Earth Planet. Sci. Lett., 38, 63.
Tolstikhin, I.N. (1978) Terrestrial Rare Gases, 33.

Sr ISOTOPES IN VOLCANIC ROCKS FROM THE SOUTH PACIFIC OCEAN:
SAMOA, RAROTONGA, RURUTU, AND MARQUESAS

Jun-ichi MATSUDA, Kenji NOTSU*, Toru KIKUKAWA
and Katsumi YASKAWA

Department of Earth Sciences, Faculty of Science,
Kobe University, Nada, Kobe 657, Japan

*Department of Chemistry, The University of Tsukuba
Sakura-mura, Ibaraki 300-31, Japan

1. Introduction

The three volcanic chains in the South Pacific: Emperor-Hawaii, Austral-Gilbert-Marshall, and Tuamotu-Line, seem to be well explained by a "hot spot hypothesis" (Wilson, 1963; Morgan, 1972). The moving lithosphere on a hot spot fixed in the deep mantle forms the volcanic islands on it and carries them next by next as it moves. Radiometric and fossil ages from the Hawaii-Emperor chain gave the strong evidence for its hot spot origin (McDougall, 1971; Clague and Jarrard, 1973; Clague et al., 1975; DSDP Scientific staff, 1971).

However, as for other two chains: Austral-Gilbert-Marshall and Tuamotu-Line, strong supports for their hot spot origin have not been obtained (Jarrard and Clague, 1977). Saito and Ozima (1977) indicated that there was no simple age progression along the line. The initial ($^{87}\text{Sr}/^{86}\text{Sr}$) ratios in volcanic rocks were quite variable, which did not suggest the single magma source under the Line islands (Matsuda, 1980). The low ($^{87}\text{Sr}/^{86}\text{Sr}$) ratio such as 0.7031 suggested that the magma sources by the hot spot were located in the "depleted" upper portion of the mantle.

Here, we report the ($^{87}\text{Sr}/^{86}\text{Sr}$) ratios in the volcanic rocks from Samoa, Rarotonga, Rurutu, and Marquesas.

2. Samples and the explanation of each island

The samples are all volcanic rocks and at first collected for the purpose of geomagnetic studies. The precise petrographic explanation was not done yet. Judging from the Rb and Sr contents almost all volcanic rocks except some from Rurutu are alkalic. The samples from Marquesas are from one site in Hiva-Oa and used to check how the ($^{87}\text{Sr}/^{86}\text{Sr}$) and Rb/Sr ratios are different from each other for one site in an island. Thirty two samples were collected from the sampling location where five or six tuff and lava flow layers were piled up alternatively to about ten meters high. We used four samples for Sr isotopic studies from thirty two samples. As for other samples the sampling locations are different for each sample in one island.

Samoa, Rarotonga, and Rurutu are geographically belonging to the Austral-Gilbert-Marshall chain which might be produced by a single hot spot (Fig. 1).

Samoa is situated on the elbow of the Austral-Gilbert-Marshall chain. If the single hot spot hypothesis for this chain is true, the age of Samoa should be about 40 m.y.

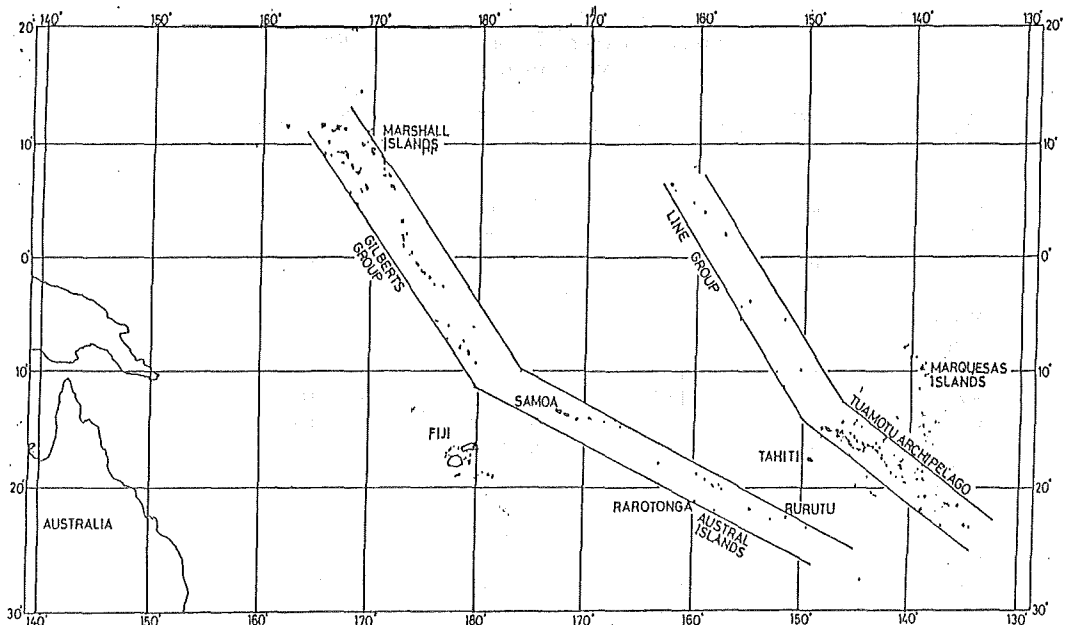


Fig. 1. The Austral-Gilbert-Marshall and the Tuamotu-Line chain in the South Pacific

which is estimated from the Emperor-Hawaii chain (Jarrard and Clague, 1977). However, active volcanism still occurs at the islands. Therefore, the Samoa islands might have been produced by another small hot spot, otherwise the volcanism still continues from 40 m.y. to the present. The chemistry and mineralogy of volcanic rocks were given by Hawkins and Natland (1975) and high ($^{87}\text{Sr}/^{86}\text{Sr}$) ratios were reported by Hedge et al. (1972).

Rarotonga is situated in the Cook-Austral islands. If Rarotonga is produced by the hot spot responsible for the Austral-Gilbert-Marshall chain (or only the Austral-Cook chain) starting from the Macdonald Seamount, the expected age of the rocks is about 20 m.y. (Jarrard and Clague, 1977; McDougall and Duncan, 1980). However, Dalrymple et al. (1975) gave the K-Ar age of 1.4 m.y. for six samples and Tarling (1967) gave the age of 2.5 m.y. for two samples (Jarrard and Clague, 1977). Therefore, this island may not be belonging to the chain produced by the hot spot of the Cook-Austral chain although there still remains the possibility that young volcanism covered the old volcanic rocks.

Rurutu is also expected to have a age of about 10 m.y. if it was produced by a hot spot for the Austral-Gilbert-Marshall chain (or only the Austral-Cook chain). Dalrymple et al. (1975) reported K-Ar ages of 1.05 m.y. for four samples, however Duncan and McDougall (1976) gave 12 m.y. of two samples. In the latter case Rurutu was one of the island chains produced by a hot spot for the Austral-Cook

Table 1 Rb, Sr and ($^{87}\text{Sr}/^{86}\text{Sr}$) ratios in the volcanic rocks from Samoa, Rarotonga, Rurutu, and Marquesas

Sample	Rb (ppm)	Sr (ppm)	Rb/Sr	$^{87}\text{Sr}/^{86}\text{Sr}$
Samoa				
B-4	42.4	621	0.0683	0.70598
C4B	34.1	843	0.0405	0.70484
G5D	66.9	439	0.1524	0.70668
J3E	36.9	642	0.0575	0.70540
M6E	23.6	735	0.0321	0.70590
Rarotonga				
A1C	148	1773	0.0835	0.70445
A4B	151	1811	0.0834	0.70450
B2A	30.4	688	0.0442	0.70413
D-2	46.3	899	0.0515	0.70445
F3A	11.8	1185	0.00996	0.70420
Rurutu				
A5	12.0	881	0.0136	0.70319
B4	8.12	722	0.0112	0.70287
E5	38.4	1194	0.0322	0.70324
G4	37.7	1207	0.0312	0.70326
J3	8.45	406	0.0208	0.70354
K3	9.15	811	0.0113	0.70348
Marquesas				
R20	56.7	702	0.0808	0.70514
R32	44.7	474	0.0943	0.70513
R1	59.9	597	0.1003	0.70512
R10	57.7	754	0.0765	0.70514

islands (McDougall and Duncan, 1980).

We can compare Sr isotopes in volcanic rocks for these three islands.

3. Experimental technique

($^{87}\text{Sr}/^{86}\text{Sr}$) ratios were measured by V-G Micromass MM30 double collector type mass-spectrometer in the University of Tsukuba. The result of repeated analyses for the standard sample NBS-987 was 0.71029 ± 0.00003 (2σ). The measurements were made twice to check the reproducibility of the measurement. The Rb and Sr contents were determined by X-ray fluorescence analyses. The precisions of the measurements were less than 5 % for both Rb and Sr. The obtained results are all listed in Table 1.

4. Discussion

(1) Marquesas

The obtained ($^{87}\text{Sr}/^{86}\text{Sr}$) ratios are essentially the same. The Rb and Sr contents are different from each other, however, these elemental abundance are quite variable and such a range of variation of Rb and Sr is not unusual. Therefore, it is confirmed that the samples are quite uniform

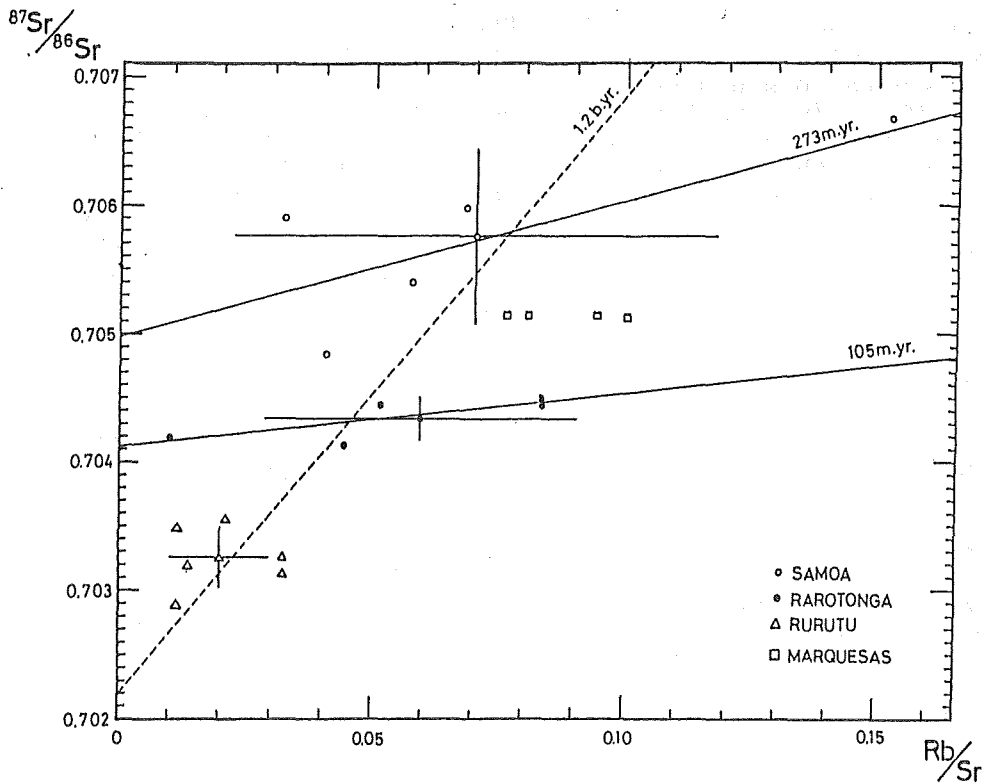


Fig. 2. $\text{Rb}/\text{Sr} - (^{87}\text{Sr}/^{86}\text{Sr})$ diagram for the samples from Samoa, Rarotonga, Rurutu and Marquesas. The points with error bars are average points for individual islands. The dotted line is the isochron for the three average points. Two lines are isochrons for Samoa and Rarotonga.

as far as they are collected from one site. The K-Ar ages from Marquesas islands gave the age progression (McDougall and Duncan, 1980), which suggested that Marquesas was produced by a hot spot.

(2) Samoa

The obtained $(^{87}\text{Sr}/^{86}\text{Sr})$ ratios are high and have a positive correlation with Rb/Sr (Fig. 2). The fitted line by the least square method gives the age of 273 m.y. and the initial $(^{87}\text{Sr}/^{86}\text{Sr})$ ratio of 0.7050 in case it is an isochron. Similar positive correlation was also obtained by Brooks et al. (1976) which gives the age of 510 m.y. and the initial $(^{87}\text{Sr}/^{86}\text{Sr})$ ratio of 0.7041. As the scattering of data around the line is large in both this study and theirs, these two ages are not quite distinguishable.

(3) Rarotonga

The positive correlation between $(^{87}\text{Sr}/^{86}\text{Sr})$ and Rb/Sr is again obtained (Fig. 2). The correlation is quite good for these samples. The fitted line gives the age of 105 m.y. and the initial $(^{87}\text{Sr}/^{86}\text{Sr})$ ratio of 0.7041.

(4) Rurutu

There is no obvious correlation between $(^{87}\text{Sr}/^{86}\text{Sr})$ and

Rb/Sr ratios (Fig. 2). ($^{87}\text{Sr}/^{86}\text{Sr}$) ratios and Rb/Sr are low compared with those from two other islands.

(5) General Discussion

The ($^{87}\text{Sr}/^{86}\text{Sr}$) ratios from each island are quite distinguishable each other and are gradually higher to the islands in the eastern side. It is noteworthy that we can not explain such a kind of variation of ($^{87}\text{Sr}/^{86}\text{Sr}$) ratios if these three islands were produced by a single hot spot. The plate itself is uniform for ($^{87}\text{Sr}/^{86}\text{Sr}$) ratios because it is produced in the East Pacific Rise where basalts were well known to have low and uniform ($^{87}\text{Sr}/^{86}\text{Sr}$) ratios. As the plate moves to the lateral direction and is cooled down, oceanic sediment or oceanic water alteration should be effective to increase the ($^{87}\text{Sr}/^{86}\text{Sr}$) of oceanic basalts (Satake and Matsuda, 1979). Such a kind of contamination to increase the ($^{87}\text{Sr}/^{86}\text{Sr}$) ratio is responsible to the magma genesis in the oceanic region. We do not know how deep the magma source is or whether the material is upwelled from the deep part of the mantle where ($^{87}\text{Sr}/^{86}\text{Sr}$) is rather high compared to the "depleted" upper portion of the mantle. However, as far as the magma source of the island always start in the same position, such a kind of effect should be the same for each island formation. Therefore, the ($^{87}\text{Sr}/^{86}\text{Sr}$) ratios should have similar values for only 40 m.y. or at least should be increased to the younger island by age effect if they have high Rb/Sr. There is no possibility of the mechanism to give the decreasing of ($^{87}\text{Sr}/^{86}\text{Sr}$) ratios as time passes as far as the magma genesis is always in the fixed position in the mantle.

Therefore, these islands should have been produced in the different position and is originated in different hot spot. The correlation lines (isochron) in Rb/Sr and ($^{87}\text{Sr}/^{86}\text{Sr}$) diagram give the age of 273 m.y. for Samoa and 105 m.y. for Rarotonga, respectively. It is interesting that if we average out the ($^{87}\text{Sr}/^{86}\text{Sr}$) and Rb/Sr ratios for each island these average points seem to lie on a line giving an age of 1.2 b.y. (Fig. 2). Therefore, it is reasonable to think that the large scale inhomogeneity of the mantle like the one under the whole island occurred at 1.2 b.y. ago, and the individual lavas in each island show a small scale heterogeneity in 100~300 m.y. time scale. Of course alkali rocks may not represent the Rb/Sr of the mantle material. Because of their small degree of partial melting, the Rb/Sr ratio in the volcanic rock is higher than that of the mantle material. In such a case the average points should be shifted to the left side in Rb/Sr—($^{87}\text{Sr}/^{86}\text{Sr}$) diagram and the real isochron will have a steep slope. Therefore, the actual age of mantle inhomogeneity is older than 1.2 b.y. Brooks et al. (1976) got the mantle isochron of 1.6 b.y. from the oceanic tholeiites, which may be a good estimate in above case.

References

- Brooks, C., S.R. Hart, A. Hofmann, and D.E. James (1976)
Earth Planet. Sci. Lett., 32, 51.
Clague, D.A. and R.D. Jarrard (1973),
Geol. Soc. Am. Bull., 84, 1135.

- Clague, D.A., G.B. Dalrymple and R. Moberly (1975), *Geol. Soc. Am. Bull.*, 86, 991.
- Dalrymple, G.B., R.D. Jarrard and D.A. Clague (1975), *Geol. Soc. Am. Bull.*, 86, 1463.
- DSDP Scientific Staff (1971), *Geotimes*, November, 12.
- Duncan R.A. and I. McDougall (1976), *Nature*, 251, 679.
- Hawkins, J.W., Jr. and J.H. Natland (1975), *Earth Planet. Sci. Lett.*, 24, 427.
- Hedge, C.E., Z.E. Peterman and W.R. Dickinson (1972), *Geol. Soc. Am. Bull.*, 83, 2709.
- Jarrard, R. and D.A. Clague (1977), *Rev. Geophys. Space Phys.* 15, 57.
- McDougall, I. (1971), *Nature Phys. Sci.*, 231, 141.
- McDougall, I. and R.A. Duncan (1980), *Tectonophys.*, 63, 275.
- Matsuda, J. (1980), *Geochem. J.*, 14, 41.
- Morgan, W.J. (1972), *Am. Assoc. Petrol. Geol.*, 56, 203.
- Saito, K. and Ozima (1977), *Earth planet. Sci. Lett.*, 33, 353.
- Satake, H. and J. Matsuda (1979), *Contrib. Mineral. Petrol.*, 70, 153.
- Tarling, D.H. (1967), *J. Geol. Geophys.*, 10, 1400.
- Wilson, J.T. (1963), *Can. J. Phys.*, 41, 863.

MAGNETOSTRATIGRAPHY AND CHRONOLOGY OF THE LATE NEOGENE
TO QUATERNARY DEPOSITS IN THE TOKACHI DISTRICT, HOKKAIDO, JAPAN

Mitsuo YOSHIDA*, Yoshiki FUJIWARA*, Mutsumi HOMMA**,
Yaeko IGARASHI* and Tokuji TONOSAKI*

- * Department of Geology and Mineralogy, Faculty of Science,
Hokkaido University, Sapporo 060, Japan.
** Girl's Senior Highschool attached to Tokyo College of Home
Economy, Tokyo, Japan.

Outlines of Geology

A series of thick marine, brackish as well as fresh water deposits including a large amount of pyroclastic deposits widely distribute in the Tokachi District, Eastern Hokkaido. These deposits are defined as the Tokachi Group at the present time. The Tokachi Group may preserve an almost complete record of the late Cenozoic history in the Eastern Hokkaido. The Tokachi Group is divided into following four formations; the Honbetsu, Ashoro, Ikeda and the Shibusan Formation in ascending order.

The Honbetsu Formation is mainly composed of conglomerate, sandstone, shale and tuff including lavaflores and pyroclastic deposits. The Honbetsu Formation is subdivided into three members; the Basal Volcanics Member, Rawan Sandstone and Conglomerate Member and the Tobushi Tuff Member in ascending order. A part of the Rawan Sandstone and Conglomerate Member is composed of marine deposits. Occurrence of generally called Takikawa-Honbetsu Fauna characterized by *Patinopecten (Fortipecten) takahashii* was reported (Fujie, 1958; Mitani, 1964).

The Ashoro Formation is mostly composed of dacitic or rhyolitic pumice flow deposits intercalating of sandstone beds. The Ashoro Formation disconformably overlies the Honbetsu Formation.

The Ikeda Formation is composed of both marine and lacustrine deposits. The relationship between the Ikeda and Ashoro Formation is a disconformity. This Formation is subdivided into two members. The Upper and Lower Member is divided by the key layer "Chiyoda pumice flow deposit". The Lower Member of the Ikeda Formation is mainly composed of conglomerate, sandstone, shale and tuff intercalating many layers of lignite beds. Warm sea temperature type molluscan fossils are recognized at near the key layer "Wine Tuff" (Tokachi Research Group, 1978). The upper limit of the appearance of *Patinopecten (Fortipecten) takahashii* covers up to the top of the Lower Member of the Ikeda Formation (Oka and Akamatsu, 1979). The Upper Member of the Ikeda Formation is mainly composed of conglomerate and sandstone. The Upper Member yields some cold sea temperature type molluscan fauna. This fauna is correlated to Plio-Pleistocene Omma-Manganji Fauna (Oka and Akamatsu, 1979).

The Shibusan Formation is mainly composed of pumice flow deposits and lacustrine deposits with lignite beds. The Shibusan Formation rests disconformably upon the Ikeda Formation. The total thickness of the Tokachi Group is estimated to be more than 2000 meters.

The climatic changes deduced from prosperity and decay of forest trees are estimated to be as follows; Subalpine zone

type conifer forest had been mostly predominated in the upper part of the Honbetsu Formation. From the beginning of the Ashoro stage, a forest belonging to the cool temperate zone had been remarkably expanded until the earliest of the Ikeda stage. This suggests the most warm paleoclimate through the whole succession. A proportion of subalpine type forest had gradually increased again at the early Ikeda stage. On the other hand, *Fagus* and Taxodiaceae disappeared at early Ikeda stage. A cool climate had been predominated until the end of this stage. Near the key layer "Kiyosumi Tuff", *Larix* observed to be remarkably increased. This suggests the most cool phase through the present stratigraphic sequence.

Paleomagnetism and Chronology

Oriented samples for paleomagnetic measurement are obtained from lavas, pumice flow deposits, tuffs and fine-grained sediments belonging to the Tokachi Group. The directions and intensities of the remanent magnetizations of the samples were measured by an automatic astatic magnetometer (Fujiwara and Yoshida, 1981) and also spinner magnetometer. The measurement was made on the samples before and after low temperature demagnetization and A.F. demagnetization.

Magnetostratigraphically, the Tokachi Group is divided into four polarity zones. The uppermost normal polarity zone is recognized from the Shibusan Formation down to the uppermost Ikeda Formation. This zone includes no reversed polarity. The K-Ar ages of Kuttari pyroclastic flow deposits belonging to the Shibusan Formation are 0.75 ± 0.38 my. and 0.96 ± 0.10 my. (Shibata et al., 1979). This normal polarity zone is correlated with the Brunhes Normal Epoch.

The reversed polarities are formed in the Ikeda Formation from the top of the key layer "Wine Tuff". The fission track age of the "Chiyoda pumice flow deposit" belonging to this reversed polarity zone is 2.0 ± 0.1 my. (Koshimizu, 1981). 1.70 ± 0.16 my. K-Ar age is also obtained from obsidian clast collected from the Upper Member of the Ikeda Formation (Shibata et al., 1979). This reversed polarity zone is correlated with the Matuyama Reversed Epoch. The normal events in the Matuyama Reversed Epoch may be represented by normal magnetized "Kiyosumi Tuff" (=Jaramillo Event) and the normal polarity found at about 10 meters above the "Chiyoda pumice flow deposit" (=Olduvai Event). These magnetostratigraphic correlations consistent with the biostratigraphic and paleoclimatic data. The time when the temperate factors decayed coincides with the time of deposition of the "Chiyoda pumice flow deposit" (=Olduvai Event). It consistent with Pliocene/Pleistocene boundary section at Italy (Nakagawa et al., 1976). Very cool phase detected near the "Kiyosumi Tuff", ie. Jaramillo Event, is also recognized in the Osaka Group (Maenaka et al., 1977), Uonuma Group (Nitobe, 1977) and the Yamato Group (Manabe, 1979-1980).

The second normal polarity zone is recognized from the Lower Member of the Ikeda Formation to the Ashoro Formation. Radiometric ages of the "Nishinaka pumice flow deposit" are 2.75 ± 0.12 my. (K-Ar), 2.82 ± 0.43 my. (K-Ar) (Shibata et al., 1979) and 2.8 ± 0.2 my. F.T. (Koshimizu, 1981). This normal zone may correlated to the Gauss Normal Epoch. A short reversed polarity episodes found in the "Senbiri pumice flow deposit" and

"Kami-aikappu pumice flow deposit" may probably correlate to the Kaena and Mammoth Event, respectively.

The second reversed polarity zone is recognized from the lower Ashoro Formation to the Honbetsu Formation. Radiometric ages of the "Naka-ashoro pumice flow deposit" (=Inashibetsu Tuff) are 4.1 ± 1.1 my. (K-Ar., Shibata et al., 1979) and 3.7 ± 0.1 my. (fission track, Koshimizu, 1981). This polarity zone may probably correlate to some time ranging from the Gilbert Reversed Epoch to Epoch 5. This result is also consistent with that the first occurrence of "*Foripecten*" is generally recognized on the Lower Pliocene or the uppermost Miocene around the Northern Pacific region (Hopkins, 1967; Gladenkov, 1976; Manabe, 1979-1980).

Consequently, age of the deposition of the Tokachi Group is correlated to the time ranging from Epoch 5 to early Brunhes Normal Epoch (see Fig.1).

References

- Fujie, T. (1958) *Shinseidai no Kenkyu* (Cenozoic Research), 26, 34.
Fujiwara, Y and M. Yoshida (1981) *J. Fac. Sci. Hokkaido Univ., Ser. IV*, 19, 519.
Gladenkov, Yu. B. (1976) *Proceeding of 1-CPNS* (Kaiyo Shuppan, Tokyo), 89.
Hopkins, D. M. (1967) *The Bering Landbridge* (Stanford Univ. Press, California), 495p.
Koshimizu, S. (1981) *J. Fac. Sci. Hokkaido Univ., Ser. IV*, 19, 505.
Maenaka, K. et al., (1977) *Quaternary Research*, 7, 341.
Manabe, K. (1979-1980) *Fukushima Univ. Sci. Rept.*, 29-30, 51-1.
Mankinen, E. A. and C. B. Dalrymple (1979) *J. Geophys. Res.*, 84, 615.
Mitani, K. (1964) *Rept. Geol. Surv. Hokkaido*, 32, 1.
Nakagawa, H et al. (1976) *Proceeding of 1-CPNS* (Kaiyo Shuppan, Tokyo), 285.
Nitobe, T. (1977) *Quaternary Research*, 7, 302.
Oka, T and M. Akamatsu (1979) *J. Geol. Soc. Japan*, 85, 691.
Shibata, K. (1979) *Bull. Geol. Surv. Japan*, 30, 231.
Tokachi Research Group (1978) *The Tokachi Plain* (Association for the Geological Collaboration in Japan, Tokyo), 433p.

(Submitted to *Jour. Geol. Soc. Japan*)

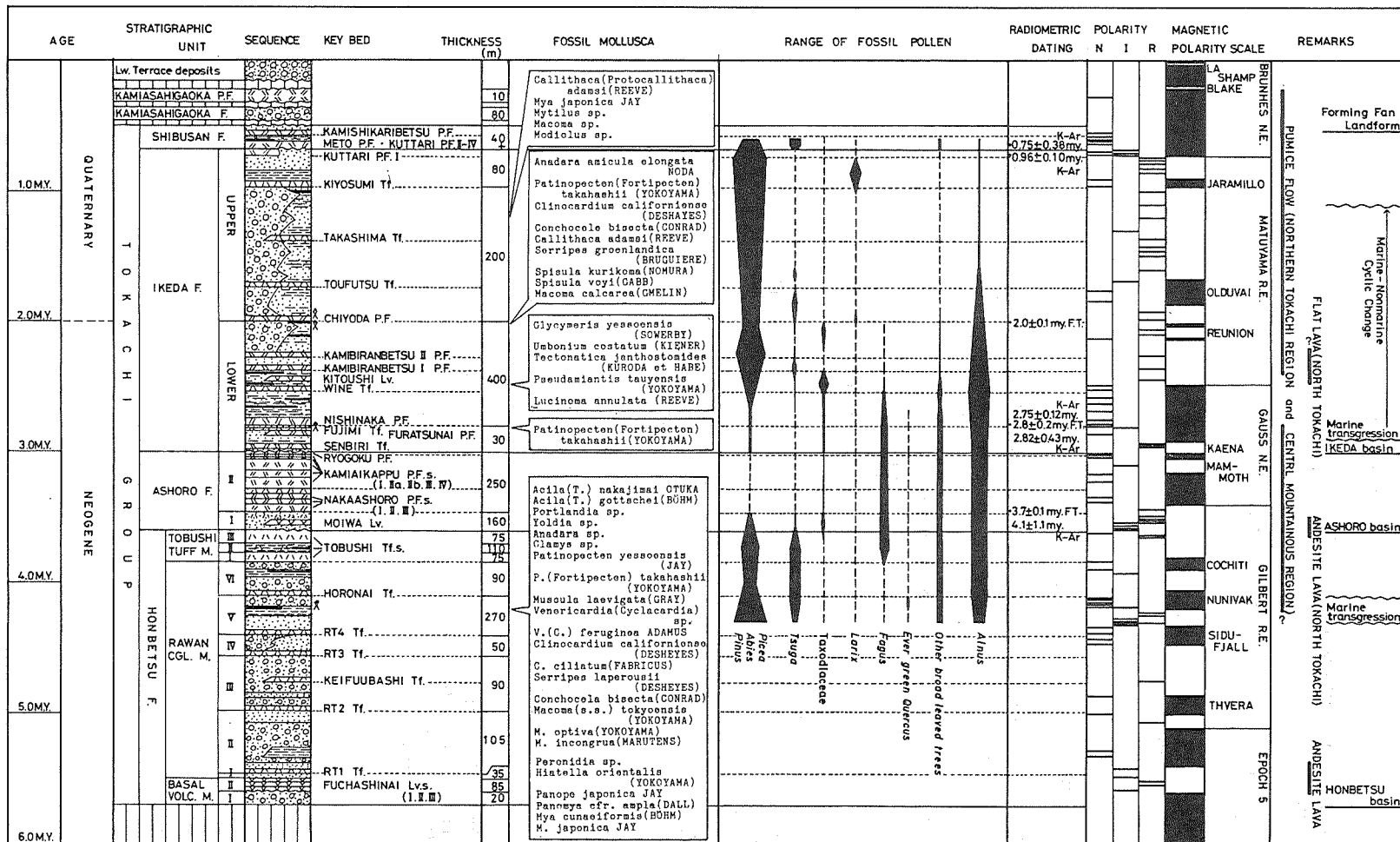


Fig.1 Paleomagnetic chronology, biostratigraphy and radiometric ages of the Tokachi Group

AUTHOR INDEX

CHUN, Liu, K. MAENAKA and S.SASAJIMA	9
DOMEN, Haruo	38, 57, 59
HAMANO, Yozo and K.YOMOGIDA	75
HEKI, Kosuke and H. TSUNAKAWA	17
HIRAJIMA, Takao	see OTOFUJI, Y.
ISHIDA, Shiro	see TORII, M.
ITO, Haruaki, K. TOKIEDA and Y. NOTSU.	40
KANEOKA, Ichiro	94
KATSURA, Ikuo and S.SASAJIMA	67
KIKUKAWA, Toru	see MATSUDA, J.
KONO, Masaru	89
KOYAMA, Masato	1
MAENAKA, Kazuaki	see CHUN, L.
MATSUDA, Junichi, K. NOTSU, T.KIKUKAWA and K. YASUKAWA	100
MIN, Kyung, Duck.	see OTOFUJI, Y.
MORIMOTO, Yuichiro	see NAKAJIMA, T.
MUNEOKA, Hiroshi	see DOMEN, H.
NAKAJIMA, Tadashi, Y. MORIMOTO	22
NOTSU, Yukio,	see ITO, H.
NOTSU, Yukio,	see MATSUDA, J.
OH, Jin, yong.	see OTOFUJI, Y.
OTOFUJI, Yo-ichiro, J. Y. Oh T. HIRAJIMA, K. D. MIN and S. SASAJIMA	46
OTOFUJI, Yo-ichiro, I. KATSURA and S. SASAJIMA	61
SASAJIMA, Sadao	see CHUN, L. OTOFUJI, Y.
SHIBUYA, H.	
SASAJIMA, Sadao	see OTOFUJI, Y.
SASAJIMA, Sadao	see SHIBUYA, H.
SASAJIMA, Sadao	see KATSURA, I.
SATO, Takaharu	85
SHIBUYA, Hidetoshi and S. SASAJIMA	53
TANAKA, Hidefumi	81
TOKIEDA, Katsuyasu,	see ITO, K.
TOSHA, Toshiyuki and H. TSUNAKAWA	28
TSUNAKAWA, Hideo	see TOSHA, T.
TSUNAKAWA, Hideo	see HEKI, K.
YASUKAWA, Katsumi	see MATSUDA, J.
YOMOGIDA, Kiyoshi	see HAMANO, Y.
YOSHIDA, Mitsuo, Y. FUJIWARA, M. HOMMA, Y. IGARASHI and T. TONOSAKI	106